UNIVERSITY OF MALAGA

PhD THESIS

Photovoltaic Lifetime Forecast: Models for long-term photovoltaic degradation prediction and forecast

Ismail Kaaya

Málaga, February, 2020

PhD THESIS

Photovoltaic Lifetime Forecast: Models for long-term photovoltaic degradation prediction and forecast

Author:
Ismail Kaaya

Supervisors:
Mariano Sidrach de Cardona Ortín
Karl-Anders Weiss

PhD program:
Mechanical Engineering and Energy Efficiency

PhD thesis presented in the SCHOOL OF INDUSTRIAL ENGINEERING of MALAGA UNIVERSITY to obtain the Doctor Degree

Director:
Mariano Sidrach de Cardona Ortín

Málaga, February, 2020

DECLARACIÓN DE AUTORÍA Y ORIGINALIDAD DE LA TESIS PRESENTADA PARA OBTENER EL TÍTULO DE DOCTOR

D./Dña ISMAIL KAAYA
Estudiante del programa de doctorado INGENIERÍA MECÁNICA Y EFICIENCIA ENERGÉTICA de la Universidad de Málaga, autor/a de la tesis, presentada para la obtención del título de doctor por la Universidad de Málaga, titulada: PHOTOVOLTAIC LIFETIME FORECAST: MODELS FOR LONG-TERM PHOTOVOLTAIC DEGRADATION PREDICTION AND FORECAST

Realizada bajo la tutorización de MARIANO SIDRACH DE CARDONA ORTÍN Y KARL-ANDERS WEISS y dirección de MARIANO SIDRACH DE CARDONA ORTÍN (si tuviera varios directores deberá hacer constar el nombre de todos)

DECLARO QUE:

La tesis presentada es una obra original que no infringe los derechos de propiedad intelectual ni los derechos de propiedad industrial u otros, conforme al ordenamiento jurídico vigente (Real Decreto Legislativo 1/1996, de 12 de abril, por el que se aprueba el texto refundido de la Ley de Propiedad Intelectual, regularizando, aclarando y armonizando las disposiciones legales vigentes sobre la materia), modificado por la Ley 2/2019, de 1 de marzo.

Igualmente asumo, ante a la Universidad de Málaga y ante cualquier otra instancia, la responsabilidad que pudiera derivarse en caso de plagio de contenidos en la tesis presentada, conforme al ordenamiento jurídico vigente.

En Málaga, a 1 de FEBRERO de 2020

Fdo.: ISMAIL KAAYA

Dr. Mariano Sidrach de Cardona Ortín, Professor in the Applied Physics department at the University of Málaga and Dr. Karl-Anders Weiss head of service life analysis in the Fraunhofer Institut of Solar Energy as Directors of the Doctoral Thesis: Photovoltaic Lifetime Forecast: Models for long-term photovoltaic degradation prediction and forecast, presented by Mr. Ismail Kaaya in the School of Industrial Engineering of the University of Málaga to obtain the Doctor Degree.
They state that this thesis is supported by the following research articles:

Paper 1. I. Kaaya, M. Koehl, A.P. Mehilli, S. de Cardona Mariano, & K.A. Weiss, "Modeling Outdoor Service Lifetime Prediction of PV Modules: Effects of Combined Climatic Stressors on PV Module Power Degradation". IEEE Journal of Photovoltaics,vol. 9, no. 4, pp. 1105–1112, May. 2019.
This paper is reprinted from the Open Access publication available at https://ieeexplore.ieee.org/document/8720037. All rights remain with the authors and editors.
Impact factor: 3.398

Paper 2. S. Lindig, I. Kaaya, K.A. Weiss, D. Moser, and M. Topic, "Review of statistical and analytical degradation models for photovoltaic modules and systems as well as related improvements," IEEE J. Photovoltaic., vol. 8, no. 6, pp. 1773–1786, Nov. 2018.
This paper is reprinted from the Open Access publication available at https://ieeexplore.ieee.org/document/8472886. All rights remain with the authors and editors.
Impact factor: 3.398

Paper 3. J. A-Vásqueza, I. Kaaya, K. Brecla, K-A. Weiss and M.Topic, "Global climate data processing and mapping of degradation mechanisms and degradation rates of PV modules". energies MDPI ,vol. 12, no. 4749 Dec 2019.
This paper is reprinted from the Open Access publication available at https://www.mdpi.com/1996-1073/12/24/4749/htm. All rights remain with the authors and editors. Impact factor: 2.707

Málaga, April, 2020
Signed:

Mariano Sidrach de Cardona Ortín | Karl-Anders Weiss

Acknowledgements

The author has carried out a big part of the research reported in this thesis at Fraunhofer Institute of Solar Energy (ISE), Freiburg, Germany, in the research group Service Life Analysis and Material Characterization. This research has received funding from the European Unions Horizon 2020 research and innovation program under the Marie Sklodowska-Curie grant agreement No 721452-Project Solar-Train.

Firstly, I would like to thank both my research supervisors: Dr. Mariano Sidrach de Ortin of the University of Malaga and Dr. Karl-Anders Weiss of Fraunhofer ISE, for their insight and mentorship, and for creating a collaborative and congenial working atmosphere for me during the process of my research.

Secondly, I would like to acknowledge the different sources of data used in this research as: Fraunhofer Instute of solar energy for sharing the module data from Negev, Gran-Canaria and Zugspitze as well as indoor test data, the Scuola universitaria professionale della Svizzera italiana (SUPSI) for sharing the TISO plant data, the Institute for Renewable Energy, EURAC Research for sharing the Bolzano system data and the Desert Knowledge Australia Solar Centre (DKA Solar Centre) for the continuous effort to provide free access photovoltaic systems data. These data sources are properly referenced in the notes and bibliography.

Special thanks go to Micheal Koehl of Fraunhofer ISE, Lindig Sascha and David Moser of EURAC Research, Julián Ascencio-Vásquez of University of Ljubljana and Alessandro Virtuani of École Polytechnique Fédérale de Lausanne (EPFL) for their fruitful discussions and collaboration during different stages of my research. I cannot forget to thank my wife Sophie Marchand of Fraunhfer ISE for her continuous support and encouragements throughout the entire research period. I could not have done it smoothly without you. I also thank my daddy Mr.Nsubuga Med and my siblings for their support in my entire academic career. Lastly I extend my gratitude to the entire Solar-Train project team for the wonderful discussions, training and informal meetings. It has been grateful to work with and learn from everyone, indeed, it has been a time of tremendous learning and growth for me both scientifically and personally.

Marie Skłodowska-Curie Actions

Abstract

As the share of photovoltaic keeps increasing in the global electricity mix, it becomes critical to assess how the overall system and module performance (power) decreases over time. This is not only important for financial reasons but also technically, because it is crucial to understand the effects of the local climate on the performance degradation. Although different models have been proposed to quantify the impact of climatic stresses on performance degradation based on indoor ageing tests, less has been done to quantify these effects in outdoor operations. The available methods for outdoor application are mainly data-driven, meaning that the performance losses are evaluated from monitored performance data without an understanding of the influencing environmental variables. Moreover, these models are suitable for performance loss rates and not for degradation rates evaluations.

Therefore, in the first part of this research, a physical model to determine the degradation rates of photovoltaic modules based on outdoor climatic variables is proposed. Through it, the impact of combined climatic loads on the module's maximum power output is quantified. In this approach, three degradation precursor mechanisms, namely, hydrolysis, photodegradation, and thermo-mechanical, are assumed to be necessary for service lifetime prediction. For each mechanism, an empirical model that describe well the physical/chemical kinetics is selected or proposed. To validate the selected or proposed models, experimental data from accelerated ageing tests are used. A generalized model to quantify the effects of combined climatic loads for outdoor applications is then derived from the three models. The generalized model is calibrated and validated using outdoor experimental data of three identical mono-crystalline silicon modules installed in three benchmarking climates: maritime (Gran Canaria, Spain), arid (Negev, Israel), and alpine (Zugspitze, Germany). Finally, using the public climate database (ERA5), climatic data is processed to extract the climatic stresses necessary for the calculation of the degradation rate. These stresses are then applied to evaluate the degradation rates based on the three precursor mechanisms and also to evaluate the total degradation rates. Therefore, global degradation risk maps based on specific precursor mechanisms as well as total degradation rate are provided. We believe that these risk maps are useful to understand the dominating degradation mechanisms according to geographical locations and hence could be used to develop photovoltaic materials depending on the operating geographical locations.

Other fundamental challenge of the available methods is their accuracy when long-term forecasts are needed after a short operation time and with limited data points. The second part of this research, addresses this challenge where a new data-driven method is proposed so as to improve the accuracy of long-term prediction with small degradation history. The model depends on the degradation patterns and a new concept of time dependent degradation rate is introduced. The model has been calibrated and validated using different photovoltaic modules and systems data with 5 to 35 years of field exposure. The new model is benchmarked against existing data-driven methods. The proposed model lowered the long-term forecast uncertainties when forecasts are made after a small performance degradation. Through this, the effects of long-term degradation to lifetime yield prediction are assessed. It has been shown that using the proposed approach, the lifetime yield predictions are more reliable due to more accurate long-term degradation forecast.

Finally, the two approaches are combined to form a hybrid model based on both the physical and data-driven methods. Indeed, the hybrid modelis aimed to provide more reliable long-term degradation forecast as well as having a physical understanding of the dominating degradation mechanisms influencing the performance degradation. We believe such a model is useful to calculate more reliable levelized cost of energy and thus the economic viability of solar energy as well as to improve the development of new PV materials according to the operating climatic conditions.

Contents

Chapter 1

Introduction

PV modules as well as systems are affected by continuous cycles of temperature, humidity, irradiation, mechanical stress, and soiling. These environmental stresses cause different degradation modes that take place within a PV module and reduce the performance of the system. In order to accurately determine the degradation rates of PV modules and to understand the effects of the operating conditions, the evolution of power in real life operation must be monitored simultaneously with the local operating condition. However, this requires waiting a considerable amount of time and huge financial investments. In this case, two main approaches are currently used to mimic the outdoor degradation rates.

The first approach is using indoor accelerated ageing tests where modules are exposed to extreme controlled operating conditions in climatic chambers in order to degrade the modules within a short time. Although these tests are carried out based on the established International Electrotechnical Commission (IEC) standards Wohlgemuth (2012), an open question remains if they can really represent outdoor degradation.

The second approach is the utilization of mathematical models to determine the degradation rates in shorter periods and to predict the lifetime of PV modules. Two modelling techniques are commonly used; physical and data driven techniques. Physical models are developed to describe the link between the modules performance degradation to environmental variables Bala Subramaniyan et al. (2018). Data-driven techniques utilize monitored operational data related to system's performance to evaluate the degradation rate Meyers et al. (2019). The biggest challenge of mathematical models is the reliability of the predicted results Jordan et al. (2020). Usually, to valid degradation models, one needs to have enough degradation data available, which is not always the case.

On one hand, according to the state-of-the-art of degradation models, most physical models are developed for accelerated indoor ageing application. Physical models to quantify the effects of outdoor climatic stresses are very helpful to understand the correlation of the different local climates with the degradation processes. This understanding is useful to develop new materials based on the operation local climates. However, such models have received relatively little attention in the industry. According to our knowledge, it is of recent that, Bala Subramaniyan et al. (2018) proposed a model to link the module performance degradation to environmental variables for outdoor application. They applied their model to predict the degradation rates of a mono-crystalline silicon module in different climatic locations. However, since PV modules are characterized by numerous degradation modes Köntges et al. (2017) and that PV modules are of different technologies, further developments for a model that take into account multiple climatic factors are still needed. Moreover, degradation models are developed on basic assumptions as well as simplifications based on the available or known degradation patterns, this makes generalization of a given model a challenge. In this case, it is important to develop different models using different assumptions describing different degradation patterns. Therefore, in the first part of research, a new physical model to quantify the effects of combined climatic stresses is proposed as a contribution to this challenge.

The new model is based on the assumptions that, three major degradation mechanisms; hydrolysis, photo-degradation and thermo-mechanical degradation are necessary for lifetime prediction. Empirical models are proposed to describe the kinetics of these three mechanism and hence to calculate the degradation rates. Through accelerated ageing tests, these mechanisms are reproduced and hence the models are validated. A model to evaluate the impacts of the combined climatic stresses is then derived from the three mechanisms. The derived model is calibrated and validated using identical mono-crystalline silicon modules installed in three different climates: maritime (Gran Canaria, Spain), arid (Negev, Israel), and alpine (Zugspitze, Germany) using real monitored meteorological data. To extend the analysis on a global scale, global climate reanalysis data is used to extract the model's climatic input variables. The extracted variables are then applied to simulate maps of degradation rates based on specific degradation mechanisms as well as the total degradation rates.

On the other hand, data-driven techniques Phinikarides et al. (2014), Meyers et al. (2019) that utilize monitored operational data related to system's are commonly used especially to evaluate the degradation rates as well as the performance loss rates of PV systems in outdoor performance. Generally, in spite of the wide application and the recognized potential of the data-driven techniques, limitations still exist for their use in PV degradation analysis. The lack of a systematic and flexible approach to select parameters of these models and their black-box character limit their understanding. Moreover, data-driven techniques for lifetime forecast are based on fitting the available systems degradation data by regression models and then extrapolating the evolution up to the time of failure. However, in practice, the system's degradation history available may be short and incomplete, and a simple extrapolation may lead to large uncertainties. Also, one other serious challenge is the accuracy of the models when applied after a shorter time interval. Data-driven models usually require enough degradation history for their training. When applied to forecast long-term degradation using a short degradation history, they often provide unrealistic degradation scenarios. For example, Taylor and Letham Taylor and Letham (2018) performed a comparison of the forecasting accuracy of different statistical models at different time horizons. In their study, most models displayed large uncertainties when applied after shorter time interval. To address these challenges, a new data-driven model is proposed specifically for long-term degradation forecast. The proposed model is aimed at improving the long-term forecasting accuracy for a shorter operation time. To achieve this, time dependent degradation factors are assumed instead of a constant one. To further improve the accuracy, different degradation factor models are proposed based on the degradation patterns. Moreover, the model has been calibrated and validated using degradation data from different sources and of different PV technologies both on module and system level.

One other drawback of the data-driven methods is the lack of a correlation of the evaluated rates with the triggering degradation mechanisms. To solve this problem, we combine both the physical and the data-driven approaches proposed in this research into a hybrid model. The hybrid model will aid to have more reliable long-term degradation forecast as well as having a physical understanding of the dominating degradation mechanisms influencing the performance degradation. We believe such a model is useful to calculate more reliable levelized cost of energy and thus the economic viability of solar energy as well as to improve the PV materials according to the operating conditions.

The structure of the thesis is as follows:

Chapter 1. Introduction of the research, the novelty of the research work is introduced with regard to the start-of-the-art.

Chapter 2. The available physical models are reviewed and Were possible a comparison of the performance of the different models is carried out using experimental data from indoor tests. At the end of the chapter the gaps for improvements are identified.

Chapter 3. In this chapter, the methodologies of the proposed models are presented. The chapter contains three major sections corresponding to methodologies for a physical, data-driven and hybrid models respectively. In the first two sections, the experimental data used for model calibration and validation are also described.

Chapter 4. Here, the results are presented and discussed in order of the sections in chapter 3.

Chapter 5. Summarises the main conclusions of the research. The references follows the chapter and the annex with the copies of the published articles that supports the research are attached after the references.

Chapter 2

Literature review

Table 2.1: Chapter Nomenclatures

Symbols	
E_a	activation energy [eV]
I	Intensity
I_{SC}	short circuit current [A]
k_B	Boltzmann constant (8.62×10^{-5}eV/K)
P_{max}	power at maximum power point [W]
R_D	degradation rate [%/hour]
T_{max}	maximum temperature [K]
T_{min}	minimum temperature [K]
R_s	Series resistance [Ω]
R_{sh}	Shunt resistance [Ω]
U	voltage [volt]
ΔT	temperature cycles [K]
Abbreviations	
BoM	bill of materials
DH	damp heat
EVA	Vinyl-acetate monomerspresent in Ethylene-vinyl acetate
LID	light induced degradation
PID	potential induced degradation
PV	Photovoltaic
RH	relative humidity [%]
RMSE	root means square error
t	time
T	temperature [K]
TOW	Time of wetness
UV	Ultraviolet [W/m^2]

2.1 Photoltaic degradation and degradation modes

Photovoltaic degradation is the reduction in efficiency with which a PV module/system converts sunlight into electricity Jordan and Kurtz (2013). Degradation modes are effects that irreversibly degrade the performance of a PV module or of a system and cloud cause safety problems Köntges et al. (2017). A great number of different degradation modes are observed in PV modules, both under outdoor operation and and also using indoor accelerated ageing testing. The most commonly observed degradation modes include Köntges et al. (2017): LID, solder fatigue failure, silver grid finger delamination, bypass diode failure, delamination, cell cracks, corrosion, polymeric discoloration, UV degradation of the cell, polymeric mechanical failure, and PID. Each of these degradation modes has different causes and is triggered by various stress factors.

Apart from the modes listed, different technical risks, which affect the PV performance and the resulting costs, were found by Moser et al. (2017) as: glass breakage, snail track, defective backsheet, hotspot, soiling, overheating, and junction box failure. An occurring degradation mode can have an increasing impact on the PV performance over time. It can develop in isolation as well as in combination with other degradation modes or technical risks and might lead to the failure of a PV module. However, despite the definitions above, a clear understanding of the definition of a degradation mode is also still a challenge and stress should be put on common nomenclature to define a degradation mode with the same terminology.

2.2 Degradation models

In general terms, degradation models are used to relate a test item's estimated failure time with the wear and tear during its usage period. It is important to note that for a PV module, failure can be related to both performance degradation and safety issues. In this regard, it is a prerequisite to describe in which context it is being used. To add on, degradation models can either be developed to evaluate electrical performance or material degradation, it is also necessary to clarify the context in this regard. Therefore, in this section, the term failure (as used throughout the entire document) is defined only in terms of performance degradation. The described as well as the proposed models quantify the evolution of PV modules performance over time.

Two modeling approaches; physical and data-driven are commonly used to evaluate the degradation rates and lifetime of PV modules.

Data-driven models are often employed to estimate degradation rates based on analysis of given data sets. Data-driven techniques can be divided into two categories: statistical techniques (regression methods, ARMA models, etc.) and artificial intelligence (AI) techniques (neural networks (NNs), fuzzy systems (FSs), etc.) Chen Xiongzi et al. (2011). The goal of the statistical analysis is to calculate the trend of the PV performance time series and to translate the slope of the trend to an annual loss rate, in units of %/year Phinikarides et al. (2014). Although these models can provide consistent performance loss rates (PLRs), which are useful for data extrapolation and service life predictions, they do not directly provide evidence for the degradation modes taking place in the module. Other effects such as diffuse soiling, snow, shading or module mismatch have also a direct impact on the performance trend.

Physical models are based on the physical/chemical understanding and assumptions of a specific degradation mode. These models represent the mechanism involved in complex physical/chemical processes. For well-known PV module degradation modes, several analytical models to predict PV module degradation are available. All these models are based on the principle of understanding the underlying process, but they are still only heuristic models, which do not include the influence of material parameters.

A significant part of the research is devoted to physical models, therefore, the literature discussion is inclined towards this directions. The statistical methods are also reviewed in the supporting article attached in the annex.

2.3 A review of the available physical models

On one hand, physical models are developed to explain experimental observations of different degradation modes and can also be used in experimental designs. A model can be applied to analyze the experimental observations by fitting experimental data to extract parameters that cannot be directly measured (e.g kinetic energy), used to study the sensitivity of performance degradation to climatic stress factors such as T, RH, ΔT, UV and other influence factors.

On the other hand, models are also used to predictive or forecast future behavior. Models are used to predict in situations where a given module needs to be analyzed under different test conditions. In this case, the measurements of the module under a given condition can be applied to calibrate the degradation models and apply the calibrated model to predict the effects of other different test conditions as illustrated in 2.1. Degradation models are used as forecasting models to know the progress of degradation for an extended time horizon. In this case, the models are calibrated on experimental data after a shorter time and then applied to extrapolate the degradation for a longer time.

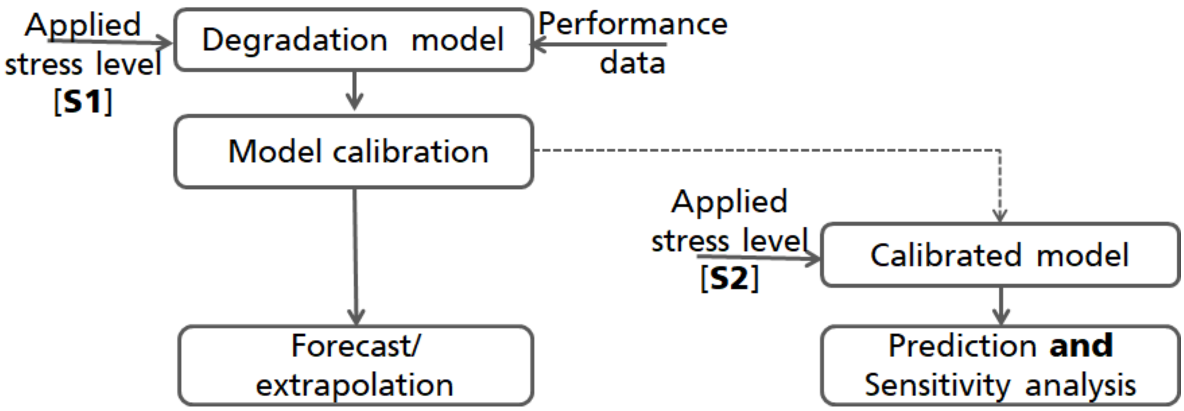

Figure 2.1: Schematic diagram showing the different applications of degradation models: forecasting, predictive, sensitivity analysis and experimental evaluation. S1 are the applied experimental stress conditions and S2 are the modeled stress conditions. At model calibration stage, the extracted parameters can be used for extrapolation, results assessment by correlating them to material properties or used as inputs to predict the degradation at different test condition as well as to perform a sensitivity analysis

Electrical parameters such as: P_{max}, I_{SC}, R_{sh} and R_s resistances are commonly modeled as degradation indicators. Hence, the environmental stresses and their interactions with the PV module components are assessed based on the reduction of the initial electrical parameter at time $(t = 0)$ before aging and at time $(t = t)$ after aging or in the field. The degradation models can be divided into two categories: models for the degradation indicators and models for the degradation rates. The degradation indicator models are mathematical functions proposed to evaluate the degradation trends of a given degradation indicator over time. Since each degradation mode or technology under investigation can have a different degradation curve, different authors have proposed models to fit the observed degradation curves. On contrast, degradation rate models evaluate the rate of change of degradation indicators. They are function of the applied stress factors.

The structure of the review is as follows; models are discussed according to specific degradation modes, how they are applied and where necessary their performances are compared and discussed.

2.3.1 Degradation models for corrosion

Corrosion is one of the most occurring degradation modes in PV modules Ndiaye et al. (2013). Corrosion is caused by the presence of high temperature and high humidity in the module. Humidity can enter the module through the backsheet or the layers of the encapsulant and spread into the module Park et al. (2013). One hypothesis is that humidity leads to the formation of acetic acid through the hydrolysis of EVA Kempe et al. (2007); Whitfield et al. (2012); Masuda et al. (2015) resulting to corrosion. Corrosion attacks the metallic connections of PV cells and results in a loss of adhesive strength between the cells and the metallic frame, as well as an increased leakage current and therefore a loss in performance Kempe et al. (2007).

Degradation indicator models based on power at maximum power point and series resistance have been proposed to fit the degradation patterns for corrosion as:

(1) Model of Pan et al. (2011)

$$\frac{P_{max}}{P_{max(0)}} = exp(-R_D t^{\beta}) \tag{2.1}$$

(2) P_{max} and R_s models according to Braisaz et al. (2014)

$$P_{max} = \frac{1 - exp(-B)}{1 + exp(R_D t - B)} \tag{2.2}$$

$$R_s = R_{S(0)} = exp(R_D t - B) \tag{2.3}$$

where P_{max} [W] and R_s [Ω] are the output power and series resistance at time (t), $P_{max(0)}$ & $R_{S(0)}$ are the power output and series resistance at time ($t = 0$), β is the experimental parameter, B is a coefficient to be calibrated and R_D [%/hour] is the degradation rate.

These functions can be applied in two way; to extract the degradation rates and also for extrapolation. The first application is used to compare the degradation rates of a similar module but with different stress conditions or to analyze the impact of applied stresses to different BoM. In this case, different modules with different BoM are tested under similar conditions and the extracted degradation rates are compared. The second application is used to forecast the evolution of degradation at an extended time horizon.

A. Comparison of Pan and Braisaz Model

The two models are applied to fit time series datasets from DH ageing tests at different conditions: DH/75^{0}C/85%RH, DH/90^{0}C/50%RH and DH/90^{0}C/70%RH. Since the loss in power could take different shapes as reported by Köntges et al. (2014), it is unlikely that a single degradation function can fit all the different shapes. Here we compare how well the two function can fit three time series dataset from DH measurements with different degradation profiles as shown in figure 2.2. The fitting is done using the least squares fitting function inbuilt in Python. In both cases the derived degradation rates, the model parameters as well as the RMSE are presented in table 2.2 . The RMSE is calculated as:

$$RMSE = \sqrt{\frac{\sum_{j=1}^{n}(f_i - m_i)^2}{n}} \tag{2.4}$$

where, m is a measured value and f is the fit value, n are the number of observations.

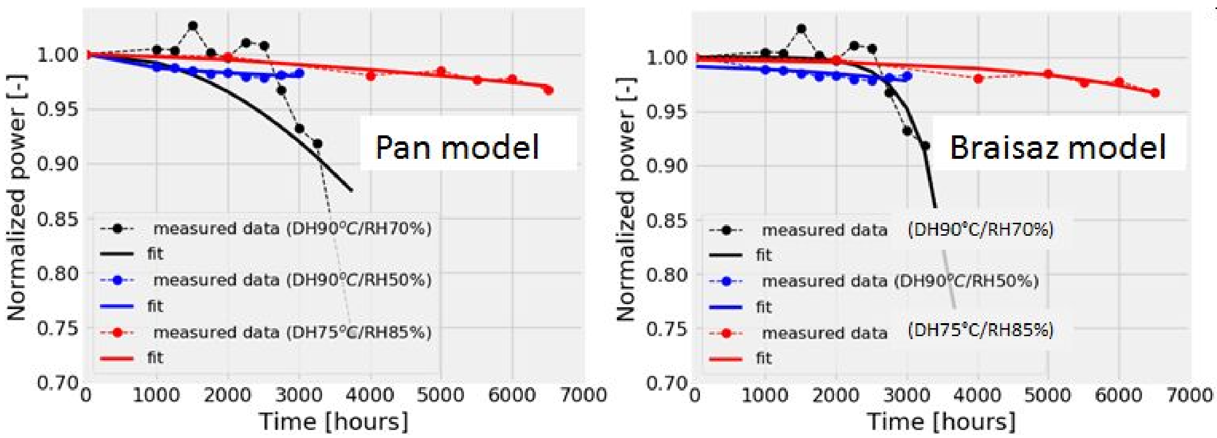

Figure 2.2: Pan and Braisaz model fit for different DH measurements, the dotted lines represent the experimental data and the thick lines are the corresponding models fit respectively. The colors represents the different experimental condition as well as the different failure profiles.

Table 2.2: Derived model parameters for different damp heat conditions

Experimental condition	R_D [%/hour]	Model parameter (β)	model parameter (B)	RMSE [%]
		Pan Model		
DH 75^{o}C/85% RH	5.66e-8	1.50	-	0.35
DH 90^{o}C/50% RH	6.40e-4	0.43	-	0.19
DH 90^{o}C/70% RH	3.15e-9	2.13	-	4.99
		Braisaz Model		
DH 75^{o}C/85% RH	4.43e-4	-	6.34	0.39
DH 90^{o}C/50% RH	4.66e-4	-	5.42	0.39
DH 90^{o}C/70% RH	2.58e-3	-	10.75	1.33

Figure 2.2 shows the experimental data with the respective models fit. It is can be seen that, depending on the degradation shape, the fitting accuracy varies for both models. For example, the model of Pan was able to fit well the red and blue curves and could not provide perfect fitting of the black curve. On contrary, the model according to Braizas was able to perfectly fit the black curve but not the the blue curve. Overall the model according to Braizas is preferable to that of Pan since the extracted degradation rates are consistent with the applied stresses. However, a model that include a shape parameter that can perfectly fit/optimize, the different degradation shapes is still needed and will be

part of this research work.

Another application of degradation models, as mentioned before, is to extrapolate the measured performance degradation to longer time horizons. Therefore, the two models are calibrated on the same dataset (i.e. DH/75^{0}C/85%RH) but only after 4000 hours. In each case the model parameters are extracted as in Table 2.3. Then the calibrated models are applied to forecast the power degradation from 4000 hours until 6500 hours. The results for all the three models are plotted with the extended measurements 2.3

Table 2.3: Model parameters for Pan and Braisaz model after 4000 hours of DH/75C/85%RH

Model	R_D [%/hour]	Model parameter (β)	model parameter (B)	RMSE [%]
Pan Model				
Pan	6.44e-10	2.07	-	0.13
Braisaz	9.00e-4	-	7.56	0.10

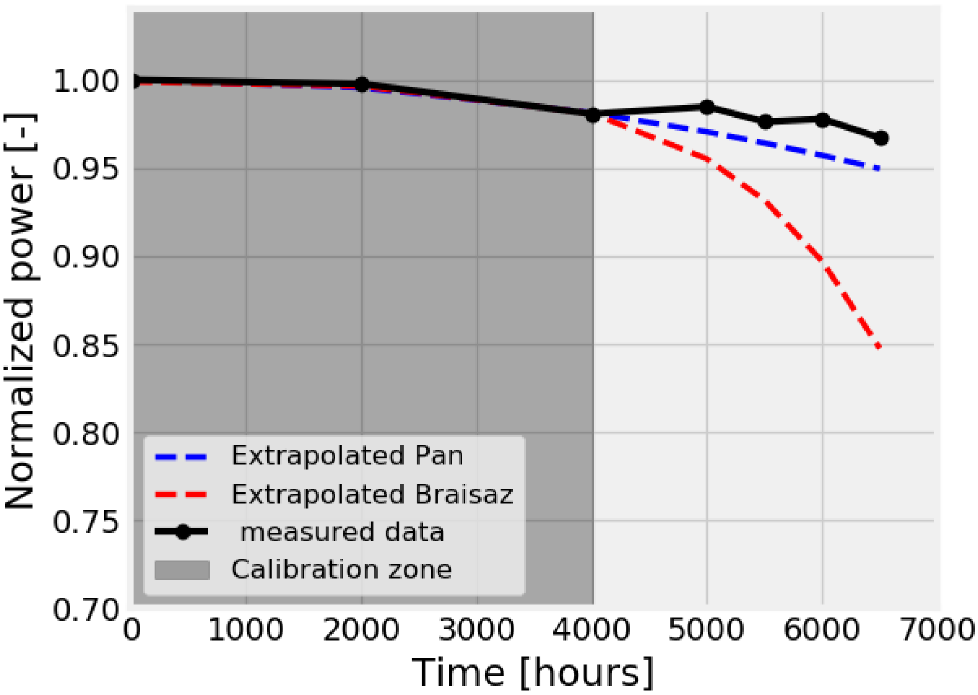

Figure 2.3: Extrapolation after 4000 hours of DH/75C/85%RH using Pan (blue) and Braisaz (red) models

Figure 2.3 shows the extrapolation of power degradation from 4000 hours to 6500 hours using of Pan and Braisaz models. Indeed, it is hard to conclude that a particular model is better than the other as this might highly depend on the degradation shape under evaluation. However, two main conclusions can be drawn:

- A perfectly fitting model does not guarantee good forecasting. This is visible for the case of Braisaz's model, with small residual deviation but instead the model demonstrates the worst performance for this data set.

- Simple extrapolation after a given interval might not be reliable for longer time extrapolation. This is visible in all the models. Indeed, this can be influenced by measurement uncertainties, nature of the degradation pattern and many other factors. Although many researchers use this kind of extrapolation, the reliability of extrapolated performance is questionable and yet an unresolved challenge. Therefore, part of this research focuses on developing methods to improve long-term extrapolation accuracy.

The degradation rates of indicator models (equations 2.1, 2.2 and 2.3 can be calculated as functions of T and RH using three common kinetics models namely; the Peck's model, the Eyring model and the exponential model Escobar and Meeker (2007); Jordan and Kurtz (2010). These models are developed on the primary assumption that the rate of degradation is proportional to the concentration of water in PV modules and that the rate constant has Arrhenius temperature dependence. The models are written as:

(3) Peck's model

$$R_{D.Peck} = A.exp\left(-\frac{E_a}{k_B T}\right) RH^n \tag{2.5}$$

(4) Eyring Model

$$R_{D.Eyring} = A.exp\left(\frac{-E_a}{k_B T} - \frac{b}{RH}\right) \tag{2.6}$$

(5) Exponential model

$$R_{D.Exp} = A.exp\left(\frac{-E_a}{k_B T}\right).exp(m \times RH) \tag{2.7}$$

where A and n, b and m are model parameters. In order to obtain A, E_a, n, b and m in the equations (2.5), (2.6) and (2.7), the equations can be fitted to experimental data or represented on a logarithmic scale by a straight line, using the following equations:

$$ln(R_{D.Peck}) = ln(A) - \left(\frac{E_a}{k_B T}\right) + n \times ln(RH) \tag{2.8}$$

$$ln(R_{D.Eyring}) = ln(A) - \left(\frac{E_a}{k_B T}\right) - \frac{b}{RH} \tag{2.9}$$

$$ln(R_{D.Exp}) = ln(A) - \left(\frac{E_a}{k_B T}\right) + m \times RH \tag{2.10}$$

A plot of $ln(R_D)$ versus $1/T(^0K)$ gives an Arrhenius plot with a slope E_a/k_B and an intercept $ln(A)$.

B. Comparison of Peck's, Eyring and Exponential models

Here we performed a sensitivity analysis of the degradation rate models 2.5, 2.6 and 2.7 to compare how the degradation rate varies with input climatic variables (temperature and humidity). To perform unbiased comparison, all the three models where fitted using the same dataset (in this case DH/75^{o}C/85% RH). Also since the Braizas model was found to have consistent results, it was selected for the calibration. For all the datasets, the model parameter B was keep the same in order to evaluate the same degradation rate. Moreover since the activation energy should be the same in the physical point of view for a similar reaction, it was kept constant for the three models. This is also good for a comparison purpose, given that, this parameter is very sensitive. The extracted models parameters used in the sensitivity analysis simulations are presented in table 2.4.

Figures 2.4, 2.5 and 2.6 show the plots of the sensitivity analysis of the Pecks, Eyring and exponential models respectively. It is clearly visible that despite a uniform calibration procedure, the sensitivity of the model varies to a big extent. This can be explained by the assumptions taken during the models formulation. Although all the models have an Arrhenius temperature dependence, the formulation of the relative humidity contribution changes the variation of the degradation rate. For example, the exponential model, assumes an exponential dependence of the relative humidity and this explain why the model is too sensitive to relative humidity compared to the Pecks and Eyring model. This high sensitivity of relative humidity together with the Arrhenius temperature dependence could deteriorate the model if used for extrapolation. Overall, the Pecks model shows a good dependence of both temperature and relative humidity.

Table 2.4: Derived model parameters used in the sensitivity analysis

Model	A	Parameters (n,b & m)	($\boldsymbol{E_a}$) [eV]	RMSE [%]
Peck	9.46	2.07	0.57	0.39
Eyring	9.97e4	6.01	0.57	0.39
Exponential	3.64e-4	0.23	0.57	0.39

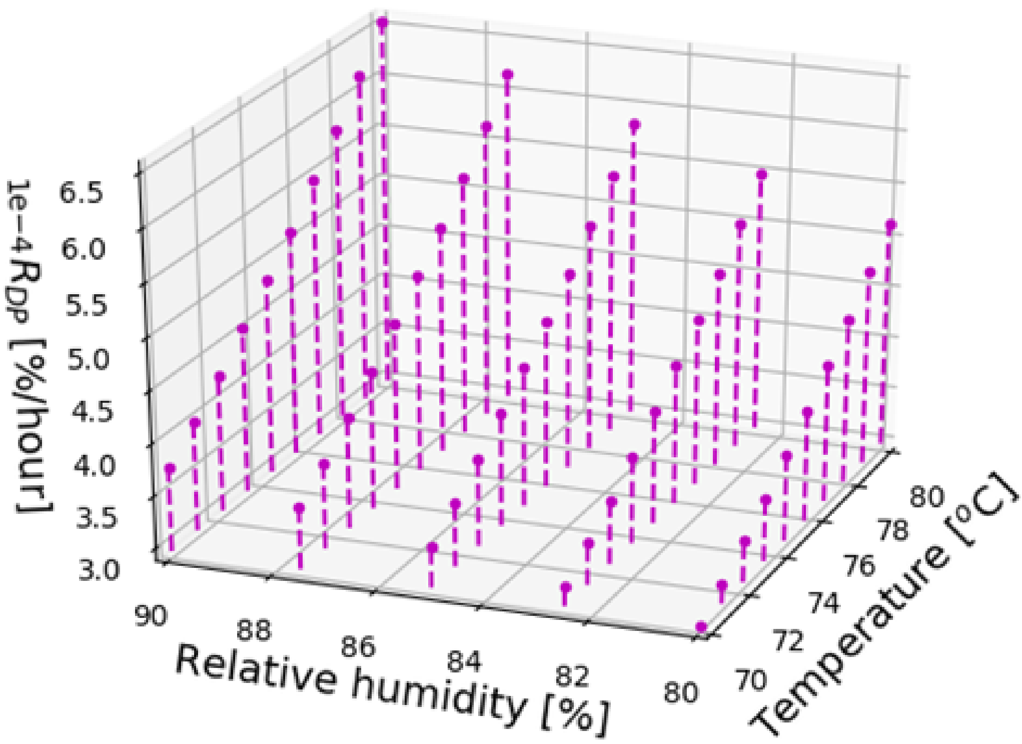

Figure 2.4: Sensitivity analysis plot of the degradation rate with relative humidity and temperature using the Pecks model (note the y axis in multiplied by 1e-4)

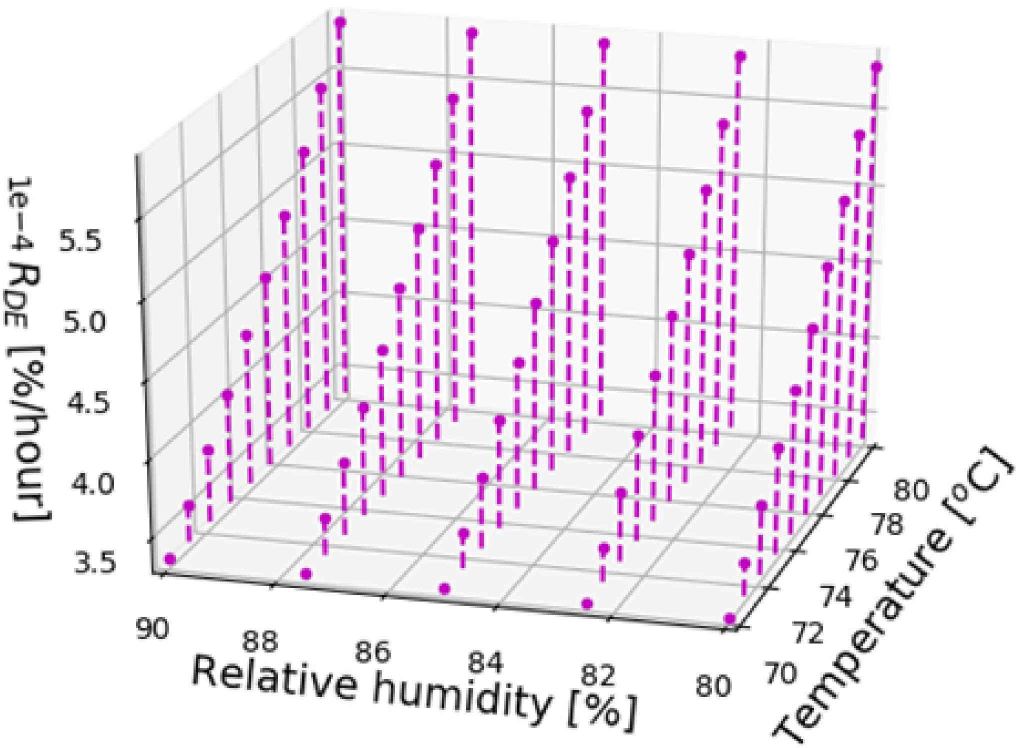

Figure 2.5: Sensitivity analysis plot of the degradation rate with relative humidity and temperature using the Eyring model (note the y axis in multiplied by 1e-4)

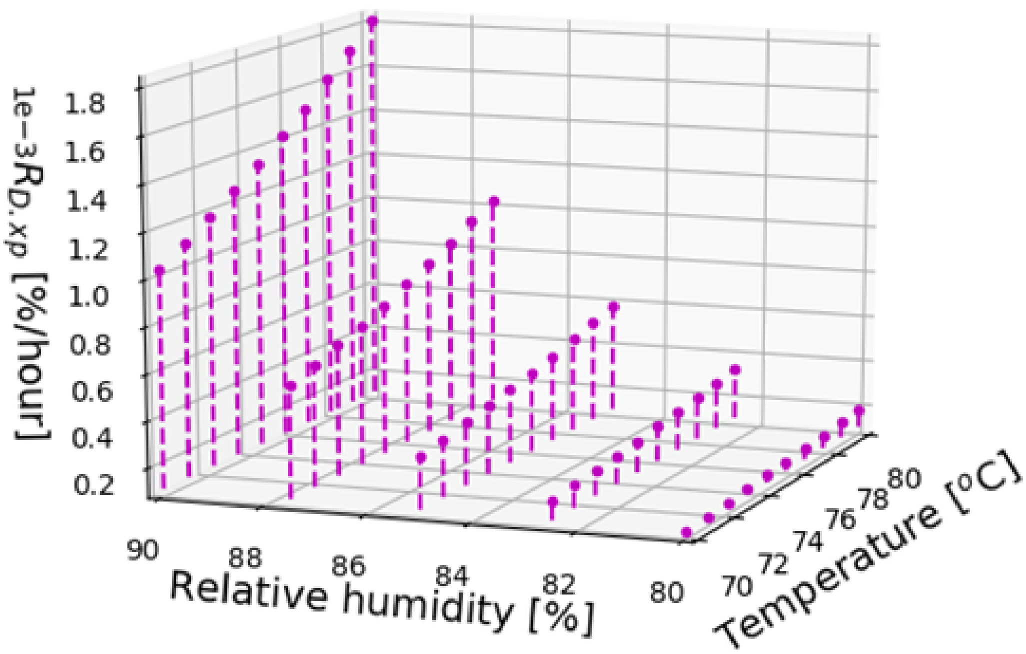

Figure 2.6: Sensitivity analysis plot of the degradation rate with relative humidity and temperature using the exponential model (note the y axis in multiplied by 1e-3)

2.3.2 Models for potential induced degradation

Potential induced degradation (PID) has been observed in all PV technologies and in almost all operating climates. It does not occur so frequently, but if it does, its effect can lead to a dramatic performance loss within a short period Moser et al. (2017); Hacke et al. (2016, 2015); Köntges et al. (2014). In general terms, PID is caused by the difference in potential between the cells and the support structure of the module. This difference drives a leakage current that can lead to power degradation. Different types of PID occur depending on the module technology. For crystalline silicon PV, two degradation modes can be identified, PID-p (for polarisation or passivation) and PID-s (for shunting). PID-p is a temporary and reversible degradation of the passivation layer, which reduces the performance due to a surface recombination increase Naumann et al. (2014); Halm et al. (2015); Swanson et al. (2005). PID-s is due to a leakage current involving an ionic flow of sodium ions (Na+) from the glass, encapsulant or cell surface into the cell, diffusing into the silicon stacking faults and shunting the cell Lausch et al. (2014). The sodium incorporation in the silicon surface degrades primarily the fill factor (FF) , the open circuit voltage (V_{oc}), and lastly the short circuit current (I_{sc}). The relevant stress factors for PID-s include Köntges et al. (2014): high temperature, relative humidity, system voltage, light, bias-junction potential and injected carriers.

Different authors Braisaz et al. (2014); Hacke et al. (2015); Annigoni et al. (2017); Hacke et al. (2016); Hattendorf et al. (2012); Taubitz et al. (2014) have proposed models to evaluate PID degradation patterns using different indicators as;

(6) PIDHACKE model

$$\frac{P_{max}}{P_{max(0)}} = 1 - A.exp\left(-\frac{E_a}{k_B T}\right) RH^n \times t^2 \tag{2.11}$$

A parabolic model was proposed by Hacke et al. (2015) to fit the power degradation of c-Si modules. The constants A and n are determined by fitting the equation to experimental results. The parameters have to be determined for each module type. This parabolic model is applicable to the beginning of the degradation phases of PID-s, as it can fit the beginning of a sigmoid and does not describe the stabilization phase of the sigmoidal curve.

(7) PID model according to Annigoni et al. (2017)

$$\frac{P_{max}}{P_{max(0)}} = 1 - A.exp\left(-\frac{E_a}{k_B T}\right) RH^n \times t^2 \times U \tag{2.12}$$

Annigoni et al. (2017) re-wrote the PIDHACKE model (2.11) including a voltage term (U) (2.12) and used the indoor data to determine coefficients of the model for distinct aging contributions (temperature, relative humidity and time) and then applied the model (2.12) to outdoor PID degradation for different climates.

(8) Hattendorf model

$$P_{max}(U,T,RH,t) = P_{max(0)}(1 - P(t)) \tag{2.13}$$

$$P(t) = P_\infty \frac{1 - exp\left(\frac{t}{\tau_1}\right)}{1 - exp\left(\frac{t - t_0}{\tau_2}\right)} \ ; \ P(U) = \left(1 + exp\left(\frac{U - U_0}{\Phi}\right)\right)^{-2} \tag{2.14}$$

$$t_0 = a \times b \times \hat{t_0}\ ;\ \tau_1(T) = b^2 \times \hat{\tau_1};\ \tau_2 = \hat{\tau_2} \tag{2.15}$$

$$a(H) = \frac{H_0}{H}\ ;\ b(T) = exp\Big(\frac{T - T_0}{\phi}\Big) \tag{2.16}$$

The model of Hattendorf et al. (2012) is based on a matrix of indoor experiments where modules are exposed to varying voltage, module temperature and ambient humidity. The conditions are varied to determine the model parameters for the module power. The model includes six adaptation parameters: $\hat{t_0}$, U_0, $\hat{\tau_1}$, $\hat{\tau_2}$, Φ and ϕ. H_0 and T_0 are scaling parameters. The function $P(t)$ describes the power loss caused by degradation. $P_\infty(U)$ is its limit for $t \to \infty$, $a(H)$ and $b(T)$ are the acceleration functions of relative humidity and temperature. For $T = 0$ and $H = 0$, they are equal to 1, therefore $\hat{\tau_1}$, $\hat{\tau_2}$ are the time constants under these conditions. τ_2 remains constant for a given module. To determine the model's parameter, the power degradation is measured as a function of time with the system voltage U as parameter and a fixed humidity H as well as temperature T. The saturating power P_∞ is extracted by fitting $P(t)$ to the measured data.

(9) Taubitz model Taubitz et al. (2014)

Shunting phase

$$R_{sh}(t) = a_S exp\Big(\frac{-t}{b_S(t)}\Big) \tag{2.17}$$

Regeneration phase

$$R_{sh}(t) = C_R + a_R exp\Big(\frac{t}{b_R(t)}\Big) \tag{2.18}$$

Transition phase

$$R_{sh}(t) = a_T(T)(t + b_T(T))^2 + C_T \tag{2.19}$$

Taubitz et al. (2014) proposed a regeneration model for shunt resistance evolution over time due to PID degradation. The shunt resistance was modeled in three phases; shunting phase, regeneration phase and transition phase. Where a_S, b_S, C_T, b_T, $a_T(T)$, $b_S(T)$, $b_T(T)$, C_R and a_R are constants and have to be determined for a specific module type. Some of them are dependent on the module temperature T. The constants are determined by measuring the times t_S, t_T, and t_R for reaching certain target values.

(10) PID model according to Braisaz et al. (2014)

$$R_{sh}(t) = \frac{R_{sh(0)}}{1 + aR_D t} \tag{2.20}$$

$$R_D = A \times U \frac{B}{1 + exp(-C(RH) + D)} exp\Big(-\frac{E_a}{k_B T}\Big) \tag{2.21}$$

The model is based on shunt resistance R_{sh} degradation as an indicator, as it is the most important parameter for PID. The evolution of R_{sh} as a function of voltage, temperature and relative humidity was modeled as (2.20). Where R_{sh} is the shunt resistance at time (t), $R_{sh(0)}$ is the initial shunt resistance, A,B,C and D are model coefficients, U is the applied voltage and R_D is the degradation rate dependent on RH, U and T.

2.3.3 Models for ultraviolet irradiance degradation

Ultraviolet (UV) light exposure has been reported to cause PV module degradation in a number of ways. As an example, it could result in discoloration of the encapsulant material Dunn et al. (2013), delamination at the glass encapsulant or cell encapsulant interface Munoz et al. (2011). The parameter most impacted by UV exposure is the short circuit current (I_{sc}). Braisaz et al. (2014) proposed a model for short circuit degradation due to UV exposure over time. They found that the degradation curve is not linear but an exponentially decreasing curve. The short circuit is modeled as a function of UV as:

(11) UV model according to Braisaz et al. (2014)

$$I_{sc}(t) = I_{sc(0)} - aD_{UV}(t) - b(1 - exp(-CD_{UV})(t)) \tag{2.22}$$

$$D_{UV}(t) = \int_0^t E(u) \times 5.5\% \, \mathrm{d}u \tag{2.23}$$

Here, D_{UV} is the UV dose in in MJ/m^2 or kWh/m^2, I_{sc} is the short circuit current at time (t), $I_{sc}(0)$ is the initial short circuit current and a, b and C are model coefficients. The multiplication by 5.5% is due to the UV radiation between (280nm – 400nm) which is approximately 5.5% of the total light spectrum $E(u)$ Koehl et al. (2009).

(12) The Schwarzschild Law

$$k = A(I)^p \tag{2.24}$$

The Schwarzschild law has been applied by Gu et al. (2015) to study the effect of intensity and wavelength of spectral UV light on discoloration of laminated glass/EVA/PPE PV modules. Here, k is a constant, I the intensity and p is the Schwarzschild coefficient.
Recommendation: When applying this expression in performance (power) prediction models where other loads are also applied, the parameter p must be calibrated according to the knowledge of severity ranking Jordan et al. (2017a).

2.3.4 Degradation models for delamination, fatigue solder failure and cell cracks

(13) Coffin-Manson's equation

$$N = \frac{\sigma}{(\Delta T)^{\beta_1}} \tag{2.25}$$

The model is used to predict degradation modes caused by temperature cycling such as encapsulant delamination, fatigue solder failure and cell cracks. According to Escobar and Meeker (2007), the model describes the number of cycles to failure as (2.25), where ΔT is the temperature range, σ and β_1 are properties of the material and test setup. The cycles-to-failure distribution for temperature cycling can also depend on the cycling rate (e.g. due to heat buildup). An empirical extension of the Coffin-Manson relationship that describes such dependencies is Escobar and Meeker (2007):

$$N = \frac{\sigma}{(\Delta T)^{\beta_1}} \frac{1}{(freq)^{\beta_2}} exp\left(\frac{E_a \times 11605}{T_{max}(K)}\right) \tag{2.26}$$

where $freq$ is the cycling frequency and E_a is a quasi-activation energy.

(14) Crack propagation model

$$C_a(t) = C_a(t-1) + \frac{1}{x\left(\frac{125}{T_a}\right)^m} \tag{2.27}$$

The model was suggested by Braisaz et al. (2014) and it was applied to simulate the degradation of the short-circuit current I_{sc} due to the expansion of cell cracks caused by temperature. $C_a(t)$ is the crack activation at time (t), $C_a(t-1)$ the crack activation at time $(t-1)$, T_a is the daily temperature amplitude, m a model parameter and x is the number of thermal cycles. The crack activation/propagation model is dependent on the daily temperature amplitude T_a.

(15) Damage accumulation model

$$D = C(\Delta T)^n (r(T))^m .exp\left(-\frac{Q}{k_B T_{max}}\right) \tag{2.28}$$

The model was used by Bosco et al. (2016) in order to calculate the solder fatigue damage in seven cities investigated in their study and compared to FEM simulated results. They found out that the model fits well to the simulated calculations. In this equation, ΔT is the mean daily maximum cell temperature change, T_{max} the mean maximum daily temperature, C a scaling constant, Q the activation energy, k_B Boltzmann's constant, $r(T)$ the number of times the temperature history increases or decreases across the reversal temperature, T the period of a year and n & m are model constants similar to those in the Coffin-Manson equation.

(16) Backsheet degradation rate model

$$R_D \approx I^X (b + m \times TOW) \times (T_f)^{\frac{T-T_0}{10}} \tag{2.29}$$

Here, I is the light intensity, X, b and m are fit parameters, TOW is the time of wetness, T the temperature, T_0 a reference temperature and T_f is a multiplier for the increase in degradation for a rise in temperature in 10 K steps.

The model is used to estimate a potential form of the degradation kinetics of the backsheet. This model was applied by Kempe (2014) to model the uncertainty in a 25 year equivalent test for module backside exposure to irradiance and temperatures in different climatic zones.

Recommendation: As also mentioned by Kempe, the parameter that describes the effect of time of wetness has very high uncertainties, we recommend careful comparison of the relative change in degradation rate with changes in TOW. In case one wants to extract thermal parameters such as activation energy, the multiplier term (T_f) can be replaced by the Arrhenius term.

2.3.5 Physical models for combined degradation modes/stresses

Since degradation of PV modules in outdoor operation is influenced by multiple environmental stresses, models based on multiple stresses are viable for outdoor service lifetime prediction. In the literature, only a few authors Gaines et al. (1978); Bala Subramaniyan et al. (2018) have proposed models based on the combination of several stresses.

(17) Model of Gaines

$$\frac{P_{max}}{P_{max(0)}} = [1 - R_D t]^{\frac{1}{\beta}} \tag{2.30}$$

$$R_D = A f_T f_{RH} f_M f_G f_\omega \tag{2.31}$$

Gaines et al. (1978) proposed a model for power output degradation based on multiple accelerated environmental stresses (2.30). Where R_D is the degradation rate and the factors f_T, f_{RH}, f_M, f_G and f_ω are associated with a decrease in power output due to effects of temperature (T), relative humidity (RH), mechanical stresses (from temperature differences) (M), gaseous concentration (G) and the frequency of the temperature excursion (ω). The mathematical form of each factor is formulated to represent the underlying physical phenomena.

An Arrhenius form is used for temperature influenced effects:

$$f_T = exp\left(-\frac{B}{T}\right) \tag{2.32}$$

B denotes a constant parameter and T denotes temperature.

The effect of relative humidity f_{RH} is represented by:

$$f_{RH} = 1 + (RH)_0.exp\left(C_0\left(\frac{1}{T_C} - \frac{1}{T_0}\right)\right)^{C-\frac{D}{T}} \tag{2.33}$$

the second term in the bracket corrects the relative humidity as a function of temperature, given a specified relative humidity at T_0. C and D are constant parameters.

The mechanical/temperature excursion factor f_M is represented by:

$$f_M = \left[\frac{exp\left(G_1\left(\frac{1}{T} - \frac{1}{T_b}\right)\right) + exp\left(-G_2\left(\frac{1}{T} - \frac{1}{T_b}\right)\right)}{D_0}\right] \times exp(J\Delta T) \tag{2.34}$$

the first term in the bracket reflects the stresses arising from differences in expansion coefficients of bonded materials. The constants G_1, G_2, D_0 and T_b are chosen to represent the estimated magnitudes of these fatigue effects. The factor $exp(J\Delta T)$ estimates the magnitude of the temperature excursion ΔT, where J is a constant.

The effect of gaseous concentration f_G is represented by:

$$f_G = \left[1 + \frac{G}{G_o}\right]^{E-\frac{F}{T}} \tag{2.35}$$

here, E and F denote constant parameters and T is the temperature.

The frequency of the temperature excursion f_ω is represented by:

$$f_\omega = \left[1 + \frac{\omega}{\omega_o}\right]^{P-\frac{Q}{T}} \tag{2.36}$$

ω is the frequency and P as well as Q are constant parameter. In a constant temperature test, T is a constant and ω is taken to be zero. In the cyclic temperature tests, reciprocal temperature is considered to be a sinusoidal function of time:

$$\frac{1}{T}(t) = \tau + \Delta\tau \sin(\omega t) \tag{2.37}$$

$$\tau = \frac{1}{2}\left[\frac{1}{T_{min}} - \frac{1}{T_{max}}\right] \tag{2.38}$$

T_{min} and T_{max} are the minimum and maximum temperatures associated with the temperature cycles.
Recommendation: The model of Gaines presents the previous approach on multiple stress modeling, however, the user should take caution that this model was developed and applied on PV modules that had a different construction from today's modules. Therefore, its application might need some modification to fit the current PV module construction types.

(18) Degradation rate model of Subramaniyan

$$Rate(T,\Delta T,UV,RH) = \beta_0.exp\left(-\frac{\beta_1}{k_B T_{max}}\right) \times (\Delta T_{daily})^{\beta_2} \times (UV_{daily})^{\beta_3} \times (RH_{daily})^{\beta_4} \tag{2.39}$$

Another model to calculate the degradation rate due to combined environmental stresses has been proposed recently by Bala Subramaniyan et al. (2018). The model takes into account the effect of both static and cyclic temperature, ultraviolet radiation and relative humidity as (2.39). Where $Rate(T,\Delta T,UV,RH)$ is the reaction rate, T_{max} the daily maximum temperature of the module [K], ΔT_{daily} the daily cyclic temperature of the module [K], UV_{daily} the daily daytime average irradiance [W/m^2], RH_{daily} the daily average relative humidity [%] and k is the Boltzmann constant. The model parameters β_0, which is the frequency factor [s^{-1}]; β_1, the activation energy [eV]; β_2, the effect of cyclic temperature; β_3, the effect of UV radiation and β_4, the effect of RH, can be estimated from measured data through data fitting techniques. In their study, the model was calibrated using outdoor measurements and then applied to predict the degradation rates in four other climates.

2.4 Chapter Overview

Based on the reviewed literature, two main aspects/challenges have been identified as;

- Degradation indicator models are developed to fit specific degradation patterns based on a specific degradation mode. A generalized model that can optimize the different degradation patterns is still a challenge. Therefore, in this research we aim to propose a model that can be generalized for different degradation patterns.

- Although several degradation rate models are developed for specific degradation modes for indoor application, little advances are made to develop models for combined climatic stresses that can be used for outdoor prediction. It is clearly seen that the need for such a model dates back in the 1970's however since then it has been of recent that Bala Subramaniyan et al. (2018) added a contribution to this effort. Therefore, further developments for a model that take into account multiple environmental stress factors are proposed in this research.

Chapter 3

Methodology

Table 3.1: Chapter 3 Nomenclatures

Symbols	
c_i	clearness index
E_a	activation energy [eV]
k	degradation factor [1/year]
k_B	Boltzmann constant (8.62×10^{-5}eV/K)
P_{max}	power at maximum power point [W]
R_D	degradation rate [%/hour]
SD_{res}	residual standard deviation
T_{amb}	ambient temperature [^0C]
T_{Dew}	dew point temperature [^0C]
T_m	module temperature [K]
Subscripts	
cal	calibration
h	hydrolysis
p	photo-degradation
t	thermo-mechanical
T	total
Abbreviations	
ΔT	temperature cycles [K]
DH	damp heat
FT	failure time
GHI	global horizontal irradiance
MSEP	mean square error of prediction
NWP	Numerical Weather Predictions
RUL	remaining usefull lifetime
STC	standard test conditions
t	time
UV	Ultraviolet [W/m^2]
WS	wind speed [m/s]
WVP	saturated water vapour pressure

In this chapter, the methodologies for the proposed physical, data-driven and hybrid models are described. The chapter is therefore, divided into three sections, 3.1, 3.2 and

3.3. In section 3.1, the physical model is described, the experimental data used for model calibration and validation as well as the methods used to process the climate data used to simulate the global degradation maps are described. In section 3.2, the data-driven approach is described as well as the experimental data used for model calibration and validation. In section 3.3, we describe how the two methods are linked into a hybrid model. For consistence and to allow the reader to follow, it is better to read section 3.1 with the corresponding results in section 4.1 and section 3.2 together with 4.2 respectively.

3.1 Methodology for the proposed physical model

In chapter 2 further development of a physical degradation rate model that take into account multiple climatic stress factors as well as a generalized degradation indicator model were identified. In this research, we contribute to these challenges by proposing a new model to quantify the impact of combined climatic stresses as well as a degradation indicator model that can optimize several degradation patterns.

3.1.1 Combined climatic stresses degradation rate model

Photovoltaic modules are exposed to a variety of climatic loads during outdoor operation. Over time, these loads trigger a number of degradation modes within the modules leading to performance loss. In section, an approach to develop a combined climatic stress degradation rate model is described.

A. Background and modelling assumptions

When developing a model for PV modules degradation prediction, three main aspects need to be considered:

- Impact of PV materials variations. New materials are proposed frequently to improve PV performance.
- The different operating climatic conditions. PV modules operate in different climates for example in arid, maritime, tropical climates.
- The different PV technologies, for example: crystalline silicon, thin films, and different module designs like bifacial, glass-glass or glass-backsheet.

However, a model that takes into account all the three aspects is rather complex and might require an extensive experimental campaign which in turn makes it expensive. Moreover the fact that, materials are changing frequently makes developing a generalized model a challenging problem. In this regard, several assumptions and simplification have to be used. In developing our model, the following assumptions are used.

- The degradation rates are assumed to be proportional to the applied stresses and to have an Arrhenius temperature dependence. Therefore, the material dependence of the model is evaluated through the activation energy.
- Three degradation processes are assumed to be necessary for service lifetime prediction as; hydrolysis, photodegradation, and thermomechanical degradation. The assumption is based on the ability to reproduce these degradation mechanism in the

laboratory using accelerated ageing tests and that, the underlying physical and(or) chemical degradation kinetics have been studied from different studies Zhu et al. (2016); Kempe (2006); Sharma and Chandel (2013); Ndiaye et al. (2013); Gok et al. (2017); Jordan and Kurtz (2013); Marín et al. (1996); Park et al. (2013); Wu et al. (2014); Koehl et al. (2017) .

Empirical kinetics models to evaluate the degradation rate constant are proposed or selected to describe the three degradation processes. These models are developed depending on the applied climatic stresses as illustrated using the general reaction equation below:

$$Stress1 + Stress2 + ...StressN \rightarrow Degradation\ precursor \tag{3.1}$$

where $Stress1$, $Stress2$, $...StressN$ are the (climatic) degradation factors triggering the degradation mechanism under evaluation. The kinetics of the dominating degradation process is quantified as the degradation rate (R_D). The mathematical form of the degradation rates of the three degradation processes is described in the following sections.

- The three processes are described based on combinations of input climatic variables. The combinations are selected based on the current indoor testing procedures Wohlgemuth (2012) which aim to reproduce degradation modes according to three main processes. Therefore, the combination of the input stresses are assumed to be responsible for triggering a specific reaction that might induce specific degradation modes. Figure 3.1 summarizes the hypothesized degradation mechanisms that are known to be induced by the applied loads.
- The effects of the applied loads is quantified on how much they affect the power output of the module, hence power at maximum power point is used as a degradation indicator in this research.

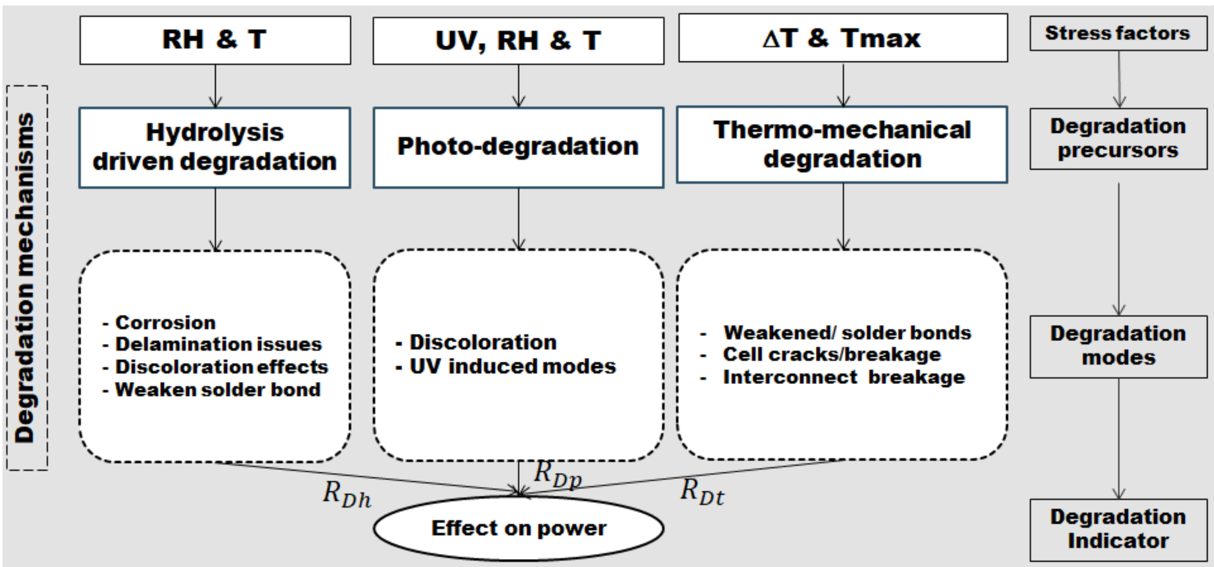

Figure 3.1: Schematic diagram of the modelling hypotheses. The combination of climatic stress triggers the three main precursor processes and the triggered processes are linked to different degradation modes

B. Hydrolysis: Temperature and Relative humidity model

The Peck's model described in chapter 2 equation (2.5) is selected to model the effect of temperature and relative humidity based on the sensitivity analysis study in chapter 2, figure 2.4. The model shows a good dependence of both temperature and relative humidity. The models is hereby re-written as:

$$R_{Dh} = A_h.rh_{eff}^n.exp\left(-\frac{E_{ah}}{k_B T_m}\right) \tag{3.2}$$

$$rh_{eff}(\%) = \frac{100}{1 + 98.exp[-9.4 \times (RH(\%)/100)]} \tag{3.3}$$

where R_{Dh} is the degradation rate constant, k_B is the Boltzmann constant $(8.62 \times 10^{-5} eV)$, T_m is the module temperature (Kelvin), A_h is the pre-exponential constant, rh_{eff} (%) is the effective module relative humidity proposed by Koehl et al. (2012), n is a model parameter that indicates the impact of relative humidity on power degradation. In this context, E_{ah} is defined as the activation energy for power degradation due to hydrolysis process.

C. Photo-degradation: UV, temperature and relative humidity model

The formulation of photo-degradation has been developed to take into account the combined effects of UV stress and moisture on PV modules. The baseline line assumption is that, UV stress alone would influence some degradation modes but also some modes might be influenced with a combined UV moisture stresses. For example, Ngo et al. (2016) has demonstrated that, UV irradiation plays a significant role in generating acetic acid with the presence of relative humidity that causes the power degradation of PV modules. Therefore to take into account the effect of UV alone and the combined UV-moisture contributions a model is proposed as:

$$R_{Dp} = A_h.UV^X.rh_{eff}^n.exp\left(-\frac{E_{ap}}{k_B T_m}\right) + A_h.UV_{dose}^X.exp\left(-\frac{E_{ap}}{k_B T_m}\right) \tag{3.4}$$

OR

$$R_{Dp} = A_h.UV^X(1 + rh_{eff}^n).exp\left(-\frac{E_{ap}}{k_B T_m}\right) \tag{3.5}$$

where R_{Dp} is the rate due to photo-degradation processes, UV is the UV irradiance (W/m^2), X is a model parameter that indicates the impact of UV on power degradation and E_{ap} is the activation energy for power degradation due to photo-degradation process.

D. Thermo-mechanical degradation: $Tmax$, & ΔT

The model used to quantify the effects of thermo-mechanical stresses is the modified Coffin-Mansion relationship that includes the effect of maximum temperature according to Escobar and Meeker (2007). The modified model is re-written as;

$$R_{Dt} = A_t.C_N.(273 + \Delta T)^{\Theta}.exp\left(-\frac{E_{at}}{k_B T_{max}}\right) \tag{3.6}$$

where $\Delta T = (T_{max} - T_{min})$ is the temperature difference (Kelvin), C_N is the cycling rate, T_{max} and T_{min} are the module maximum and minimum temperatures, E_{at} the activation energy of power degradation due to thermo-mechanical process.

E. Combined ($RH, T, UV\ Tmax$ & ΔT) model

The transition from indoor degradation rate evaluation to outdoor is a challenging task as the interaction of different stresses and processes leading to PV degradation is not well known. The underlying assumption deployed in this research is that: some degradation processes might lead to specific degradation modes independent of the others and that some might have a synergistic nature as described in the schematic figure 3.2, which results in a variety of degradation modes.

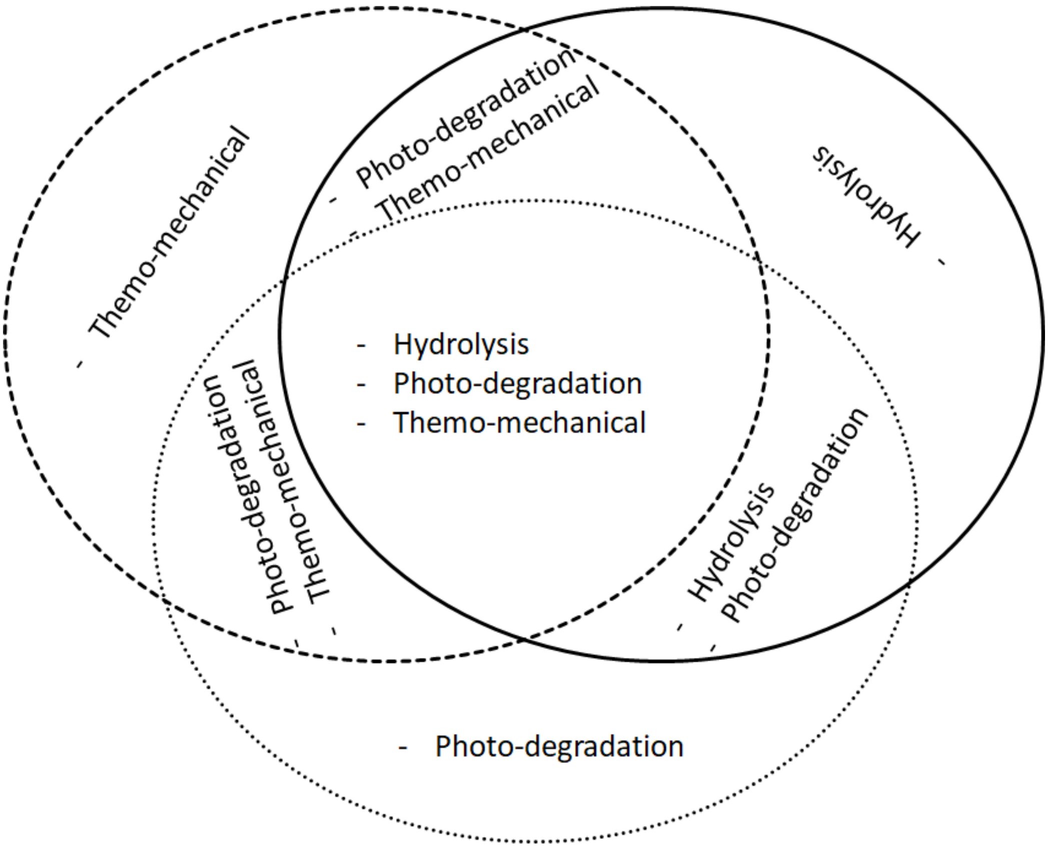

Figure 3.2: Schematic showing possible interactions of the three degradation processes

Hence, this assumption allows us to evaluate the total degradation rate as the sum of both independent and dependent processes. The mathematical form of the total rate is expressed as:

$$R_{DT} = A_N(R_{Dh} + R_{Dp} + R_{Dt} + R_{Dh}.R_{Dp} + R_{Dh}.R_{Dt} + R_{Dp}.R_{Dp} + R_{Dh}.R_{Dp}.R_{Dt}) \tag{3.7}$$

OR

$$R_{DT} = A_N(1 + R_{Dh})(1 + R_{Dp})(1 + R_{Dt}) - 1 \tag{3.8}$$

OR

$$R_{DT} = A_N.\prod_{i=1}^{n}(1 + R_{Di}) - 1 \tag{3.9}$$

where R_{DT} (%/year) is the total degradation rate, R_{Di} is the i^{th} rate constant and n is the total number of degradation processes. A_N is the normalization constant of the physical quantities, in this case it takes the units ($year^{-2}\%$).

3.1.2 Degradation indicator model

As already mentioned in chapter 2, different electrical parameters such as: P_{max}, I_{SC}, R_{sh} and R_s are commonly modeled as degradation indicators to quantify the effects of the applied stresses. In this study, P_{max} is considered as the degradation indicator. The reasons to use P_{max} as an indicator are: it is easily calculated from the current-voltage (I-U) curves unlike R_{sh} and R_s that are derived from fitting procedure of the illuminated I-U curve with diode equations. Moreover, it's a parameter needed for energy yield evaluation and a metric used by manufacturers to give warranties.

A. Proposed power degradation model

Usually a linear-shaped power loss is assumed for outdoors degradation analysis and lifetime predictions. However, as reported by Jordan et al. (2017b), non-linearity of power loss is often observed in the field depending on the modules technologies or degradation modes. In their study, the effect of the different degradation curves, observed (approximately) in field performance on the levelized cost of energy (LCOE) was quantified using Monte Carlo simulation. Köntges et al. (2014) also reported that, the loss in power can take different shapes, for example the following categories: exponential-shaped, linear-shaped, steps degradation and saturating power loss over time. A simplified non-linear power degradation model that can optimize most these degradation shapes has been proposed as;

$$\frac{P(t=t)}{P_{Initial}} = 1 - exp\left(-\left(\frac{\Gamma}{R_{Di}.t}\right)^{\mu}\right) \tag{3.10}$$

where $P(t=t)$ and $P_{Initial}$ are the module output power at time t and the initial output power, respectively. Γ is the power susceptibility, which is assumed to be a material property, μ is the shape parameter and R_{Di} is the degradation rate constant of degradation process i or the total degradation rate.

B. Failure time function

The failure time (FT) is defined in this study as a 20% loss of the nominal power (common manufacturer's warranty). Using equations (3.8) and 3.10, the failure time can be derived as:

$$FT = \frac{\Gamma}{R_{DT}.(|log(0.2)|)^{\frac{1}{\mu}}} \tag{3.11}$$

3.1.3 Experimental part

In order to calibrate and valid the models, two sets of experiments where carried out; first using indoor accelerated ageing tests and second, using outdoor monitoring tests.

A. Experimental: Indoor accelerated aging

Distributed damp heat (DH), thermal cycling (TC) and combined DH-UV stress tests were carried out at different test conditions as shown in 3.2. The condition are varied because one set is used for model calibration and the other set is used for model validation. Table 3.3 shows the time steps and the measured power degradation at the different applied test conditions. The tested modules are from the same manufacturer with p-type homo-junction crystalline silicon (c-Si) cells, with a thermoplastic encapsulant material and no aluminum layer as additional moisture barrier.

Table 3.2: Experimental conditions for DH, combined UV/DH and TC tests

	Test conditions	
Experimental	Test conditions for model calibration	Test conditions for model validation
DH	$75^0C/85\%RH$ (6500 hours)	$85^0C/85\%RH$ (6500 hours)
UV/DH	$180W/m^2/65^0C/55\%RH$ (4000 hours)	$180W/m^2/85^0C/55\%RH$ (4000 hours)
TC	$-40^0C/40^0C$ (3500 cycles)	$-40^0C/85^0C$ (1200 cycles)

Table 3.3: Time steps and measured power degradation at different test conditions

DH: $75^0C/85\%RH$										
Time steps[hours]	0	2000	4000	5000	5500	6000	6500			
Normalized power	1.000	0.991	0.967	0.993	0.986	0.990	0.987			
DH: $85^0C/85\%RH$										
Time steps[hours]	0	500	1000	1500	2000	2500	3000	3500	4000	
Normalized power	1.000	1.000	0.995	0.991	0.991	0.983	0.977	0.953	0.944	
UV/DH: $180W/m^2/65^0C/55\%RH$										
Time steps[hours]	0	2000	2500	3000	3500	4000				
Normalized power	1.00	0.976	0.972	0.964	0.953	0.945				
UV/DH: $180W/m^2/85^0C/55\%RH$										
Time steps[hours]	0	2000	2500	3000	3500	4000				
Normalized power	1.00	0.984	0.960	0.928	0.872	0.845				
TC: $-40^0C/40^0C$										
Cycle steps	0	2000	2010	2050	2100	2600	3000	3200	3400	3600
Normalized power	1.00	0.979	0.978	0.975	0.976	0.926	0.968	0.972	0.975	0.960
TC: $-40^0C/85^0C$										
Cycle steps	0	200	400	600	800	1000	1200			
Normalized power	1.00	0.965	0.957	0.941	0.937	0.920	0.888			

B. Experimental: Outdoor monitoring

To clearly assess the effect of combined climatic stresses on performance degradation, three identical experimental mono-crystalline silicon (mc-Si) modules are exposed and under monitoring in three climatic zones, maritime in Gran Canaria, Spain; arid in Negev, Israel; and alpine in Zugspitze, Germany (see Figure 3.3). At each test site, the electrical performances and climatic conditions are under monitoring at high time-resolution. In Gran Canaria, the tilt angle is 23^0, and the azimuth angle is 169^0 of PV modules. In the Negev the tilt angle is 31^0, and the azimuth angle 180^0 for PV modules. The module in Gran Canaria has been exposed for over 7 years and the ones in Negev as well as in Zugspitze have been exposed over 5 years. A more detailed descriptions focusing on the test sites and categorization of weathering stresses for PV modules in Koehl et al. (2011, 2018). Apart from the electrical performance measurements, the modules temperatures are also recorded every 10 minutes. The sensors for measuring modules temperatures are located under one of the central cells. They are Pt100 sensors, which are attached from the back using adhesive aluminum tapes. Other meteorological data such as: relative humidity, global irradiation, UV irradiance and wind speed are also under monitoring in all the three zones with a one minute resolution. Figure 3.4 shows the temperature distribution

Figure 3.3: The outdoor test facilities: Alpine: Zugspitze, Germany; Desert: Negev, Israel; and Maritime: Gran Canaria, Spain.

in the three locations, the annual averages of UV dose and RH as well as the performance measurements of (P_{max}).

C. Data processing of the three location

An irradiance filter between (800-1200 W/m^2) is used for all locations and the power is corrected to standard test conditions (STC) of irradiance. The irradiance bin ensures that only clear sky conditions were considered in order to have irradiance conditions near to STC and to model a common situation for all the climates. The temperature filter applied varied from location to location depending on the most frequent temperature that a module experiences over its lifetime in each location (see figure 3.4. Forexample a temperature filter between (30^{0}C-35^{0}C) is used for Gran Canaria, (35^{0}C-45^{0}C) for negev and (5^{0}C-25^{0}C) for Zugspitze. To make sure that the power degradation observed for outdoor modules are not due to soiling effects, periodic cleaning of the modules is done. To avoid seasonal effects in climatic variables evaluation, five years data is averaged to calculate the models input values (see table 3.4). Indeed, this ensures that, the values used in degradation prediction correspond to what a module will experience during its lifetime. The mean value of the module minimum and maximum temperature has been computed considering upper and lower temperature bins as in figure 3.4 C. This also ensures that extreme values corresponding to measurement anomalies are not used in degradation rates calculations.

3.1.4 Global climate data processing

The studies over large geographical regions can be made by processing global gridded data estimated from NWP including satellite or reanalysis models Urraca et al. (2018). Even

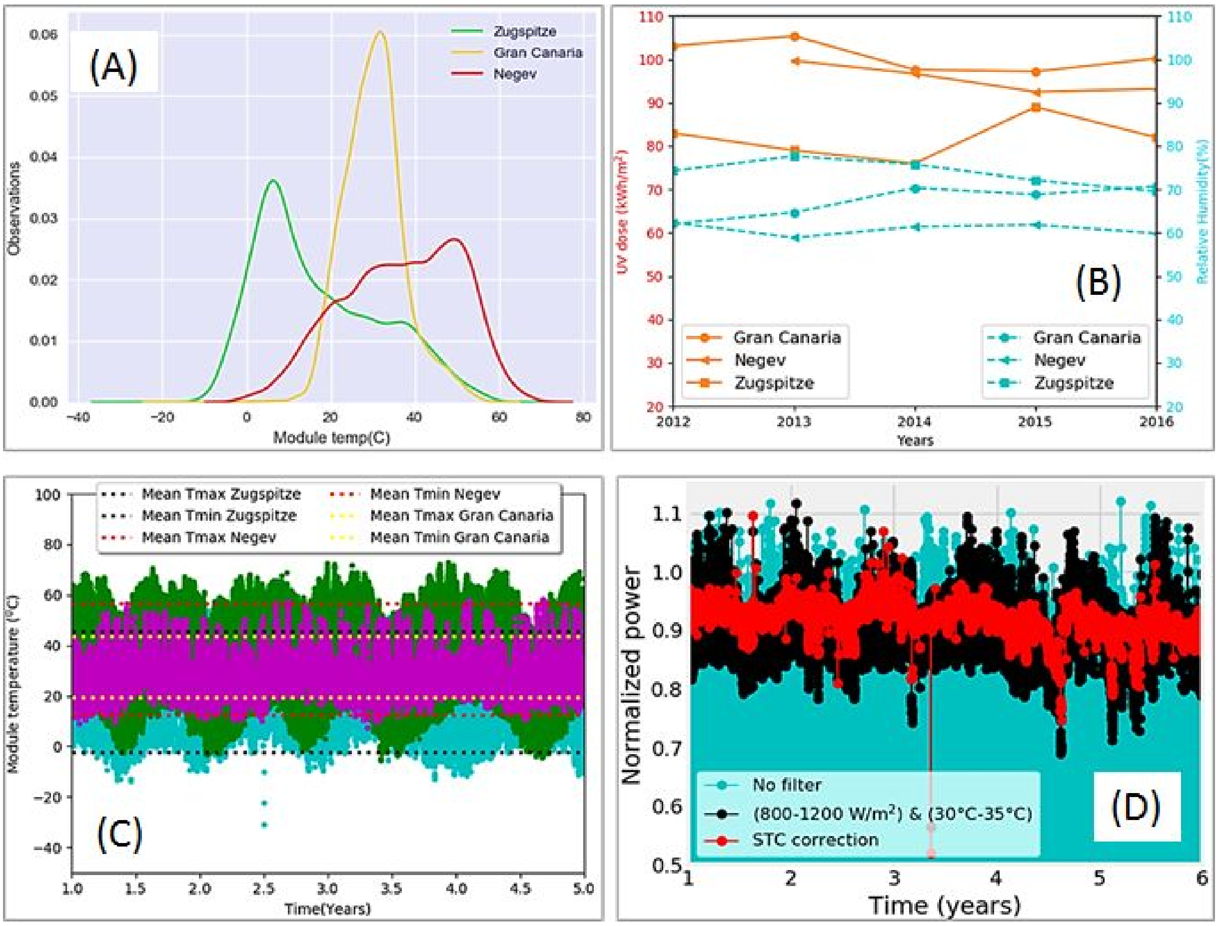

Figure 3.4: (A): Distribution of module temperature in the three climatic zones. (B): Total UV dose and average annual relative humidity for the three zones measured for 5 years. (C) : Ten minutes values of module temperature for 5 years. The dotted lines show the mean maximum and minimum temperatures. (D) : Raw and filtered power measurements in Gran Canaria, Spain. In cyan is the power raw data (before applying filters), in black is the data after applying the irradiance and temperature filters and in red is the data after STC correction.

Table 3.4: Summary of 5 years average climatic inputs used in simulation.

	Input parameters				
Location	RH [%]	T_m [^0C]	UV [kWh/m^2]	T_{max} [^0C]	T_{min} [^0C]
Negev	61.0	36.8	87.7	56.7	12.7
Canaria	68.0	30.6	101.0	43.6	19.6
Zugspitze	74.0	18.7	81.0	44.7	-2.30

though satellite-based estimations can be more accurate than the reanalysis-based ones, the advantage of the second is the possibility to extract all the essential variables together in the same data-set, without gaps and identical timestamps.

In this research, the ERA5 climate reanalysis data-set (C3S) (2017) was processed to extract and model the climatic stresses necessary for the degradation rate evaluation. This dataset provides a spatial resolution of 31 km and temporal resolution of hourly data from 1979. The estimated climate data is compared and validated with real ground measurements taken from the World Radiation Monitoring Centre - Baseline Surface Radiation Network (WRMC-BSRN) Driemel et al. (2018) (the validation procedure is described in the annex). Although not all variables required are directly available from the ERA5, we calculate the missing local climate variables, WS, RH and UV irradiance from existing models as described below. The derived maps are presented in the annex.

A. Evaluation of relative humidity

The relative humidity is not extracted directly from ERA5, so it is estimated using equations 3.12 and 3.13. The saturation water vapour pressure (WVP) over water and ice is calculated using the Buck's formula Buck (1981) from the dew point temperature (T_{Dew}) and ambient temperature (T_{amb}):

$$WVP(T)[kpa] = \begin{cases} 0.61115.exp\left(23.036\frac{T}{333.70}\right).\left(\frac{T}{279.82+T}\right) & for \;\; T<0 \\ 0.61115.exp\left(18.678\frac{T}{234.84}\right).\left(\frac{T}{257.14+T}\right) & for \;\; T\geq 0 \end{cases} \tag{3.12}$$

$$RH[\%] = \frac{WVP(T_{Dew})}{WVP(T_{amb})}.100[\%] \tag{3.13}$$

B. Evaluation of UV

Regarding the UV irradiation, although this variable is included in the ERA5 dataset, it considers a wavelength-range up to 440 nm. In our case, the effective UV irradiance covers up to 400 nm, since that is a typical average value where encapsulates change the transmittance properties Miller et al. (2015). For this reason, we neglect the UV irradiance given by ERA5, and model it using a formula proposed by Crommelynck and Joukoff (1990) as expressed in equations 3.14-3.17. It is based on the clearness index (c_i) and the global horizontal irradiance (GHI). The c_i is calculated by dividing the GHI and the top-of-atmosphere irradiance extracted from ERA5. Unfortunately, the lack of valid measurements disallows us to do a benchmarking of UV models.

$$c_i = max(0.1, min(c_i, 0.7)) \tag{3.14}$$

$$UV_B = (1.897 - 0.860.c_i).1e^{-3}.GHI \tag{3.15}$$

$$UV_A = (7.210 - 2.365.c_i).1e^{-2}.GHI \tag{3.16}$$

$$UV = UV_A + UV_B \tag{3.17}$$

C. Evaluation of wind speed (WS)

The WS is a parameter of interest in this study because it is used to estimate the PV module temperature (T_m) due to the related cooling effect of materials. The WS is calculated and height corrected according to equation 3.18 and equation 3.19 Huld and Amillo (2015), where $\hat{u}_{wind}$ and $\hat{v}_{wind}$ are the vector components of the wind, h_{ERA} is the height from ground which the wind is modelled in the ERA5 dataset, and h_{ERA} is the assumed height of the PV modules equal to 2 meters. The 2 meters height assumed are in accordance with the height of modelled ambient temperature (T_{amb}) and dew point temperature (T_{Dew}) given by ECMWF.

$$WS_{ERA} = \sqrt{\hat{u}^2_{wind} + \hat{v}^2_{wind}} \tag{3.18}$$

$$WS = \left(\frac{h_{mod}}{h_{ERA}}\right)^{0.2} . WS_{ERA} \tag{3.19}$$

D. Modelling module temperature

The module temperature is the most effective parameter in degradation rate evaluation, since the rate models are built on the assumption that, the degradation follows an Arrhenius temperature dependence . In most cases, the module temperature is estimated from, ambient conditions of temperature, irradiance and wind speed using a number of different models proposed by Kratochvil et al. (2004), Segado et al. (2015), Faiman (2008). In this research the Faiman model (equation 3.20) is selected for module temperature evaluation because it has been reported that, it provides a good accuracy under different climate conditions for crystalline silicon PV modules Faiman (2008); Schwingshackl et al. (2013) The model estimate the PV module temperature as a function of the GHI, WS and T_{amb} as:

$$T_m = T_{amb} + \frac{GHI}{u_0 + u_1 . WS} \tag{3.20}$$

where u_0 is a coefficient describing the effect of the radiation on the module temperature $(W/^0Cm^2)$ and u_1 describes the cooling by the wind $(Ws/^0Cm^2)$. In this research, the values of u_0 = 26.9 $(W/^0Cm^2)$ and u_1 = 6.2 $(Ws/^0Cm^3)$ according to Huld and Amillo (2015). The presented calculations consider an open-rack flat mounting configuration for the PV modules at all locations. However, the installation over rooftops or any other surface and the re-positioning can increase the thermal stress due to higher reception of photons from the sun or more circulation of air.

3.1.5 Statistical error analysis methods

To analyse how well a set of data points fit with a given model, the residual standard deviation as a measure of a goodness-of-fit is used. Given that,

$$Residual = Y_m - Y_f \tag{3.21}$$

The residual standard deviation (SD_{res}) is expressed as:

$$SD_{res} = \sqrt{\frac{\sum(Y_m - Y_f)^2}{n-2}} \tag{3.22}$$

where Y_m measured value, Y_f fitted value and n number of data points.

To check the prediction accuracy and to evaluate the uncertainties of the model, the percentage mean square error of prediction (MSEP) is used according to McKay et al. (1999) as:

$$MSEP = 100 \times \left[V[P_p] + \left(\mu_{pp} - \mu_{pm}\right)^2\right] \tag{3.23}$$

Where $V[P_P]$ is the variance of predicted power, μ_{pp} and μ_{pm} are the mean of predicted and measured power respectively.

3.2 Methodology for data-driven model

Different from the physical model presented in the previous section, here a data-driven methodology for long-term degradation forecast is described. In this approach, the lifetime forecast is based on the existing degradation history observed in the field and not on the climatic stress factor. The schematic figure 3.5 summarises the methodology.

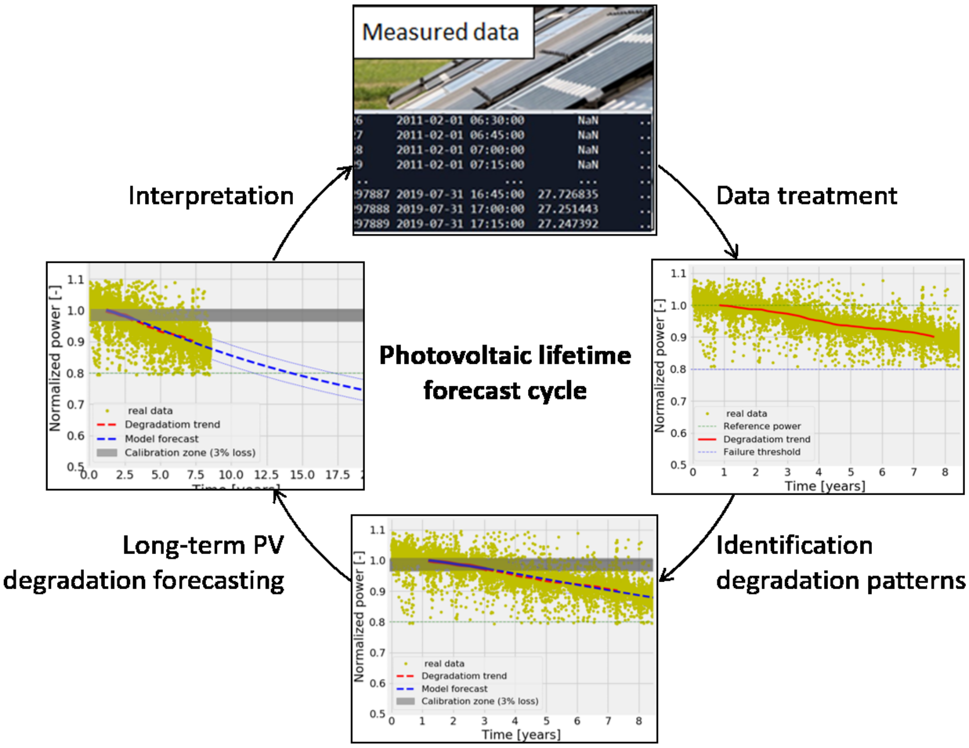

Figure 3.5: Illustration of the overall objective of the data-driven methodology. The major steps are; data treatment, identification of degradation pattern and selection of the best degradation model for long-term forecast

3.2.1 Background

The ever-growing secondary market of PV systems (that is, the transaction of solar plants ownership) calls for reliable and high quality long-term PV degradation forecasts to mitigate the financial risks. Data-driven techniques that utilize monitored operational data related to system's performance are used in many fields, for example in the aircraft industry Zhang et al. (2018); Listou Ellefsen et al. (2019) to forecast the future trend or the remaining useful lifetime. They are normally applied to complex systems where developing a physical model could be more complex and expensive.

For PV applications, a few authors have proposed data-driven prognosis models to evaluate the remaining useful lifetime of PV modules. For example, Laayouj et.al Laayouj et al. (2016) proposed a smart prognostic method for PV module health degradation and remaining useful lifetime prediction. The model is based on two approaches; the on-line diagnosis and data-driven prognosis. Also, Sheng et al Sheng et al. (2019) proposed an autoregressive moving average model-filtered hidden Markov model to predict the residual life for complex systems with multi-phase degradation. They applied the model to predict the residual life of a specific PV module system. Although both methods are reported to provide good predictions, the biggest drawback of these methods is that their performances are not rigorously validated or analysed with different degradation datasets. Both methods are calibrated, validated and applied based on a single PV module or system dataset. Moreover, for the later, the methodology was applied to simulated performance measurements for its reliability evaluation and residual life prediction. PV modules can exhibit different degradation scenarios Köntges et al. (2014) especially due to different technologies, different failure modes as well as different operating local climates. Therefore, it is very unlikely that a model calibrated and validated on a single dataset can be generalized to apply to other degradation scenarios. In this regard, we propose a model based on a rigorous analysis of degradation data of several PV modules as well as systems of different technologies and installed in different locations. Hence the proposed model is aimed to be generalized to the different degradation scenarios. Also related work is that of Rizzo et.al Rizzo et al. (2018) where an algorithm for lifetime extrapolation, prediction, and estimation was proposed. However, their algorithm is proposed only for emerging PV technologies and for shorter time forecasts.

Generally, in spite of the recognized potential of empirical data-driven techniques for time series forecast, limitations still exist for their application in long-term PV degradation evaluation. Different factors such as outliers in the dataset, seasonal variations and many other reducing factors (e.g. soiling) should be separated from long-term non reversible degradation. The lack of a systematic and flexible approach to select parameters of these techniques and their black-box character limit the understanding and control of their performance. We address this issue by proposing a systematic and flexible approach with adjustable model parameters to evaluate the degradation trend based on the nature of the dataset under evaluation. The proposed method aims to evaluate the irreversible long-term degradation of PV modules as well as systems. To achieve this we propose an iterative algorithm for degradation trends evaluation that allows to separate seasonal variations and other reversible performance reducing effects from irreversible degradation.

Another drawback of the available data-driven techniques is their accuracy when long-term predictions are required after a short time interval and with limited data points. For example, Taylor and Letham Taylor and Letham (2018) performed a comparison of the forecasting accuracy of different statistical models at different time horizons. In their study, most models displayed large uncertainties when applied after shorter time interval. Indeed, the available techniques are based on fitting the available systems degradation data using regression models and then applying a simple extrapolation to forecast the lifetime. However, in practice, the system's degradation history available may be short and incomplete, and a simple extrapolation could lead to large uncertainties hence degrading the reliability of the forecasts. To address this challenge, the proposed model is aimed at improving the long-term forecasting accuracy using a small degradation history and few data points. To achieve this, we propose a new concept using time dependent degradation factor for degradation extrapolation instead of using a simple extrapolation for lifetime forecast. To further improve the accuracy and to have a generalized model, the concept of multiple degradation factor models dependent on degradation patterns is proposed.

3.2.2 Modelling assumptions

To begin with, the concept of the proposed data-driven model is based on the work reported by Jordan et al Jordan et al. (2017), that associating specific degradation and failure modes with specific time series behavior can aid in service life prediction. Based on this understanding, our model is based on analysing time series degradation patterns to extracted different parameters (see Figure. 3.6).

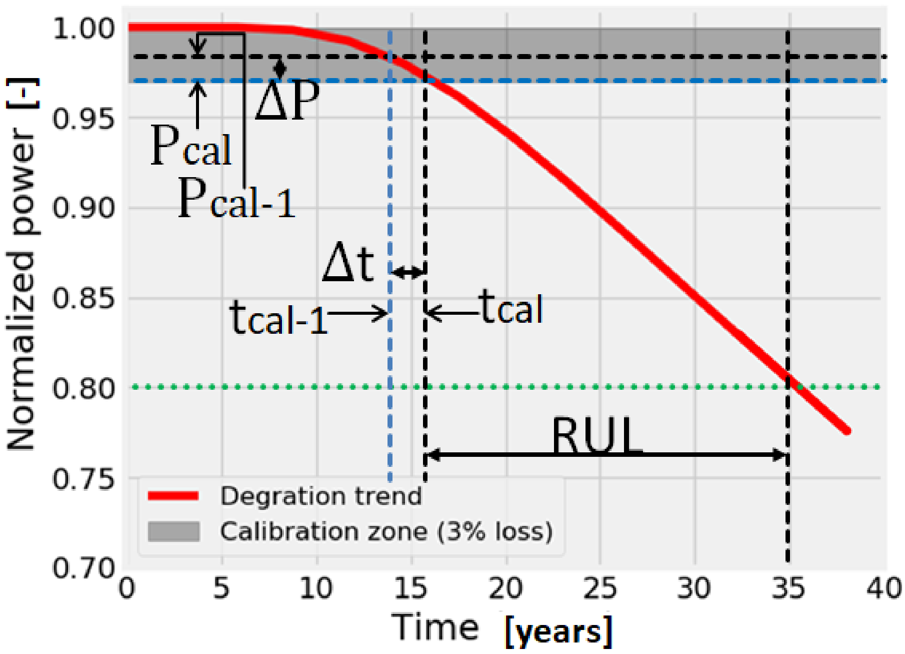

Figure 3.6: Illustration of the different degradation pattern parameters extracted during calibration and the remaining useful lifetime (RUL)

The extracted parameters are then used to formulate degradation rate functions. In developing the model, we also use the following assumptions:

- Different degradation modes might cause differences in degradation patterns meaning that it is unlikely that a single degradation function can represent all expected degradation patterns. Therefore the approach depends on multi-degradation rate functions.

- Some degradation modes might be triggered by other degradation modes and might appear at certain stages of a module's lifetime, meaning that using a constant degradation rate extracted at a given stage of PV operation to represent the entire lifetime could affect the forecast accuracy. Therefore, time dependent degradation rates are proposed. Moreover, the usage of degradation factor is preferable to degradation rate since we consider a non-linear degradation with a non-constant degradation rate.

A. "Time and degradation pattern" dependent models

Taking the aforementioned assumptions into consideration, we propose different degradation factor models dependent on time and degradation pattern. The degradation factor models are expressed as:

$$k_1 = k_{cal}\left(1 + A_1.k_{cal}.ln\left(\frac{1}{\Delta P}\right).\tau_1^{y_1}.\tau_2^{x_1}.\rho^{z_1}.t\right) \tag{3.24}$$

$$k_2 = k_{cal}\left(1 + A_2.k_{cal}.\left(\frac{1}{\tau_1}\right).\rho^{z_1}.t\right) \tag{3.25}$$

$$k_3 = k_{cal}\left(1 + A_3.k_{cal}.ln\left(\frac{1}{\Delta P}\right).\left(\frac{1}{\tau_1}\right).\tau_2^{x_1}.\rho^{z_1}.t\right) \tag{3.26}$$

Table 3.5: Definition of coefficients and parameters

Coefficients and parameters	Definitions
t_{cal}	Time at calibration threshold
P_{cal}	Power at t_{cal}
$SD_{P_{cal}}$	Standard deviation of calibrated data
$\tau_1 = \sqrt{max(t_{cal})}$	-
$\tau_2 = \lvert ln\Delta t\rvert = \lvert ln(t_{cal} - t_{cal-1})\rvert$	-
$\rho = ln\left(\frac{1}{SD_{P_{cal}}}\right)$	-
A_1 $[year^{-3/2}]$, A_2 $[year^{-1/2}]$ and A_3 $[year^{-1/2}]$	Proportionality constants
y_1, z_1 and x_1	Optimization parameters

It should be noted that, these models are purely empirical without any physical implication, they are derived from degradation pattern parameters shown in figure 3.6 as they describe well the specific degradation patterns. It is also important to note that the model parameters are extracted after an initial 3% performance degradation threshold. The 3% optimization threshold is calculated from the degradation trend that excludes early degradation effects. The reasoning for using a 3% threshold are further described and demonstrated in the results section.

B. Power degradation model

The power degradation function proposed in section 3.1, equation (3.10) is used to fit the degradation data also in this part. However, since the evaluation is independent of material properties evaluation or analysis, the model parameter Γ is fixed to one. Therefore, the power degradation function can be re-written as:

$$\frac{P(t=t)}{P_{Norm}} = 1 - exp\left(-\left(\frac{1}{k_{cal}t}\right)^{\mu}\right) \tag{3.27}$$

where P_{Norm} is the maximum power of the degradation trend and k_{cal} is the degradation factor [a^{-1}] at calibration. In this case the degradation factor is preferred for use instead of the degradation rate because of the non-linearity of the power degradation and non-constant degradation.

3.2.3 Modeling approach

A. Failure time and remaining useful lifetime definitions

Chen Xiongzi et al Chen Xiongzi et al. (2011) defined the RUL of a system or a component as the length from the current time to the end of its useful life. The question is how to define the "useful life". In this study the useful life is defined as the non-reversible performance loss such that the module or system power decreases by 20% of the "maximum stable power" measured in the field. The notion of a maximum stable power is introduced to separate long term degradation from early stage degradation events such as light induced degradation (LID) for p-type crystalline silicon modules Köntges et al. (2014) or light and elevated temperature induced degradation (LeTID for multicrystalline silicon and modules with passivated emitter and rear cell (PERC)Kersten et al. (2017); Philipp et al. (2019). It also helps to separate other reversible effects reducing module performance such as soiling Zorrilla-Casanova et al. (2013) and seasonal variations Cañete et al. (2014). Moreover, due to these effects and variation of the outdoor conditions, the power printed on the PV module label substantially deviates from the initial PV module power outdoors. From our point of view, the maximum stable power can be easily compared among systems and is describing the system performance well which is not necessarily the case for the nominal power. The nominal power of a PV module/system may deviate substantially from the real power since it is recorded under STC. These well defined conditions of 1000 W/m^2 and 25°C are almost never prevalent as shown in the histogram in figure 3.7b.

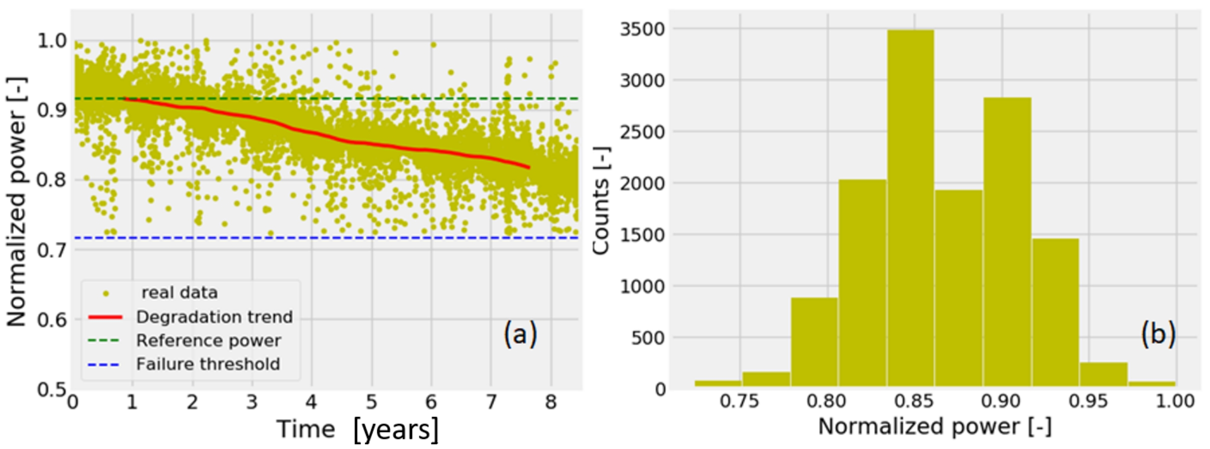

Figure 3.7: A, Illustration of the stable power (red line) used in this study, the green doted line is "maximum stable power" (reference power) and the blue dotted is the failure time threshold. B, Histogram of the data distribution throughout the 8.5 years

Although, the term failure time has already been defined in subsection 3.1.2 it is re-defined here accordingly to the context. In this study, we therefore, define the FT as a reduction in the module or system performance by 20% of the maximum stable power (indicated by the green dotted line in figure 3.7). The 20% loss is purely arbitrary and it is used in this case because of its consistence with the warranties given by manufacturers. It might be interesting to predict the module or system performance for its entire lifetime (until the module stops working), however, such a prediction could be more unreliable and unrealistic since certain future events are unpredictable. Moreover, the longer a module stays in the field the more sensitive it becomes to different degradation modes. That might lead to a dramatic increase in the degradation rate which cannot be easily modeled. Therefore, according to FT definition, the RUL is the length between the current time (CT) to the FT and can be expressed as:

$$RUL = FT - CT \tag{3.28}$$

1. Data filtering

The first filter applied to the input dataset is an irradiance filter. The upper limit for irradiance was set and fixed at 1200 W/m^2 and the lower limit was chosen flexible between 600-900 W/m^2 depending on the location under evaluation. This clear sky filter is used as a way to separate low performances due to low irradiance from degradation. The filtered power is then corrected to STC of irradiance by applying a linear correction of power to 1000 W/m^2 irradiance. The second step is to remove outliers. Because of the stochastic behavior of outdoor conditions and anomalies in the measuring equipment, data measured from outdoor PV modules as well as systems is usually subject to outliers. When not treated well, Outliers might lead to large uncertainties, especially in degradation trend evaluation. The outliers are removed by computing the standard deviation (SD) around the mean value of the entire dataset, whereby all points that are out of the range of $(Mean \pm 2 \times SD)$ are eliminated. For LID or LeTID sensitive systems, it is a crucial step to analyse the degradation pattern during the first year of operation. These degradation modes are characterized by strong non-linear trends in the initial phase which might either stabilize gradually or undergo a regeneration phase Kersten et al. (2017); Philipp et al. (2019). If the regeneration phase is detected, we recommend to eliminate the data until the onset of this phase.

2. Data decomposition

Time series data is characterized by four major components; level, trend, seasonality, and noise. There are two models that are used to model the effects of these components; additive (linear) and multiplicative (non-linear) Brownlee (2017). In our case a multiplicative model is used. The model suggests that the components are multiplied together as follows:

$$y(t) = Level \times Trend \times Seasonality \times Noise \tag{3.29}$$

This function is implemented and available for free use in the python library. The function uses a moving average (MA) method to extract a degradation trend in the time series data. The averaging depends on the required resolution (weekly, monthly or yearly) of one's interest and it determines the extracted degradation trend in this case.

In outdoor conditions seasonal and other different effects can reduce the performance of a PV module or system. For non-reversible performance degradation evaluation it is crucial to choose a good averaging temporal interval that eliminates seasonality and other reversible effects. It has been reported that reversible effects such as inverter failures and soiling of PV modules have a higher impact on performance loss rates than the actual performance degradation which is non-reversible Klünter et al. (2019). These effects could be module technology dependent, for example Virtuani et al. Virtuani et al. (2015) reported that amorphous silicon (a-Si) systems are more affected by variations in the incident spectrum then crystalline silicon (c-Si) systems because of there narrower spectral sensitivity. Therefore, it is important to separate these performance reducing effects from long term degradation by choosing a good averaging temporal interval. The selection of a good temporal interval could be very tedious if one has to do it manually. An iterative algorithm has been implemented to assist in determining a proper interval for degradation trend evaluation depending on the datasets being evaluated.

3. Iterative algorithm for degradation trend evaluation

One way to completely remove any variation in the degradation trend will be to apply a strict constraint, which removes the difference between each nth and $(n+1)^{th}$ value of the trend that is greater or equal to zero, that is; $trend[n-(n+1)] \geq 0$. However, according to the stochastic behavior of outdoor conditions, outdoor measurements usually contain unavoidable outliers which can appear even after applying certain filters. This implies that applying such a strict condition to outdoor datasets is quite unrealistic; in most cases this condition is not fulfilled or might require a considerable amount of computation time to converge depending on the nature of the dataset. Therefore , a tolerance (tol) is introduced and the condition is applied as:

$$trend\left[\left|\frac{max(dn)-min(dn)}{min(dn)}\right|\right] \leq toll, \quad for: \quad dn = n-(n+1) \tag{3.30}$$

The process begins by initialising the temporal interval by: initial temporal interval = 2% of the total length of the time series. Afterwards, the iterative loop is repeated until the condition in 3.30 is fulfilled. The tolerance depends on the nature of the dataset under investigation, for example it can be correlated with the resolution of the data or the magnitude of outliers in the datasets. This makes the process of temporal interval selection a quasi-automated process. By analyzing a number of datasets, a range of tol values can be set granting the flexibility for application on broad datasets of the different distributions.

3.2.4 Experimental

Different data-sets for PV modules as well as systems that have been exposed for quiet a long period of time with considerable degradation were used in this study. The data-sets are from three different sources:

1. The first set of data are those of the TIcino SOlare (TISO)-10-kW PV plant in Lugano (Switzerland) Virtuani et al. (2019); Annigoni et al. (2019). The TISO-10 PV system has been connected to the grid since 1982, and is the oldest installation of this kind in Europe (We shall refer to them as ”TISO-Modules” here after). The performance (i.e. current-voltage curves) of 18 selected reference modules were measured at regular intervals between 1982 and 2017. After 35 years in the field, these modules show a degradation rate ranging from -0.2 to -0.7%/year considering a ± 3% measurement uncertainty. In this study 10 of the 18 modules with a considerable degradation have been used in module calibration and validation stages.

2. Another source of data is a PV plant installed at the airport of Bolzano/Italy (position ca. 46.46 N, 11.33 E, elevation: 262 m) including 11 experimental PV systems, which are in operation for 8.5 years and covering the time period from 01 February 2011 until 31 July 2019. They are referred to as ”Bolzano systems”. Most major PV system technologies are included, namely one and three junction amorphous silicon (a-Si), cadmium telluride (CdTe), CIGS, silicon solar cells made out of a heterojunction with an intrinsic thin layer (HIT), mono-crystalline silicon (mc-Si), poly-crystalline silicon (pc-Si) and poly-crystalline silicon string ribbon (ribbon). All systems are part of one experimental PV plant, they are ground mounted with an orientation of 8.5^{o} west of south and a fixed tilt of 30^{o}. The installed nominal power for the systems range from 1 to 4 kWp per individual installation. According to a new PV sensitive climate classification, proposed by Ascencio-Vázquez et al. Ascencio-Vásquez et al. (2019), the climate in Bolzano is categorized as a temperature climate with medium irradiation. The irradiance is measured with a Kipp & Zonen CMP11 pyranometer. Calibrations are performed in regular intervals and the measurement uncertainty is between 2% and 4%. Additionally, climate data are taken from a ground based meteo-station installed in close proximity to the test side.

3. Finally, data from the Desert Knowledge Australia Solar Centre (DKA Solar Centre) DKASC (2019), named hereafter as ”DKA systems”, are used. The data can

be downloaded through [1]. The data sets used in this study are given as monthly yield in kWh of three different systems; Kyocera-5.4kW-Poly-Si Dual (2008), eco-Kinetics-26.5kW-mono-Si-Dual (2010) and trina-23.4kw-mono-dual (2009). For the first system (Kyocera), data from 01 January 2009 to 01 December 2018 was used in the analysis, for the eco-Kinetics system from 01 January 2011 to 01 December 2018 and for the Trina system, data from 01 January 2014 to 01 June 2019. More information about these systems and datasets are available on the DKA Solar Centre website. It should be noted that the data plotted here have been normalized to the maximum power and were subject to the outlier filters described in the previous section.

3.2.5 Statistical errors analysis

The error measurement employed for the performance evaluation of the proposed forecasting method is the root mean square error (RMSE). Given a measured (m) and a predicted (p) value, respectively, for a given quantity and number of observations (n), the RMSE is expressed as.

$$RMSE = \sqrt{\frac{\sum_{j=1}^{n}(p_i - m_i)^2}{n}} \tag{3.31}$$

The metric deployed to compare the performance of the proposed method with other methods is the relative difference. This is a relative comparison of the failure time forecasted after a 3% interval and on the full dataset. It is expressed as,

$$Rel_{diff} = \frac{|FT_{3\%} - FT_{full}|}{max(|FT_{3\%}|or|FT_{full}|)} \tag{3.32}$$

where, Rel_{diff} the relative difference is, $FT_{3\%}$ and FT_{full} are the failure time evaluated after a 3% degradation and using the entire dataset respectively.

[1]DKA data download: http://dkasolarcentre.com.au/locations/alice-springs/graphs?sources=91

3.3 Methodology of a hybrid model

The described physical models is very useful when one need to correlate the predicted lifetime to the influencing climatic factors as well as dominating degradation mechanisms. However, one draw back is on the accuracy when it comes to long-term degradation prediction. And also, the described data-driven model could help to improve the long-term prediction accuracy, however, it provides no information about the influencing degradation mechanisms. A model that can provide more accurate long-term predictions as well as information of the dominating degradation mechanism is of great importance for financial evaluation as well as material development. In this regard, the two approaches are combined into a hybrid model to achieve these two aspects. The combination of the two approaches is illustrated in the schematic diagram (figure 3.8)

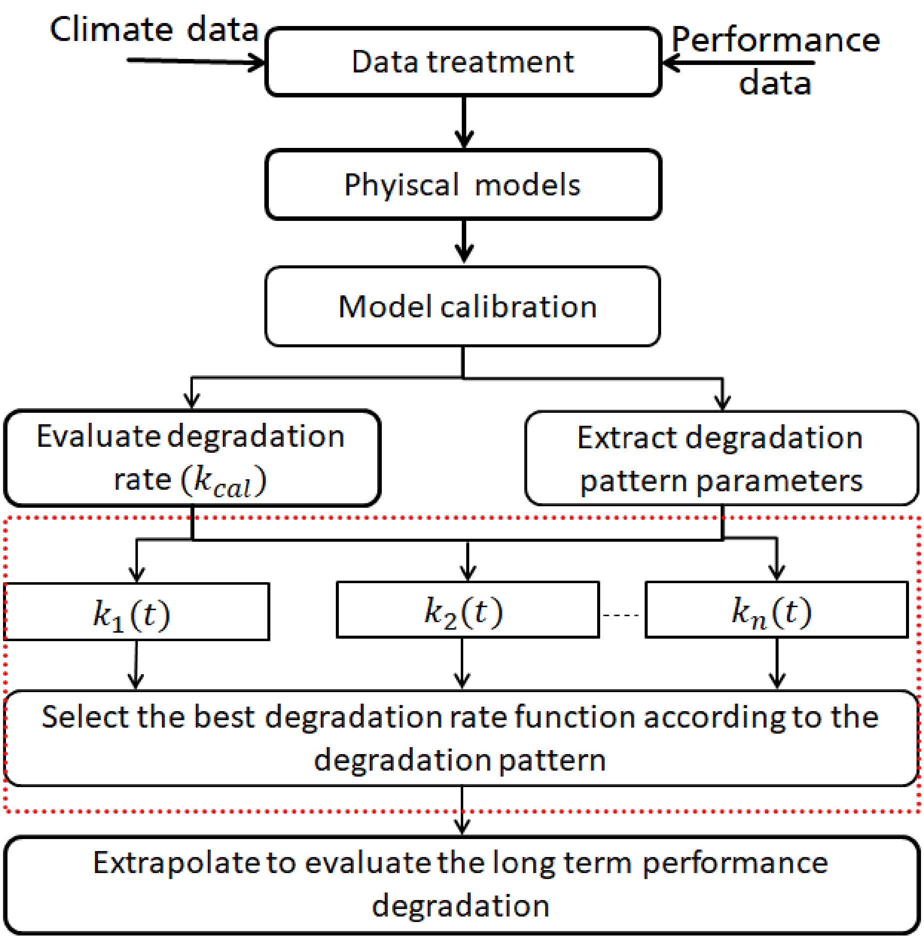

Figure 3.8: Flow chart illustrating the link between the physical and data-driven approach. The red dashed square is the data-driven part, we implement an algorithm to identify the degradation patterns and to select the appropriate rate function

Figure 3.8 illustrate the link between the physical and the data-driven approaches. The fundamental assumption in this link is that, the module experience the same degradation pattern in other geographical locations. This means that the degradation pattern parameters extracted in the training location can be applied in other locations to select the best degradation function for long-term predictions. Therefore, the differences are within the calculated degradation rate at calibration (k_{cal}) which is dependent on the climatic stresses of a given location.

Chapter 4

Results and Discussion

Table 4.1: Chapter 4 Nomenclatures

Symbols	
c_i	clearness index [-]
E_a	activation energy [eV]
k	degradation factor [1/year]
$FT_{3\%}$	Failure time calculated using -3% degradation [year]
FT_{full}	Failure time calculated complete dataset [year]
k_B	Boltzmann constant (8.62×10^{-5}eV/K)
P_{max}	power at maximum power point [W]
R_D	degradation rate [%/hour]
Rel_{diff}	relative difference
SD_{res}	residual standard deviation
T_m	module temperature [K]
T_{mm}	measured module temperature [^0C]
T_{mp}	modeled module temperature [^0C]
(μ)	shape parameter [-]
Subscripts	
cal	calibration
h	hydrolysis
p	photo-degradation
t	thermo-mechanical
T	Total
Abbreviations	
AH	tropical with very high irradiance
AK	tropical with high irradiance
BH	desert with high irradiance
BK	desert with very high irradiace
KGPV	Köppen-Geiger-Photovoltaic
FP	Facebook prophet
MSEP	mean square error of prediction
PR	performance ratio
RUL	remaining usefull lifetime
STC	standard test conditions

In this chapter, the results of the physical model, data-driven model as well as for the hybrid model are presented and discussed respectively.

4.1 Results for the physical model

4.1.1 Properties of the proposed power degradation function

As already mentioned that, non-linearity of power loss is often observed in the field depending on the module technologies or degradation modes. And also that, the loss in power can take different shapes, for example: exponential-shaped, linear-shaped, steps degradation and saturating power loss over time. Moreover, since energy yield could highly depend on how the performance degradation evolves over time (see figure 4.1b), it is very crucial to choose a degradation model to take into account the different failure patterns. A simplified non-linear power degradation model proposed in this research aims to take into consideration these non-linearity dependencies of power degradation. To do this, a shape parameter μ has been introduced to model all the degradation shapes as shown in figure 4.1a.

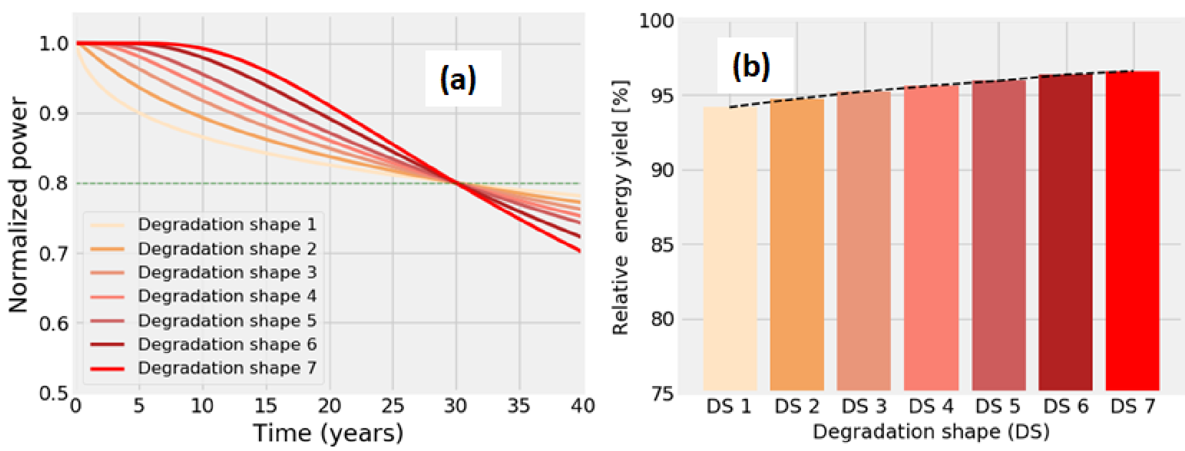

Figure 4.1: A) Optimization of power degradation shapes by altering the shape parameter μ and B) Relative energy yield corresponding to the degradation shapes

Figure 4.1a shows the simulated degradation shapes 1-7 corresponding to different values of μ = 0.1, 0.2, 0.3, 0.4, 0.5, 0.8 & 1.0 respectively. On the one hand, when $\mu = \mathbf{0.1}$ and $\mu = \mathbf{0.2}$, one can achieve the commonly observed degradation shape in thin film technologies with a faster degradation at early stages of exposure and followed by stabilization Jordan et al. (2017b). On the other hand, one can expect the degradation shape similar to that when μ= 1.0 for glass-glass modules if we speculate that for this module design there are less moisture pathways and moisture ingress compared to glass-backsheet modules. Therefore, the moisture induced degradation modes are slower at the earlier stages of the module lifetime. However, as the breathable pathways and drying are also limited, the moisture will accumulate over the years, leading to a dramatic increase in degradation rate.

4.1.2 Calibration and validation of the specific degradation rate models

Two basic approaches are applied for the calibration of the different degradation rate models: (a) optimization of model performances and (b) through prior knowledge from previous studies. Optimization of model performance, which compares measured and simulated data, is applied by the help of a built-in nonlinear least-squares solver in the GNU Octave software. Prior knowledge, with the aid of sensitivity analysis, is used as a baseline to select the initial fitting guesses and also as a confirmation that the extracted values are in a meaningful range.

To derive the model parameters, equations 3.2, 3.5 and 3.6 are fitted on experimental data from the indoor accelerated ageing tests at given specific test conditions as presented in chapter 3 table 3.2. The extracted parameters are presented in table 4.2 together with the percentage residual standard deviation ($\boldsymbol{SD_{res}}$) (see equation 3.22). To further ensure a better calibration procedure, in each case the distribution of the residuals is plotted and analysed (to check if the residuals follow a normal distribution). The parameter Γ of the power function in equation (3.10) has been normalized to one and the extracted shape parameter ($\boldsymbol{\mu}$) is 0.7 for hydrolysis, 0.4 for photo- and thermo-mechanical degradation in figure 4.2.

To validate the models, different sets of data measured at different test conditions (see table 4.2) are used and by using the extracted parameters the simulations are compared with the measured data points through evaluation of the mean square error of prediction (MSEP, see equation 3.23) as also presented in table 4.2. The MSEP is also used as a metric to correlate the uncertainties in model calibration with the predictions when compared with the $\boldsymbol{SD_{res}}$. For example, a 0.5% $\boldsymbol{SD_{res}}$ led to 0.025% MSEP for the hydrolyisis model, a 1.65% $\boldsymbol{SD_{res}}$ resulted into 0.216% MSEP for the thermo-mechanical model and 0.19% $\boldsymbol{SD_{res}}$ led to 0.168% MSEP for the photo-degradation model. Although, there is a correlation of the uncertainties due to model calibration as its evaluated in the thermo-mechanical model, the uncertainties in experimental data sets used for validation can also influence the evaluated mean square error therefore it's also useful to plot and interpret the results basing on the degradation trend. Evaluating a confidence interval of the prediction can also help to analyze the model performance.

Table 4.2: Extracted parameters for the three rate models and the percentage residual standard deviation ($\boldsymbol{SDres}$) as well as the mean square error of prediction (MSEP)

Extracted models parameters						
Degradation rate model	$\boldsymbol{A_i}$	$\boldsymbol{E_a}$ [eV]	$\boldsymbol{n}$	$\boldsymbol{X}$ & Θ	$\boldsymbol{SD_{res}}$	MSEP
Hydrolysis: Eq(3.2)	6.11e4	0.91	1.90	-	0.5%	0.025%
Photodegradation: Eq(3.5)	1.20e-3	0.43	1.80	0.63	0.2%	0.168%
Thermo-mechanical: Eq(3.6)	9.10e-5	0.40	-	2.24	1.6%	0.216%

Figure 4.2 shows calibration and validation results for the hydrolysis, photo-degradation and thermo-mechanical models (equations 3.2, 3.5 and 3.6) respectively. In black is the measured power for DH 75^0C/85RH; red is the respective model fit with a violet line at 5000 hours representing the optimized data points. The blue line is the predicted power at DH 85^0C/85RH, the light blue patch is the 95% prediction confidence interval and in green the measured power at DH 85^0C/85RH, used for model validation. The vertical lines on measured data points indicate a 2.5% measurement uncertainty. The color usage

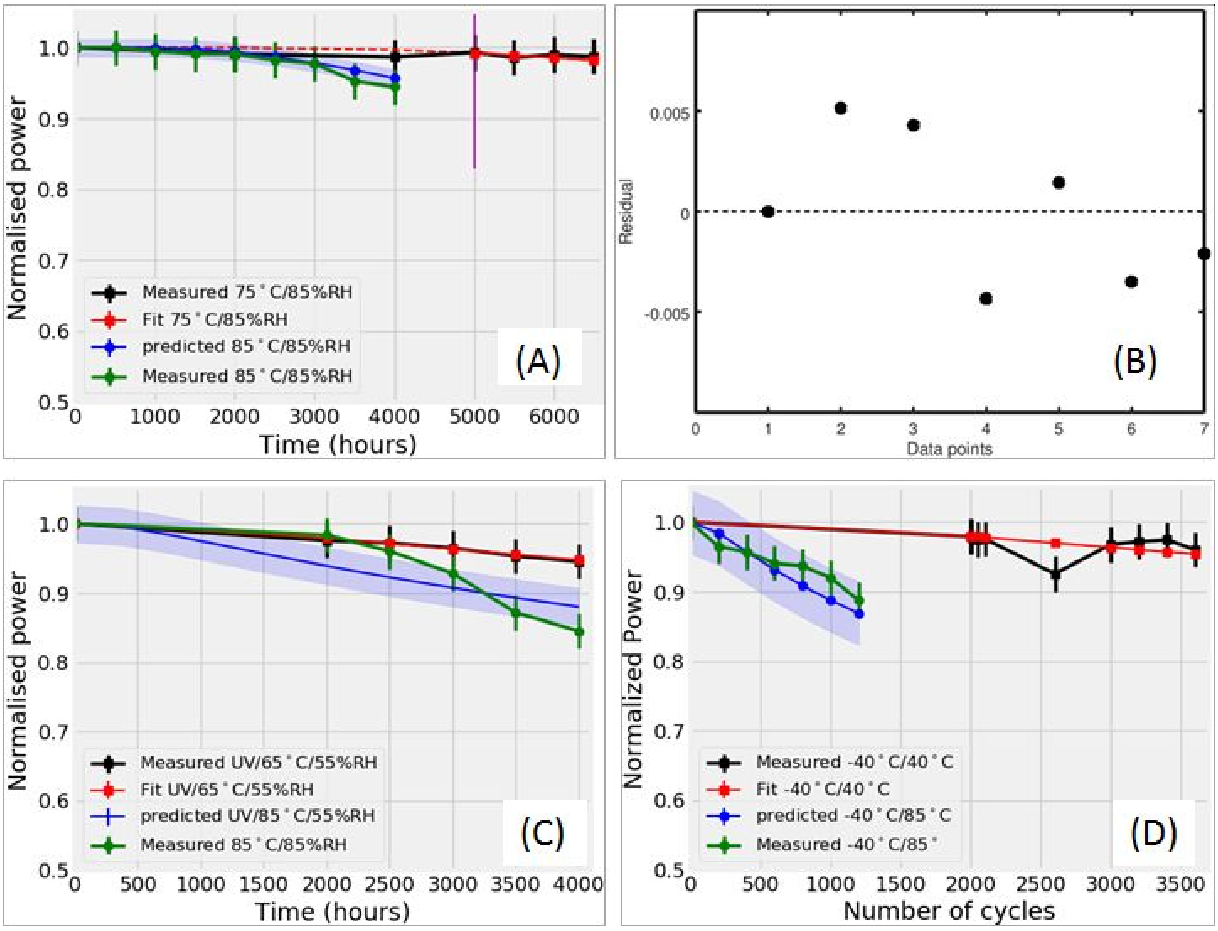

Figure 4.2: A: Hydrolysis model Eq(3.2) calibration and validation, the vertical violet line represents the optimized data points; B: Residual distribution of the fitted data points of the DH test; C: Photo-degradation model Eq(3.5) calibration and validation, and D: Thermo-mechanical model Eq(3.6) calibration and validation. The blue patch is the 95% confidence interval of prediction.

and explanation above are consistent for photo-degradation and thermo-mechanical graphs using respective data sets. For all the models, the predictions are satisfactory and are within a 95% confidence interval. The observable variations could be linked with the measurement uncertainties.

It important to note that, when applying the physical models, the extracted parameters are usually valid only for a particular module type. Meaning that the parameters have to be evaluated when the module type or technology changes.

4.1.3 Calibration and validation of the combined degradation rate model

The combined/total degradation rate (equation 3.8) is calibrated using outdoor measurements of Gran Canaria. The dataset of Gran Canaria is selected over Negev and Zugspitze because the module in Gran Canaria has been exposed longer compared to the ones of Negev and Zugspitze, and moreover it shows a clear degradation trend. The extracted model parameters are presented in table 4.3. On calibration, the residual standard deviation is 2.34% and the derived parameters, $\Gamma = 190$ and $\mu = 0.19$ for the power degradation function in equation 3.10.

Table 4.3: Extracted model parameters of the individual rate models using the combined rate model 3.8 and with Gran Canaria data

Extracted models parameters				
Degradation rate model	A_i	E_a [eV]	n	X & Θ
Hydrolysis: Eq(3.2)	4.91e7	0.74	1.90	-
Photodegradation: Eq(3.5)	71.83	0.45	1.90	0.63
Thermo-mechanical: Eq(3.6)	2.04	0.43	-	2.24

The model is validated by using the derived model parameters to simulate the degradation rates using the climatic datasets of Negev and Zugspitze. By comparing the simulated degradation trend with the measured data (see figure 4.3), the accuracy of the model is verified.

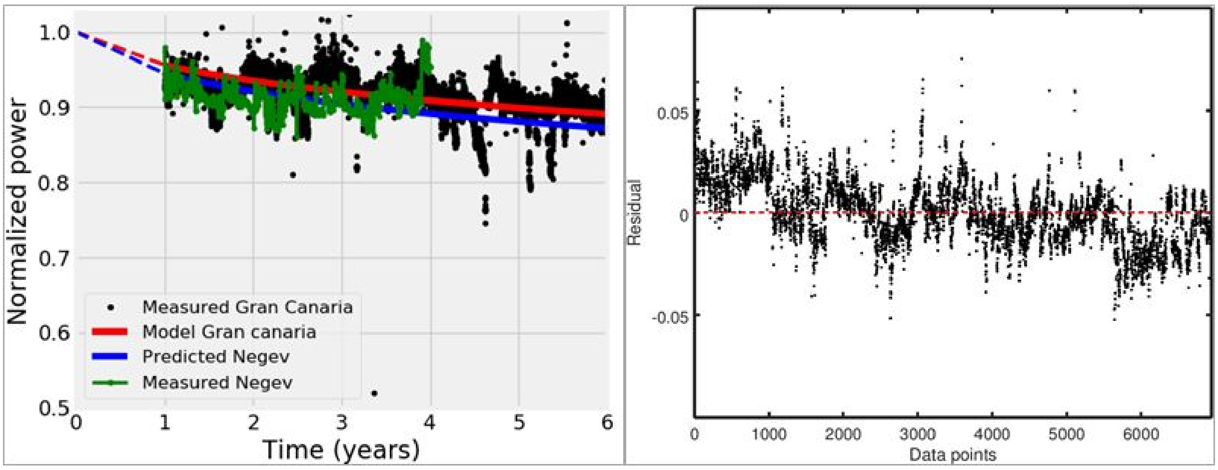

Figure 4.3: Right: Dotted black points are the measured data of Gran Canaria (calibrated dataset); thick red line is the model fit; in green is the measured data of Negev, thick blue line is the model prediction for Negev and the dashed lines indicate normalization to the initial laboratory power values before outdoor exposure respectively. Left: Residual distribution of the calibrated data points.

Figure 4.3 on the right shows the calibrated data of Gran Canaria and the predicted degradation for Negev plotted together with the measured degradation. The alpine predictions were left out to avoid too much information on the graph due to data fluctuations. The outdoor predictions show a good agreement with the measured power degradation.

4.1.4 Degradation rates and lifetime prediction

Depending on the climate a module is installed in, different degradation modes might dominate over the others. Using the proposed degradation models, equations (3.2), (3.5), (3.6), (3.8) and the outdoor derived model parameters, it is possible to predict the dominating degradation precursor and the total degradation rate as well as the failure time from equation (3.11) for any location with known climatic loads. In this section, annual degradation rates of the mc-Si modules were predicted using input climatic loads of Zugspitze, Gran Canaria and Negev as shown in table 4.4.

High thermo-mechanical degradation is predicted for Zugspitze in comparison to Gran Canaria because of high module temperature variations in this climate zone. On the contrary, small degradation due to hydrolysis is predicted in Zugspitze despite the high levels of relative humidity. This could be explained by the low average module temperatures experienced in this region, hence slowing hydrolysis processes and the absolute water vapor concentration. In all cases, high rates are predicted in Negev. This can be explained again by the higher temperatures in this zone that determines the reaction rates for other degradation processes caused by other degradation factors such as hydrolysis by humidity and photo-degradation by UV dose. The predicted failure time defined as a 20% loss in power, show more severe degradation of maximum power output in arid climates where temperatures are higher such as expected. This further confirms the previous studies Annigoni et al. (2017) that temperature could be the primary accelerator of degradation.

Table 4.4: Predicted degradation rates of the mc-Si modules and failure time in the three climatic zones with a 95% lower and upper confindence interval (CI).

Predicted rates and FT							
Location	R_{Dh} (%/year)	R_{Dp} (%/year)	R_{Dt} (%/year)	R_{DT} (%/year)	FT (years)	Lower 95% CI (years)	Upper 95% CI (years)
Negev	0.169	0.216	0.225	0.74	21.4	16.7	27.1
Gran-Canaria	0.122	0.212	0.104	0.50	31.6	25.0	40.0
Zugspitze	0.043	0.103	0.129	0.3	52.8	42.7	65.0

4.1.5 Comparison of the proposed physical model with other physical model

We compare the predictions of the total degradation rate and failure time using the proposed physical mode and the model proposed by Bala Subramaniyan et al. (2018) in equation (2.39). For meaningful comparison and to avoid any bias, both models are calibrated using the same dataset (from Gran Canaria). Moreover, the model parameters are also derived to be in range with those reported in their paper Bala Subramaniyan et al. (2018). The simulated degradation rates and failure times are as presented in table 4.5. Note that the values of Gran Canaria are perfectly the same because they are the reference calibrated dataset for both models. The comparison is then made on the predictions of the other two locations that is; of Negev and Zugspitze.

The evaluated rates are quite comparable for Negev but show very high difference for Zugspitze. To further analyse the cause of this high discrepancy in the prediction, the sensitivity analysis of the input variables is carried out. Temperature (T), relative humidity (RH) and UV dose bins between (15^0C-45^0C), (40%-100%) and (80-120kWh/a/m^2) respectively are used to generate 500 combinations of T, RH and UV. The sensitivity of the degradation rate with the climatic variables is as shown in figure 4.4.

As shown in figure 4.4, the model according to Bala Subramaniyan et al. (2018) has a higher sensitivity to the input variable especially to the module temperature. At lower or higher values of temperatures, the model overestimates or underestimates the degradation rate respectively and this explains the observed variations in the predictions especially in Zugsptize where the module temperatures are considerably low. The reason to this higher

Table 4.5: Comparison of the proposed model with the model according to Bala Subramaniyan et al. (2018)

Location	R_{DT} [% years] (Proposed) Eq(3.8)	FT [% years] according to Eq(3.11	R_{DT} [% years] (Subramaniyan) Eq(3.8)	FT [% years] according to Eq(3.11)
	Predicted rates and FT			
Gran Canaria	0.50	31.6	0.50	31.6
Negev	0.74	21.4	0.80	20.0
Zugspitze	0.30	52.8	0.14	113.5

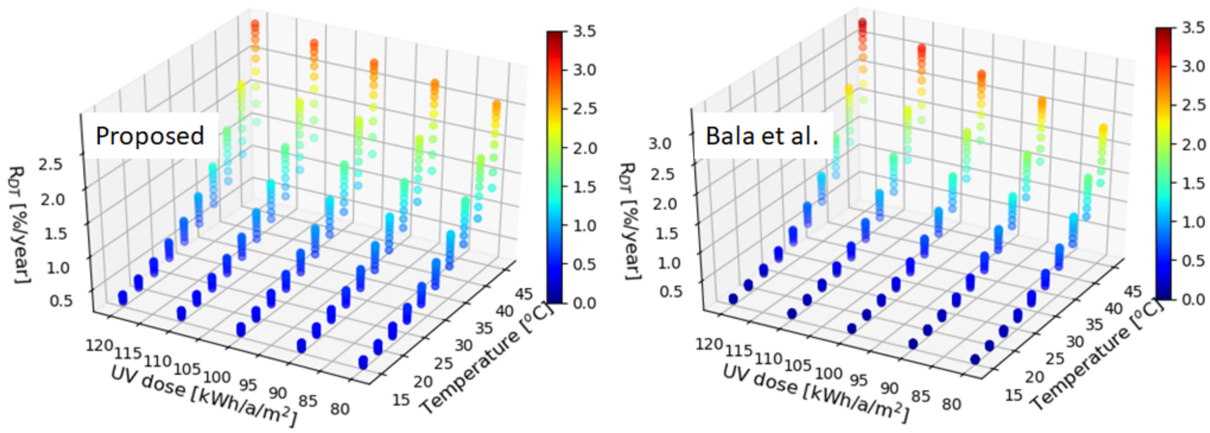

Figure 4.4: Sensitivity analysis of the proposed and the model according to Subramaniyan. Note, each dot represents a value of relative humidity and increases to the bottom.

sensitivity on temperature could be attributed to the model assumption that, all the degradation processes triggered by the combination of the four stresses have the same activation energy. From a physical point of view, this is usually not the case as one can expect different processes to have different kinetics and hence different activation energies. Also, assuming a single activation energy could be too much simplification hence deteriorating the model performance.

4.1.6 Global degradation rates mapping: A global PV degradation risk analysis

The evaluation of the degradation rates dependent on specific degradation processes and the total degradation rate is extend from the three available location to a global scale. The aim is to create a global risk map of the three proposed mechanism and also the total degradation rate. The climate datasets used are extracted, modelled and averaged from the ERA5 reanalysis dataset for the years 2016, 2017 and 2018.

Figures 4.5, 4.6 4.7 and 4.8 show the worldwide degradation rates for hydrolysis, photodegradation, thermo-mechanical and total degradation respectively. The generated maps are in accordance with the parameters from the studied mono-crystalline modules.

According to the recently proposed Köppen-Geiger-Photovoltaic (KGPV) climate scheme Ascencio-Vásquez et al. (2019), hydrolysis-degradation presents the smallest contribution in almost all the KGPV zones, but is considerable high for the tropical climates AH (trop-

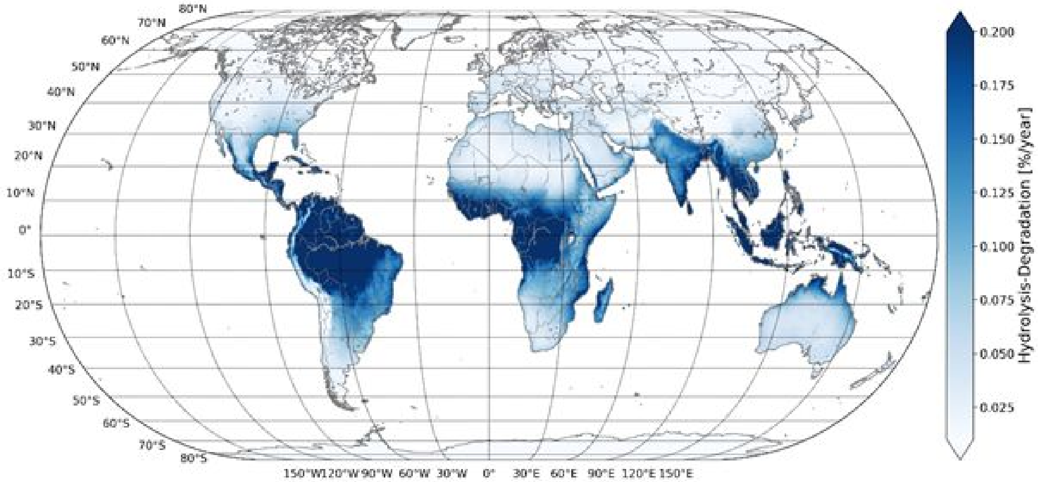

Figure 4.5: Global mapping of hydrolysis degradation rate

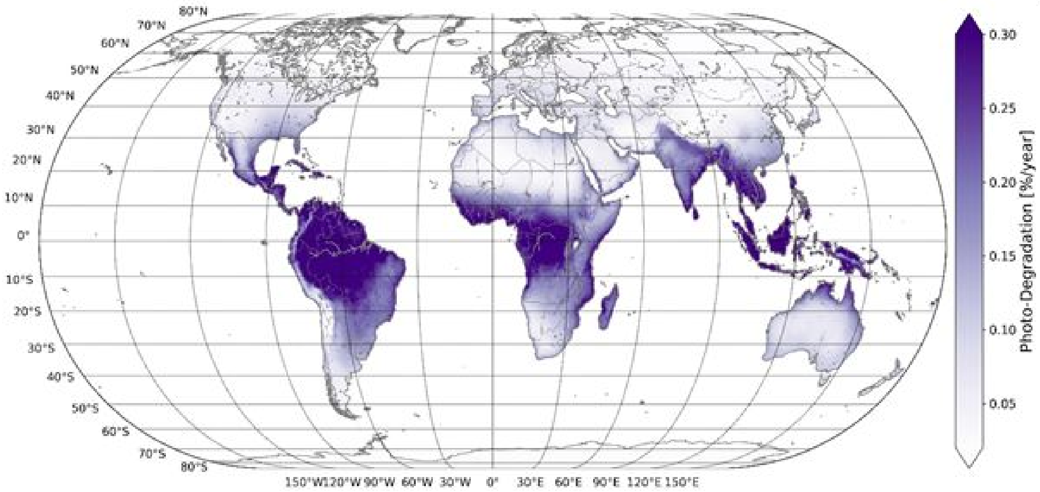

Figure 4.6: Global mapping of photo-degradation rate

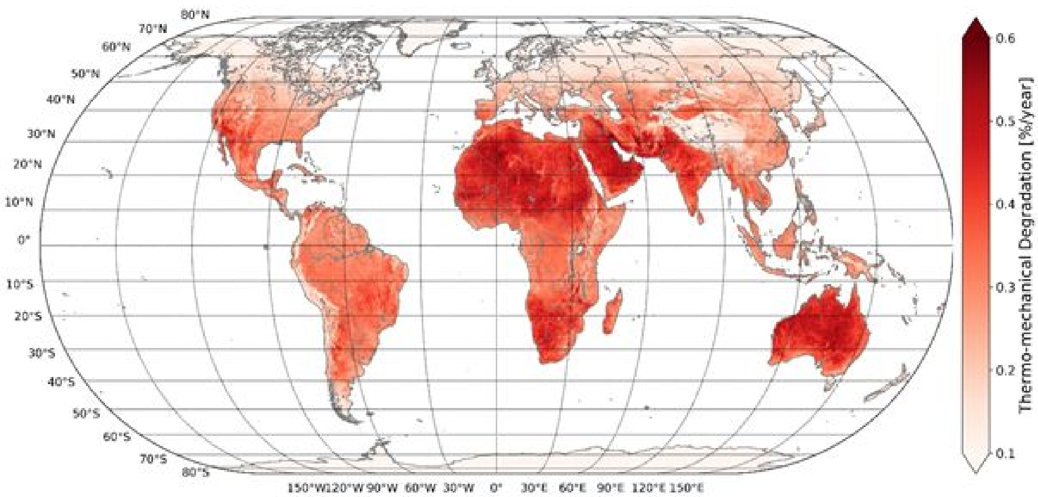

Figure 4.7: Global mapping of thermo-mechanical degradation rate

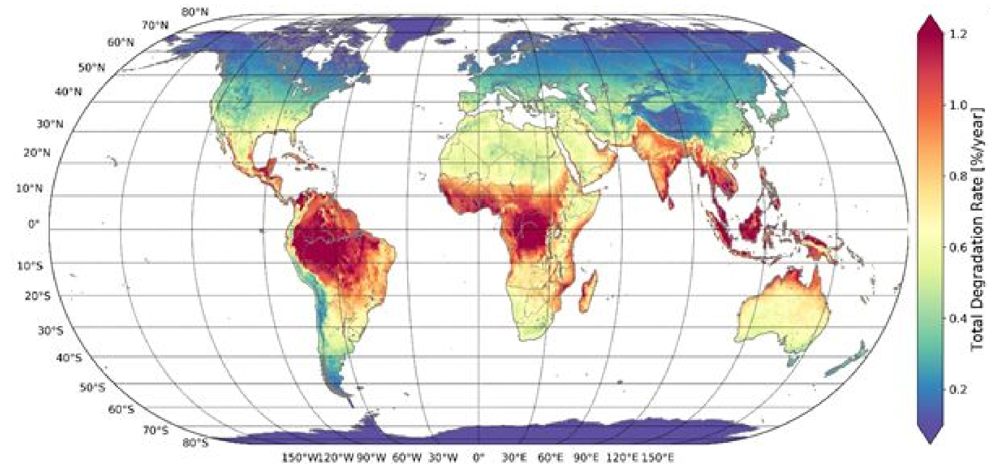

Figure 4.8: Global mapping of total degradation rate

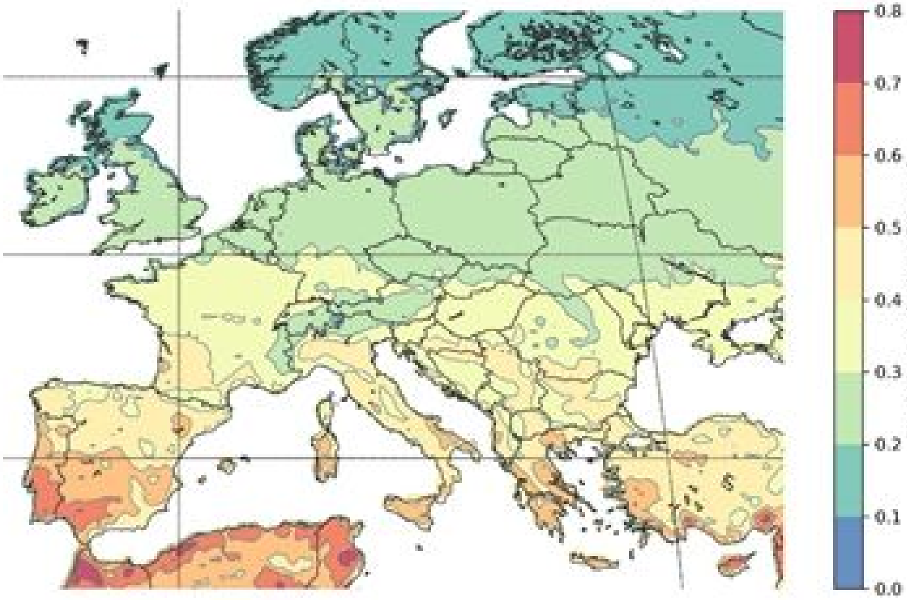

Figure 4.9: European categorization of total degradation rate based on temperature, humidity and UV irradiance for a mono-crystalline silicon PV module.

ical with very high irradiance) and AK (tropical with high irradiance), which zones are related with high precipitation levels (humid areas) and temperature levels. This process can provoke the moisture ingress leading to delamination of polymers or corrosion of solder bonds Koehl et al. (2018).

Photo-degradation has the second-highest contribution to the total degradation rate. This indicator combines the humidity, temperature and UV irradiance impacting the PV module. The impact is similar to the hydrolysis-degradation but higher in terms of absolute values due to the process triggered by UV irradiation. For desert areas, even though the UV irradiation is high, the low humidity in the air decreases the damage of the PV cells due to this mechanism Ngo et al. (2016). The photo-degradation is considerable high in AH (tropical with very high irradiance) and AK (tropical with high irradiance) zones due to the high climatic stresses of all variables (temperature, humidity and UV irradiation). It is surprising that the highest degradation due to photo-degradation was not predicted in the desert with high irradiance (BH) and desert with very high irradiace (BK) climates, for example in the northern part of Africa where the UV is expected to be higher compared to the tropical regions of central Africa. The reason to this can be attributed to the low values of relative humidity in the dessert areas hence lowering the impact of the degradation modes influenced by the combined UV-RH stresses.

Thermo-mechanical degradation exhibits the highest contribution to the total degradation rate in almost all zones. This parameter is affected by the seasonal temperature cycling (the difference between the maximal and minimal temperature of the year) and also the annual average maximum temperature.

The total degradation rates calculated by the combination of the previous three degradation mechanisms is also mapped. In accordance with the literature Omazic et al. (2019), the highest degradation rate is identified in tropical areas (hot and humid). Interestingly, the AK presents lower degradation than the AH, due to lower photo-degradation contribution (related to lower humidity). Globally the highest degradation rates (above 1.4 %/year) are identified in locations next to the equator line. To facilitate the visualization and use of degradation maps, we categorize the locations into bins of 0.2%/year ranging from 0 to 0.8%/year for Europe The categorized map is shown in figure 4.9 The total degradation rates could reach 0.8%/year in the hottest areas of the south of Spain and Portugal for Europe. In real operating conditions, external degradation factors, such as soiling might increase the degradation rate if taken into account, but the degradation presented here assumes only gradual and non-reversible degradation processes.

4.1.7 Uncertainties evaluation of the physical model

In order to be able to develop reliable predictive models, it makes it crucial to evaluate the different sources of uncertainties that can deteriorate the model performance. Therefore, in this section, the different sources of uncertainties are analyzed and discussed.

A. Uncertainties related to data quality

The quality of input data can highly affect the accuracy of the predictions. Here, the impact of data outliers is analysed. The module power measurements were done every five minutes, such high-resolution measurements and the frequently fluctuating environmental conditions outdoors, lead to unavoidable noise even after applying filters and corrections. By using an hourly moving average to minimize the noise in the datasets, the process of model calibration and validation is repeated. The effect of the noise to the derived model parameters as well as on failure time estimation is evaluated. Because the parameters: $\boldsymbol{E_a}$, $\boldsymbol{n}$, $\boldsymbol{X}$ and of the degradation rates models are very sensitivity, they are assumed constant in this analysis. Therefore, we evaluate the noise effect using the parameter Γ of the power degradation function (3.10). In order to illustrate this effect, the simulations of the failure time for the three location have been repeated using the hourly time-resolution and compared with the five minutes resolution. The MSEP and relative difference in failure time estimation with a five minutes and hourly resolution data are presented in table 4.10. Figure 4.10 shows a plot of the simulated and measured data. Note, the dataset of Gran-Canaria is still used as training or calibration dataset. The residual standard deviation reduced to 2.04% and the derived model parameter reduced to $\Gamma = \mathbf{182.3}$.

Although the residual standard deviation improved from 2.23% for 5 minutes resolution to 2.04% for hourly resolution, the improvement did not considerably led to reduction in MSEP. However, it led to a 4.05% relative difference of the predicted failure time. This is

Table 4.6: Percentage mean error in prediction (MSEP) and relative difference of the estimated FT for different data resolutions.

Uncertainties evaluation					
Location	Data Resolution	Parameter Γ	MSEP [%]	FT $[year]$	Relative difference
Negev	5 min	190.0	0.0230	21.4	4.05%
	Hourly	182.3	0.0240	20.5	
Zugspitze	5 min	190.0	0.0152	52.8	4.05%
	Hourly	182.3	0.0150	50.7	

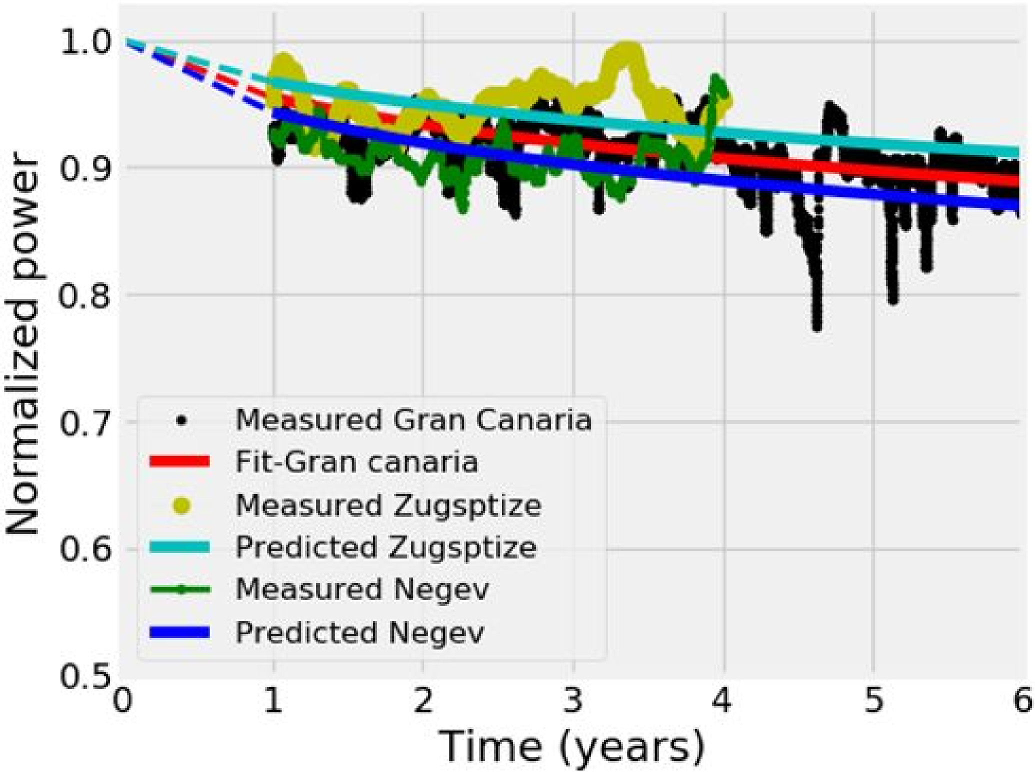

Figure 4.10: Model calibration and validation with hourly resolution

consistent with the observations from indoor results that, the uncertainties in experimental data sets used for validation can also influence the evaluated MSEP.

B. Uncertainties related to climatic variables evaluation

In most cases, the essential input climate variables (temperature, humidity and UV irradiation) are evaluated from national or private weather services such as EAR5 used in this study to evaluate the global degradation map. The key challenges with these databases is that they are not developed for PV module or systems evaluation. In most cases the required variables such as relative humidity and UV irradiation are not directly measured. Therefore, they have to be evaluated from other variables such as precipitation and global irradiation using specific mathematical models. Indeed, these models are associated with their own uncertainties since they are difficult to calibrate and validate. Indeed, using such calculated parameters poses a question on the absolute values accuracy of the predict degradation rates or failure time. Moreover, parameters such as ambient temperatures which is widely measured and available are not directly used as model inputs since they have to be converted to module temperature for degradation evaluation. This also influence the evaluated degradation rates and failure time. Since temperature is considered as the main factor that influences the degradation mechanisms, here we demonstrate the uncertainties involved in module temperature evaluation by comparing the predictions of the modeled and measured module temperatures in the three locations.

As can be seen in table 4.7, the relative difference in measured (T_{mm}) and modeled (T_{mp}) module temperatures can be as high as 47%. Also depending on the location where the module is installed; this difference can lead to as much as 59.3% relative difference between the degradation rate evaluated with the measured module temperatures (R_{DTmm}) and the degradation rate evaluated using modeled temperatures (R_{DTmp}). One important observation is that, the uncertainties in rates or lifetime prediction due to the uncertainties in module temperatures evaluation, are location dependent. For example, the modeled module temperature showed high uncertainties for Zugspitze as compared to Gran Canaria, on contrary high uncertainties in degradation rates are evaluated for Gran Canaria compared to Zugspitze. This can be explained by the Arrhenius temperature dependence in the degradation rate models. The effect can be clearly explained by the temperature against the degradation rate plot Figure 4.11.

Table 4.7: Comparison of predicted rates and FT using measured and modeled module temperature.

	Predicted rates and FT							
Location	T_{mm} [^{0}C]	T_{mp} [^{0}C]	relative difference	R_{DTmm} [^{0}C]	R_{DTmp} [^{0}C]	TF_{Tmm} [$years$]	TF_{Tmp} [$years$]	relative difference
Negev	36.63	25.35	44.47%	0.75	0.471	33.60	21.09	59.27%
Gran-Canaria	30.12	23.81	26.51%	0.48	0.345	45.80	33.0	38.79%
Zugspitze	4.98	3.65	36.38%	0.23	0.22	71.41	69.22	2.74%

At lower temperature, large variation of temperatures leads to small change in the degradation rate and at high temperatures a small variation in temperature leads to a relatively large change in the degradation rate. Hence, the uncertainties in module temperatures evaluations have a more drastic effect on the accuracy of the predictions in locations with high module operating temperatures.

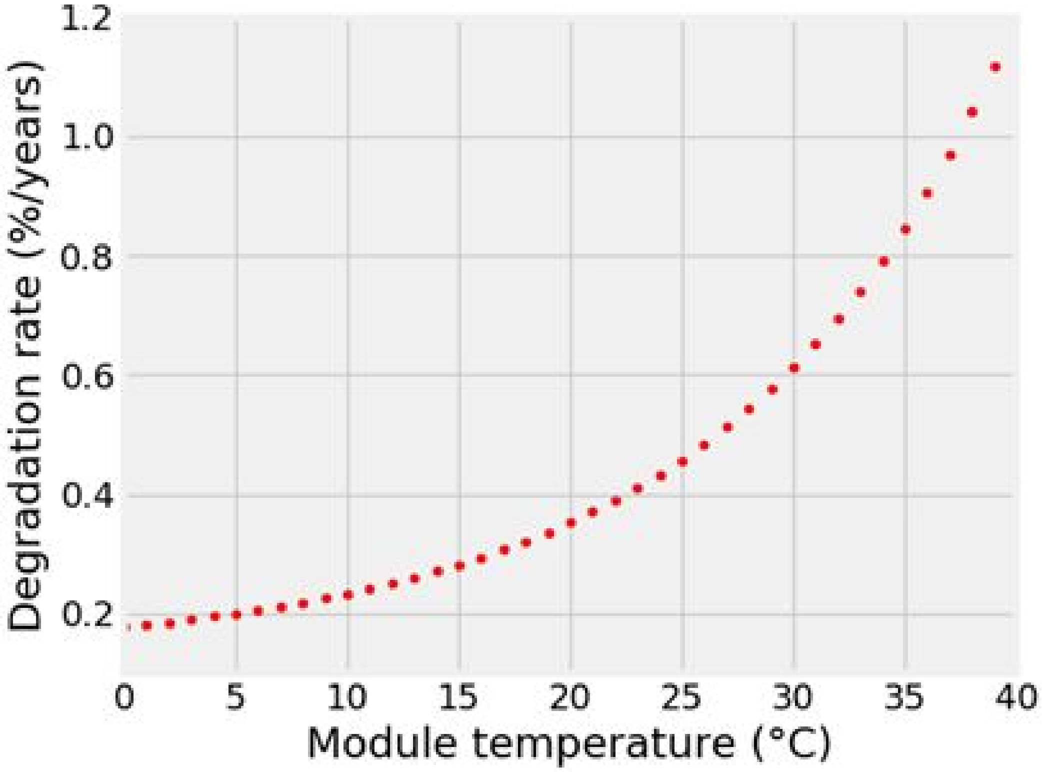

Figure 4.11: Module temperatures against the degradation rate

4.2 Results for the data-driven model

4.2.1 "Time and degradation pattern" dependent models as well as 3% degradation threshold

To validate the assumptions used in this approach, here the pitfalls of using a constant degradation rate for long-term degradation forecast are illustrated. Also, the dependence of the model on time series degradation patterns is illustrated.

The power degradation function (equation 3.27) is calibrated at different performance degradation intervals (at P = -1%, P = -2% and P = -3%). At each interval, a simple extrapolation with a constant degradation rate at calibration (k_{cal}) is performed and failure time evaluated. To analyse the dependence on degradation patterns, two of the TISO-modules named TEA5 and TEA6 are used as shown in figure 4.12.

It is clearly visible that although the model fits the data very well at all calibration intervals, the evaluated failure time is very different at each calibration interval. This effect is observed for both modules TEA5 and TEA6. This result demonstrates three aspects: one, a perfectly fitting model does not guarantee better forecast or prediction. Two, a model that assumes a constant degradation factor/rate is not appropriate for long-term PV performance degradation forecast. Three, the model forecast accuracy might highly depend on a specific degradation pattern. This effect is visible in the two modules, for example high discrepancies are visible for the TEA6 module compared to TEA5 module even at similar calibration intervals. Therefore, based on these three observations, the concept of "time and degradation pattern" dependent degradation factor was introduced.

It is also visible that the forecasting accuracy improves as the calibration interval or performance degradation increases, which seems like an obvious observation. However, since the objective is to perform the prediction at the early stages of the module's operation, a 3%

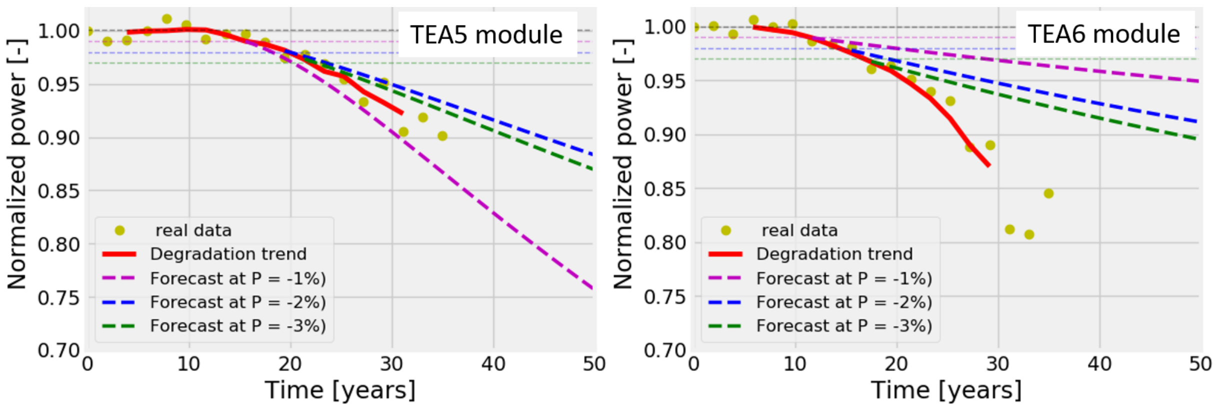

Figure 4.12: Fit and RUL prediction at different percentage power loss of two TISO modules, namely TEA5 and TEA6. The dotted lines represent forecasts at the three calibration intervals

threshold was selected. This threshold was found optimal since it provided good forecasts compared to values less than 3% loss. Moreover, another reason is that in situations where the degradation trend is not monotonically decreasing as in many outdoor datasets, using performance degradation of less than 3% might lead to misinterpretation of degradation with seasonal variation or other performance reducing factors which are reversible. For example, the TEA5-module in figure 4.12 shows that prediction after only 1% performance degradation resulted in under-estimations compared to the measured degradation trend, which is attributed to the variations in the degradation trend due to reversible effects.

4.2.2 Model calibration

The power degradation model 3.27 was fitted on measured datasets to extract the model parameters (k_{cal} and μ). At the same time the degradation pattern parameters ΔP, Δt and t_{cal} are evaluated. During the calibration process, a total of 7 TISO-modules (named TEA1, TEA4, TEA6, TEA8, TEA10, TEB1, TEB2) and 2 DKA systems where optimized. From these modules and systems, different failure patterns where extracted by altering the tolerance (which changes the degradation trend). Despite the strong degradation and huge variations in the data points observed for the DKA systems, they are selected for the calibration process because the objective of proposed methodology is to be applicable on a wide set of data distribution.

Figure 4.13 shows an example of one of the TISO-modules (TEA1) with annual measurements for 35 years and one of the DKA systems (Kyocera system) with monthly average values for 9 years, used for model calibration. The extracted parameters are used as the basis to set logical conditions to select which degradation factor model represents better a given degradation pattern. Over 10 logical conditions where achieved to represent the different degradation patterns as presented in table 4.8.

Figure 4.14a shows the 7 TISO-modules used in this study for model calibration. Figure 4.14b is the corresponding change of the degradation factor over time of the 7 modules. It is clearly visible that the rate of degradation factor variation is dependent on the degradation patterns. This is evident for TEA1 module that displays a strong degradation but with a low rate of change of the degradation factor over time. Furthermore, for some degradation patterns like the one of TEA10, a constant degradation factor ($k = k_{cal}$) was sufficient to evaluate the long term degradation. Hence, for such a degradation pattern, it is enough to

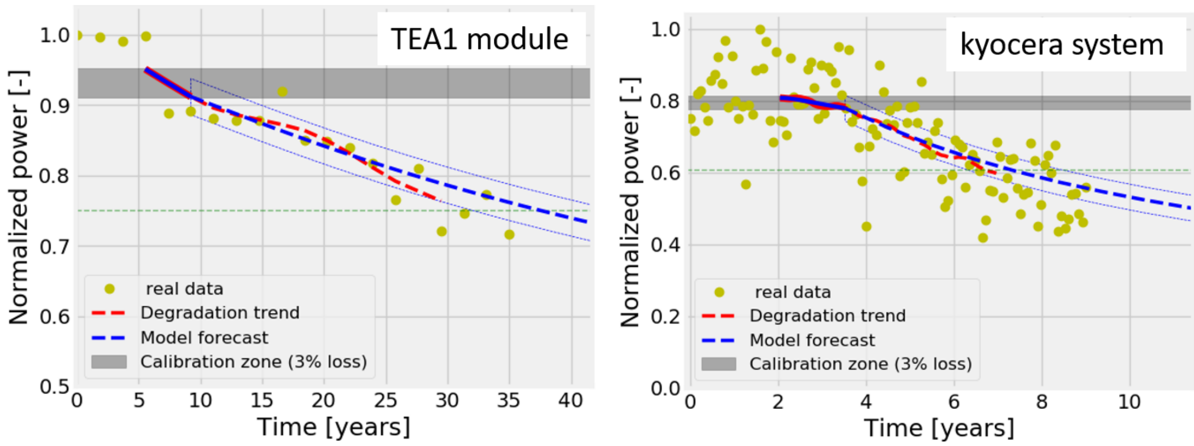

Figure 4.13: TEA1 module (from the TISO-Modules) and Kyocera system (from DKA systems) selected for calibration. In yellow are the measurements and red is the extracted degradation trend and in thick blue line is the model prediction with the 95% confidence interval. The horizontal green dotted line shows the -20% failure threshold of the degradation trend

Table 4.8: Logical conditions for model selection and the corresponding extracted optimization model parameters

Logical conditions	Model	Parameter y_1	Parameter x_1	Parameter z_1
$\mu \leq 0.45$ & $k_{cal} \leq 9.0e-4$	k_1	2.0	1.0	1.0
$\mu \geq 0.45$ & $k_{cal} \geq 0.01$	k_1	1.0	0.1	1.0
$\mu \leq 0.3$ & $\Delta P \geq 0.01$	k_1	1.0	0.1	1.0
$\mu \geq 0.45$ & $\Delta P \geq 0.01$	k_1	1.0	1.5	1.0
$\mu \geq 0.55$ & $k_{cal} \leq 0.005$	k_1	-	4.0	1.0
$\mu \leq 0.4$ & $\Delta P \leq 0.01$ & $k_{cal} \leq 0.005$	k_1	-	4.5	1.0
$\mu \leq 0.35$ & $\Delta P \geq 1.0e-4$ & $t_{cal} \leq 5$	k_2	-	-	3.5
$\mu \leq 0.45$ & $\Delta P \leq 1.0e-4$ & $k_{cal} \leq 0.009$	k_3	-	0.1	1.0
$k_{cal} \geq 0.01$ & $\Delta P \leq 5.0e-5$ or $\mu \geq 0.45$	$k = k_{cal}$	-	-	-
$k_{cal} \leq 0.013$ & $\Delta P \leq 9.5e-6$ & $\mu \geq 0.43$	k_3	-	0.1	0.5
else:	k_1	0.0	2.5	1.0

forecast the lifetime by using only the simplified power degradation model e.g. equation 3.10.

4.2.3 Validation

The most important and challenging part of all predictive models is the validation process of the models which usually requires different sets of measured data from the ones used in the calibration process. In this study, PV modules and systems with a considerable performance degradation were used to valid the performance of the model. An example is shown in figure 4.15 for Trina and CIGS systems. By comparing the measured trend line and the prediction line, the accuracy of the model was verified.

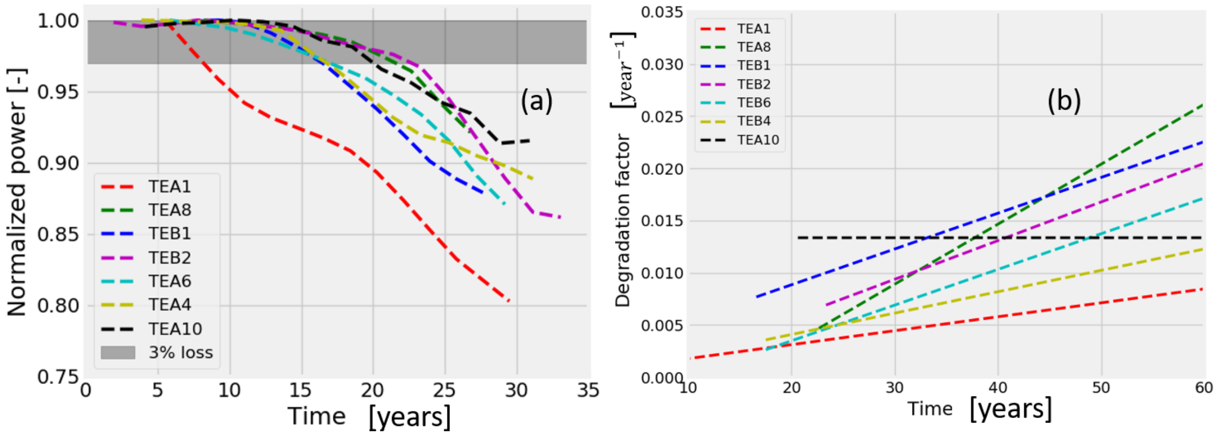

Figure 4.14: A, Different TISO-modules used in model calibration. B, Change of the degradation factor over time of the 7 modules respectively

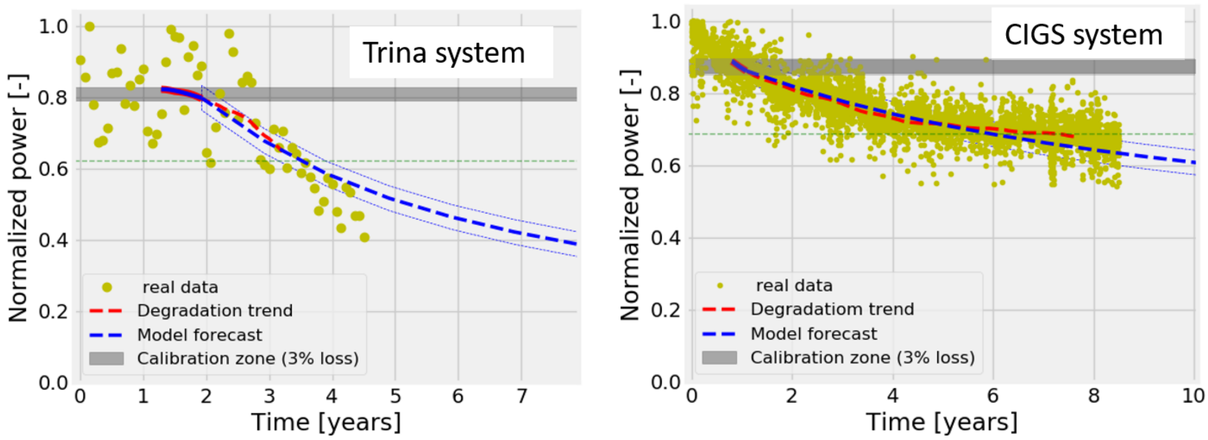

Figure 4.15: Model validation with experimental datasets of Trina (from DKA systems) and CIGS (from Bolzano systems). In yellow are the measurements, in red is the extracted degradation trend and in thick blue line is the model prediction with the 95% confidence interval. The horizontal green dotted line shows the -20% failure threshold of the degradation trend

4.2.4 Model application and comparison with statistical models

The performance of the proposed method is benchmarked against those of two statistical forecasting methods, namely ARIMA and Facebook prophet (FP). The reasons to select these methods is based on a study by Taylor and Letham Taylor and Letham (2018), where the performance of the different statistical models in long-term forecast was compared. In their study, FP was found to be outstanding in comparison with other models. The ARIMA model was characterized with the highest uncertainties. We selected the best and the least performing models to compare the accuracy of the proposed model and to investigate whether the nature of the data under evaluation could affect the models' performance. Moreover, both methodologies are simple to apply and commonly used in different fields. For example, the FP algorithm is implemented in common programming languages such as python and R [1]. The methodology was created as a flexible time series model which is configurable by non-experts. It is based on a decomposable time series model including

[1]The code can be accessed at: http://https://facebook.github.io/prophet/

trend, seasonality, holidays (not important for our application) and an error term. The model gives the opportunity to chose linear and logistic time series evolution, the second being suited for the non-linear behavior of PV performance. Furthermore, among the seasonality settings for different time resolutions, yearly seasonality was selected to detect yearly variations in power production due to the seasons of a year. The ARIMA model has free online packages Hyndman et al. (2018) and Hyndman and Khandakar (2008). In this study an auto-arima function which uses the akaike information criterion (AIC) to get the optimal model was used.

Table 4.9: Comparision of ARIMA, Facebook prophet and the proposed model at two prediction intervals. where, mc1 is mc-Si1, mc2 is mc-Si2, 1j is 1j-a-Si1, 3j is 3j-a-Si1, pc1 is pc-Si1, pc2 is pc-Si2, pc3 is pc-Si3 and rib is ribbon1

System	HIT1	mc1	mc2	pc1	pc2	pc3	1j	3j	rib	CdTe1	CIGS1
ARIMA											
$FT_{3\%}$[years]	21.4	NA	18.8	10.1	14.2	18.2	16.2	NA	13.8	16.4	NA
$RUL_{3\%}$[years]	12.9	NA	10.2	1.6	5.7	9.7	7.8	NA	5.3	7.9	NA
FT_{full}[years]	21.2	NA	14.5	NA	22.3	26.5	15.0	NA	21.8	12.5	4.0
RUL_{full}[years]	12.8	NA	6.0	NA	13.8	18.0	6.5	NA	13.3	4.0	-4.5
Rel_{diff} [%]	0.9	-	22.8	NA	36.3	31.3	36.7	-	21.8	23.8	NA
Facebook prophet											
$FT_{3\%}$[years]	34.6	37.8	13.8	9.8	9.5	15.3	15.1	21.0	9.4	14.9	NA
$RUL_{3\%}$[years]	26.1	29.3	5.3	1.3	1.0	6.8	6.6	12.5	0.9	6.4	NA
FT_{full}[years]	16.7	37.8	14.7	33.1	24.7	18.7	14.9	21.0	24.5	12.8	5.6
RUL_{full}[years]	8.2	29.8	6.2	24.7	16.2	10.2	6.4	12.5	16.0	4.2	-2.9
Rel_{diff} [%]	51.7	-	6.1	70.3	61.5	18.2	36.9	-	61.6	14.1	NA
Proposed											
$FT_{3\%}$	16.5	82.5	17.2	17.8	25.2	25.4	18.7	25.2	25.2	15.8	5.8
$RUL_{3\%}$ [years]	8.0	74.0	8.7	9.3	16.7	16.9	9.9	16.7	16.7	7.3	-2.7
FT_{full}[years]	15.4	82.5	17.2	14.7	24.3	18.8	21.8	25.2	24.3	15.2	6.5
RUL_{full}[years]	6.9	74.0	8.7	6.2	15.8	10.3	13.3	16.7	15.8	6.7	-2.0
Rel_{diff} [%]	6.7	-	0	17.4	3.6	25.9	14.2	-	3.6	3.8	10.8

The performance evaluation is carried out using the 11 Bolzano system datasets. The comparison of the three models is twofold: first, the models are compared on the lifetime forecast after a small performance degradation interval and second, on the consistence of the forecast at two different forecasting intervals. In the first attempt, the same system input data (normalized and STC irradiance corrected power time series with 3% performance degradation as training data) were tested on ARIMA and FP models. Unfortunately, no meaningful predictions were achieved because the number of calculated change points is greater than the number of observations in the dataset. Instead, the monthly Performance Ratio (PR) was used as the input parameter. The PR sets the actual yield of a PV system in relation with the expected yield at STC conditions IEC61724-1 (2017). For model comparison, the models are calibrated at two different intervals: first , at an interval corresponding to the 3% performance degradation and second , using the entire datasets corresponding to 8.5 years interval. The respective lifetime and RUL forecasts are shown in table 4.9.

Considering a 3% calibration threshold, it is visible that there are high discrepancies as well as unrealistic forecast scenarios (see figure 4.16) for both FP and ARIMA models.

In table 4.9 it is also observed that the failure times are either over- or under-estimated for the ARIMA and Facebook models. The over- and under-estimations can be correlated with the evaluated degradation trend which is influenced by the nature of the dataset as well as the number of data-points. Considering the calibration using the entire dataset, the FP and the proposed model show good agreement in the failure time forecast for most of the systems. This excludes the mc-Si1 system that appeared to be very stable with a performance degradation of less than 2% after 8.5 years. For this system, the proposed model shows an over-estimation of the failure time because the evaluated degradation is too small to achieve optimal calibrations. Comparing the variations in predictions at different calibration intervals, it can be seen that the proposed model displays a good consistency (on average 9.5% relative difference) compared to the other two models that displayed unrealistic scenarios. Although the FP showed a good agreement with the proposed model when calibrated using the entire dataset, it however displayed big variations in lifetime forecast between the two calibration intervals. Overall, the ARIMA model does not perform well in this study since it failed to converge for four systems. The model also tends to overfit the data, hence making it more sensitive to reversible performance reducing events. This is visible when looking at the pc-Si1 system (figure 4.17) where the model failed to converge when calibrated on the entire dataset. This implies that such a model is not useful for performance degradation forecast.

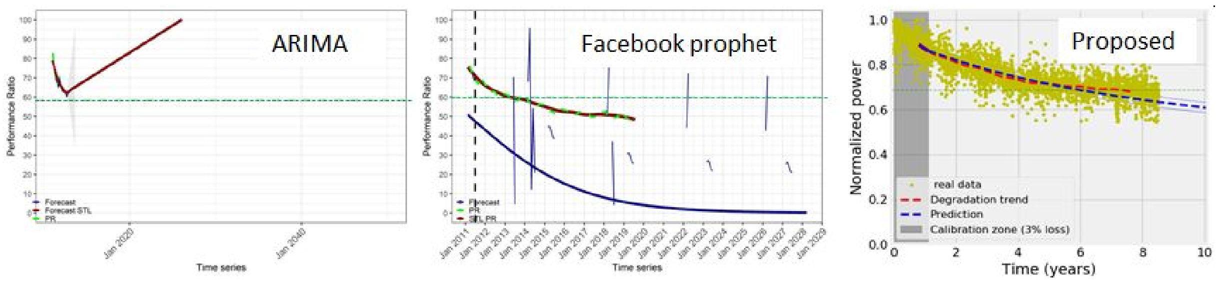

Figure 4.16: ARIMA, Facebook prophet and proposed methods when applied on a CIGS system with fewer data-points using a 3% threshold. The horizontal dotted green line shows the failure time threshold.

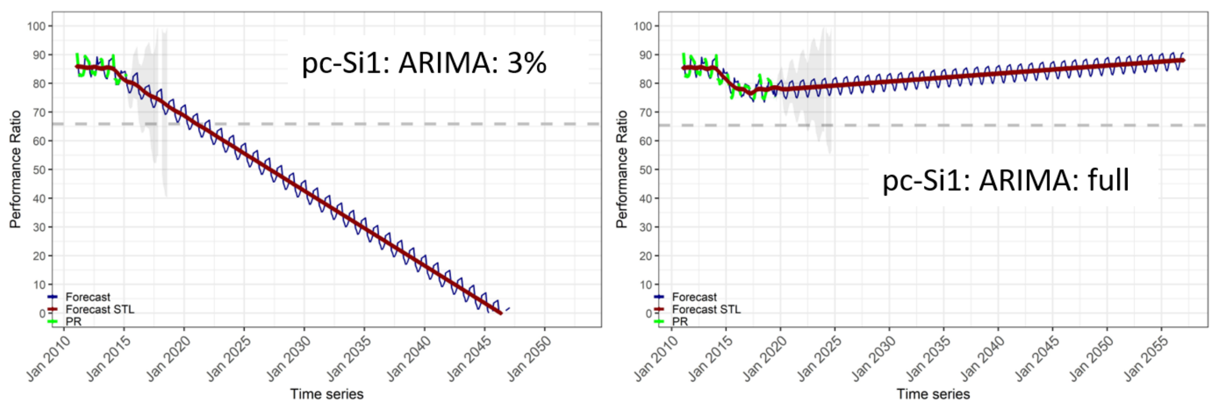

Figure 4.17: Forecast at 3% and entire data-set calibration thresholds using auto-ARIMA model. The figure shows overfiting when calibration is done on the entire dataset.

Considering the calibration using the entire data-sets, the Facebook and the proposed model showed a good agreement in the failure time forecast for most of the systems. This excludes the mc-Si1 system that appeared to be very stable with a performance degradation of less than 2% after 8.5 years. For this system, the proposed model shows an overestimation of the failure time because the evaluated degradation is too small to achieve optimal calibrations. Comparing the variations in predictions at different calibration intervals, it can be seen that the proposed model displays a good consistence compared to the other two models. Although the Facebook prophet showed a good agreement with the proposed model when calibrated using the entire data-sets, it however displayed big variations in lifetime forecast between the two calibration intervals. Overall, the ARIMA model showed the under-performance in this study since for over four systems it failed to converge. The model also tends to overfit the data, hence making it more sensitive with performance reducing events that could be reversed. This can be clearly displayed in pc-Si1 system (figure 4.17) where the model failed to converge when calibrated on the entire dataset. This implies, that such a model is not sufficient for performance degradation forecast.

4.2.5 Model limits and uncertainties

Although the proposed model has displayed a good performance on a number of PV modules and systems, it is however bound to some limits and uncertainties that could deteriorate the prediction accuracy. The model limits and uncertainties are identified as:

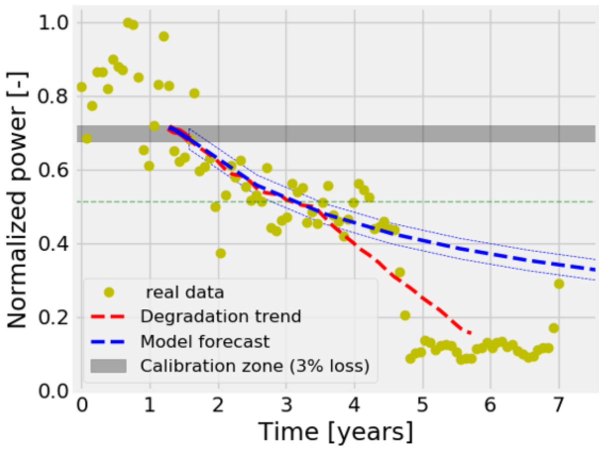

Figure 4.18: System showing a sudden drop in power (around the green box), in blue is the model forecast. The horizontal green dotted line shows the -20% failure threshold of the degradation trend

The model works well when the degradation is gradual and continuous, it cannot forecast events that might lead to dramatic or sudden power losses, such as breakage, fire, or catastrophic failures. For example, figure 4.18 shows one of the DKASC Alice Spring systems; eco-Kinetics-26.5kW-mono-Si-Dual (2010), which experiences a sudden drop in performance. According to the information from the DKA website, this sharp drop in performance was attributed to one PV module in this PV array that was damaged during a windstorm. Hence, the cause is identified as a partial failure of one array string in which this damaged module is connected.

The model is based on degradation patterns; hence it is influenced by the extracted degradation trends. The degradation trend is extracted from time series data by applying the condition in equation 3.30. Changing the tolerance (tol) value affects the extracted degradation trend as shown in figure 4.19a. Figure 4.19b shows how the calibration as well as the forecast error varies with tol. The RMSE was calculated using equation 3.31 and is converted to percentage.

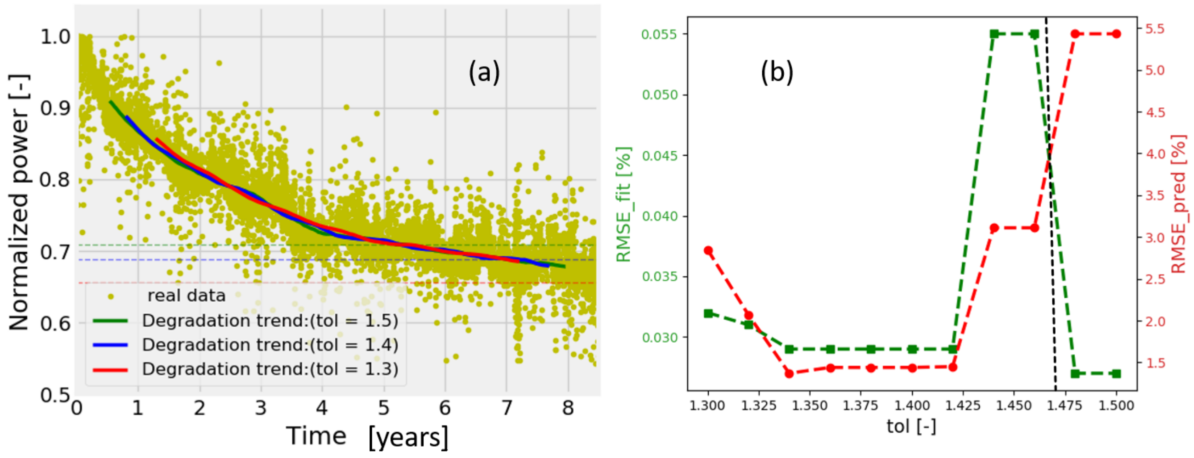

Figure 4.19: A, Variation of the extracted degradation at different values of tol, the horizontal dotted lines show the -20% failure threshold of the degradation trend. B, is the variation of the fitting error (RMSE-fit) and forecast error (RMSE-pred) with different values of tol

According to the evaluated datasets in this study, the value tol and the extracted degradation trend highly depend on the resolution and the outliers in a given dataset. For data sets with a monthly or yearly resolution, the values of tol ranged from 0.9 to 1.25 while datasets with high resolution of 15 minutes, the values were between 1.4 and 1.65. The tolerance factor tol is very useful as it provides a parameter for optimization adapted to the datasets variability unlike the black box automated algorithms.

4.2.6 Assessing the effects of PV modules long-term degradation on lifetime energy yield

To mitigate the financial investment risks for PV systems stakeholders, it is a prerequisite to reliably predict the long-term energy yield. Recently Reise et al. (2018) have reported the different sources of uncertainties in PV systems yield predictions and assessments. A big challenge was on how the degradation effects are taken into account during long-term yield predictions. Indeed, the authors reported that, this is the most unexplored challenge and varies from analysist to analysist. Therefore, in this section we show how the proposed model could be applied to long-term yield predictions to lower the uncertainties associated to long-term performance degradation and hence improve the long-term yield prediction accuracy. Hence we point out that, the scope of the study is limited to analyzing the impact (sensitivity) of degradation to long-term yield prediction and not to propose a model for yield prediction.

The described method is applied to 7 of the TISO modules (TEA1, TEA4, TEA6, TEA8, TEA10, TEB1, TEB2) to extract the degradation trends independent of measurement uncertainties and to forecast the power degradation from a -5% to a 35 years time frame (the current modules age). To expand our analysis, three degradation scenarios; linear with a constant rate, non-linear (proposed but with a constant degradation rate) as well as non-linear (proposed with a time dependent degradation rate) are assumed. The comparison with a linear approximation is of ultimate importance because it is commonly used during long-term yield evaluation according to Reise et al. (2018). Figure 4.20 shows the results of two of the modules TEA1 and TEA8 that showed the best and the worst forecasts when using the linear approximation.

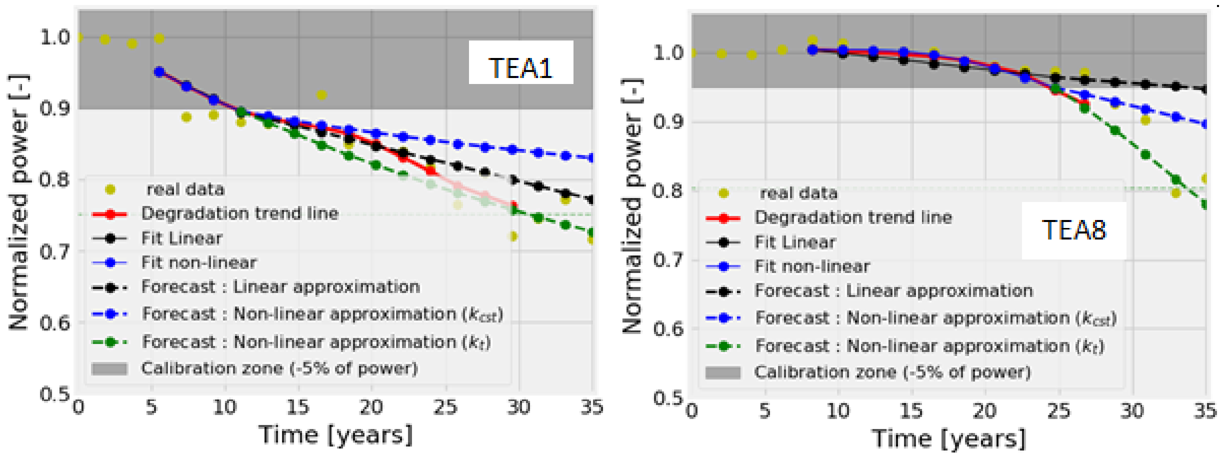

Figure 4.20: (TEA1) and (TEA8) TISO modules that displayed lower and higher uncertainties when long-term predictions are made with a linear approximation (black). The green and blue curves show the forecasts with the non-linear degradation with time dependent rate and with a constant rate respectively. In yellow are the measured data points and in red is the degradation trend

It can be seen that the new approach (non-linaer with a time dependent degradation rate) displays consistent results considering the measured data (real data). Since the intended exercise is to assess how this will affect the long-term yield predictions, all the approximations are correlated to the uncertainties in yield evaluations. This was achieved by comparing the relative loss of lifetime energy yield of the measured degradation for the 35 years with the predicted ones as shown in table 4.10. It can be seen that using the proposed long-term degradation method (non-linear with a time dependent rate) reduced the prediction uncertainties to 37.6% on average. Moreover, it is seen that a linear approximation with a constant degradation rate is associated with the highest uncertainties of over 64.7 on average. Indeed, the dependence of the prediction uncertainties to the degradation patterns is clearly visible in the two modules. For module TEA1 with a linear degradation pattern the uncertainty is small compared to module TEA8 with an exponential degradation pattern. Moreover, the residual standard deviation calculated according to equation 3.22, further confirms these discrepancies. Meaning that the linear approximation cannot reliably fit or describe the different degradation patterns observed in the field.

Table 4.11 shows the failure time (defined as the time needed for power to decrease by -20% of the initial value). It is observed that using the proposed method (non-linear approximation with a time dependent rate), consistent failure time forecasts are achieved. On contrary, using a linear as well as a non-linear approximation but with a constant rate, some unrealistic scenarios are predicted for some modules. Indeed these scenarios are correlated with the degradation patterns. These calculations demonstrate that if these scenarios are included in the lifetime yield predictions, they can lead to over estimation of the lifetime yield. Hence the proposed model could provide a solution to improve the lifetime yield accuracy.

Table 4.10: Comparison of evaluated loss in lifetime energy yield in 35 years using the 3 degradation approximation scenarios. Relative uncertainty is calculated according to the measured yield loss

Module name	TEA1	TEA4	TEA6	TEA8	TEA10	TEB1	TEB2
Measured							
Loss of lifetime energy [years]	-19.04	-7.86	-9.07	-6.58	-5.09	-8.87	6.97
Linear							
Loss of lifetime energy [years]	-15.70	-3.38	-0.46	+0.37	-0.29	-5.70	-3.57
Relative uncertainty [%]	17.5	57.0	94.9	105.7	94.3	35.7	48.8
Non-linear with a constant rate							
Loss of lifetime energy [years]	-12.74	-3.84	-1.38	-1.47	-1.21	-6.47	-4.93
Relative uncertainty [%]	33.1	51.1	84.7	78.6	76.2	27.1	29.3
Non-linear with a time dependent rate							
Loss of lifetime energy [years]	-39.7	-16.89	-4.25	-13.55	-2.46	-8.86	-6.81
Relative uncertainty [%]	52.0	53.4	52.8	51.4	51.6	0.1	2.3

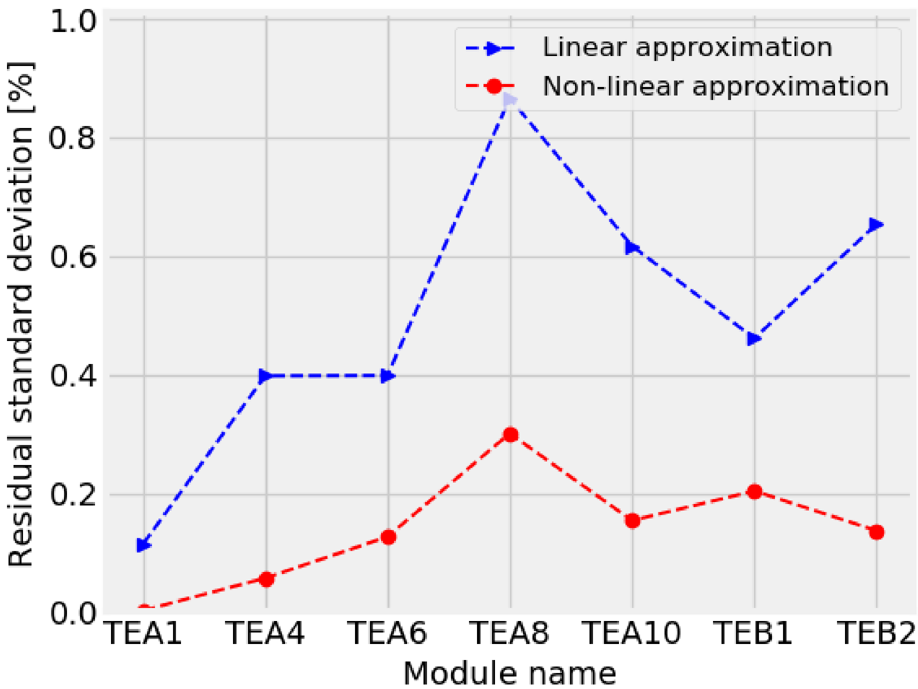

Figure 4.21: Residual standard deviation of the 7 TISO modules fitted at -5% degradation using linear and non-linear models respectively

4.2.7 Simplified User Interface (PVLife Toolbox)

After optimizing, testing and further validating our model under different data scenarios, the described approach is embedded into a simplified user interface for PV lifetime forecast called 'PVLife toolbox' as shown in figure 4.22. This simplified interface is aimed to be applicable by any user, even without deep knowledge in data analysis. The toolbox has for main buttons; the browse button that allows to enter the data path, the run button

Table 4.11: Comparison of evaluated loss in lifetime energy yield in 35 years using the 3 degradation approximation scenarios. Relative uncertainty is calculated according to the measured yield loss

Module name	TEA1	TEA4	TEA6	TEA8	TEA10	TEB1	TEB2
Linear							
Failure time [years]	38.7	82.7	96.4	123.7	112.0	75.9	116.6
Non-linear with a constant factor							
Failure time [years]	95.0	92.5	82.8	52.8	77.1	73.9	67.1
Non-linear with a time dependent factpr							
Failure time [years]	29.8	33.1	38.0	33.4	44.1	38.8	39.9

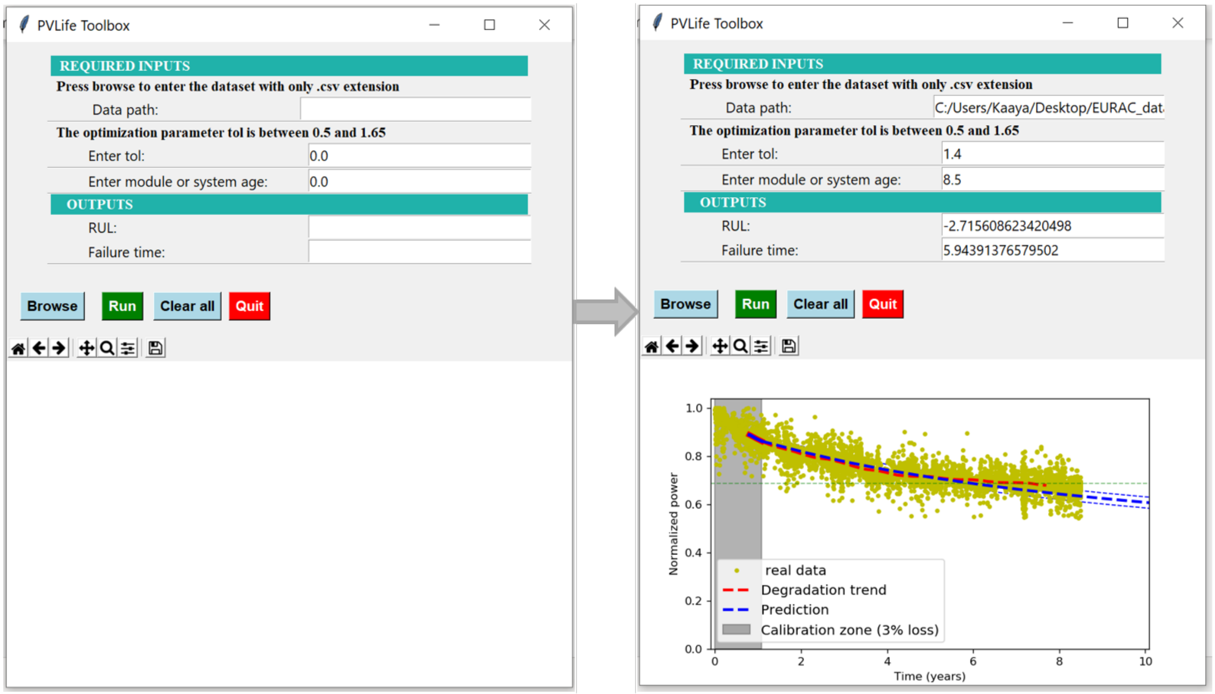

Figure 4.22: PVLife Toolbox, on the left is the layout before simulation and on the right is the layout after simulation

that starts the simulation, the clear button that deletes the current inputs-output to allow entrance of new inputs and the quit button that exits the toolbox. The toolbox has been created using the module Tkinter in python therefore it can run on the python interface.

4.3 Results for the hybrid model

4.3.1 Application of the hybrid model

After calibration and validation of both the physical and the data-driven methods, both approaches are combined into a hybrid model as described in section 3.3. The hybrid model is then applied to re-calculate the failure time of the three mono-crystalline modules. The results are compared with the one from the physical model as in table 4.12. Figure 4.23 shows the evolution of the degradation trends for the physical as well as the hybrid model. If we base our argument on the module installed on Zugspitze and on the current bill of materials, we can conclude that the predicted failure time with the hybrid method is more probable as compared to the failure time evaluated with only a physical model.

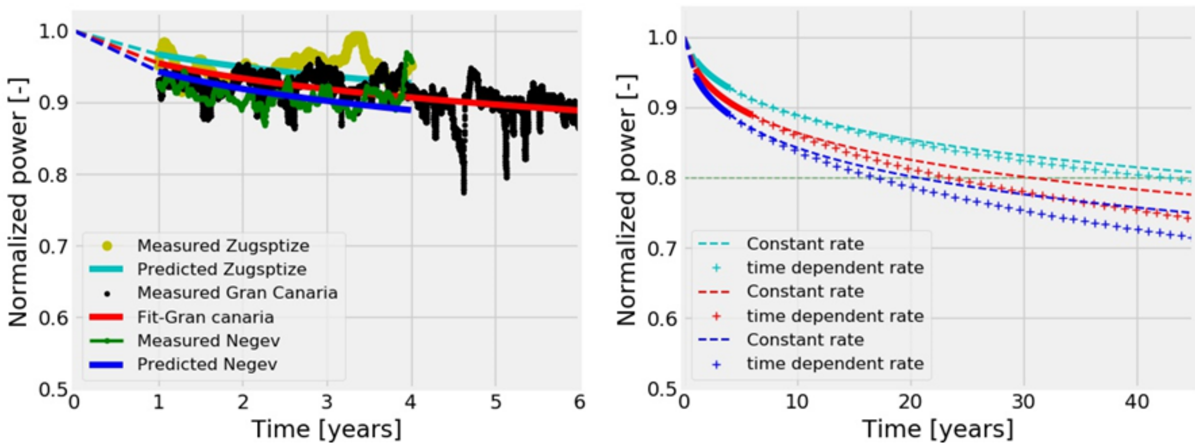

Figure 4.23: On the right: model and measured degradation trend until the time of exposure. On the left: bold lines, measured trend, dotted lines model forecast for with a physical model (using constant rate) and with a hybrid model (using time dependent rate). The colors represent the three climatic locations.

Table 4.12: Comparison of the physical model and the hybrid models

Module Location	Failure time [years]		Relative difference
	Hybrid model	Physical model	
Zugspitze	42.4	52.8	19.7 %
Gran Canaria	23.6	31.6	25.3 %
Negev	17.0	21.4	20.6 %

Chapter 5

Conclusion

When exposed in outdoor environment, PV modules as well as systems are affected by continuous cycles of temperature, humidity, irradiation, mechanical stress, and soiling. These environmental factors cause different degradation modes to take place within a PV module and reduce the performance of the system. Therefore, it is necessary to develop diagnostic techniques, lower the performance uncertainty, and predict the behavior of PV systems with higher accuracy. In this research, two main modelling approaches to predict the degradation rates, the failure time and the remaining useful lifetime of PV modules as well as systems have been proposed.

On the one hand, a physical model for quantifying the impact of combined climatic stresses on module maximum power output degradation is proposed. Degradation rate models are proposed and validated with indoor measurements for specific degradation precursors. A combined degradation rate model is developed. The model is calibrated and validated with real field data sets using three identical mono-crystalline modules installed in three climatic zones: maritime, arid and alpine. Severe degradation is predicted in the arid climate characterized by high temperatures. Using EAR5 reanalysis datasets to evaluate the model's input climatic variables, global risk maps of the specific degradation mechanisms and the combined rate model are created. The maps are evaluated based on the studied mono-crystalline modules, and they represent a correlation of different climatic zones to the different degradation mechanisms. For-example, according to the the Köppen-Geiger Photovoltaic (KGPV) climate classification, thermo-mechanical degradation is the harshest for the studied PV module in mostly all climate zones, presenting the highest impact in very high irradiation zones. Photo-degradation and hydrolysis-degradation show similar global spatial distribution, but the first one is higher since it comprises also UV irradiation as a degradation factor. Although, due to the high uncertainty in real degradation rate of PV systems (solar resource, methodology of calculation, quality of operational data, bill-of-materials of PV modules, etc.), the presented maps might not be representative of the actual absolute degradation rates, however, they can be used as a guide to identify possible risk areas in terms of climate stresses.

On the other hand, a data-driven approach is also proposed, the model is aimed to improve the long-term degradation forecasting accuracy using a shorter degradation history. In developing the model, multiple degradation factor models dependent on the degradation patterns as well as time are proposed to describe the different degradation patterns. The data-driven method is based on the monitored degradation and has been calibrated to provide reliable forecast using a short degradation history of only 3%. During the model development, a focus is put on data treatment especially on extraction of the degradation trends independent of any reversible performance reducing effect or measurement uncertainties. Therefore, a computer aided approach is proposed to extract the degradation trends from the outdoor data. The model has been validated using different PV module and system datasets with observed long-term degradation. The performance of the proposed model is benchmarked against two statistical methods, namely ARIMA and Facebook prophet, using the time series of 11 experimental PV plants (with different PV technologies). The proposed model displays outstanding performance when forecasts are made after a shorter time compared to the two statistical models which displayed unrealistic forecasts. The model also displays consistent results with a 9.5% average relative uncertainty of the evaluated failure time when forecasts are made at different intervals, which is not the case for the two statistical models. Therefore, the obvious advantages of the proposed model over other data-driven models are that, it is applicable after a small performance degradation of only 3%, which usually can be observed after a short operation time and it is applicable on fewer data points. Another advantage of the proposed approach is that, it is based on a systematic approach for selecting the data and parameters of the models making it applicable for degradation evaluation on a wide range of data distributions. Hence, the models' performance can be well understood and a correlation of different parameters can be achieved, which is not the case for many empirical, data-driven techniques, especially those with a black-box character. Moreover, the model is also applicable to all PV technologies.

On addition, the proposed data-driven model has been applied to assess the effects of long-term degradation to lifetime yield prediction. The assessment has been carried out by assuming three degradation scenarios; linear and non-linear with a constant degradation rate as well as non-linear with a time dependent degradation rate (proposed). Using the latter made it possible to lower the long-term yield prediction relative uncertainty to 37.6% on average compared to 54.4% and 64.7% for a non-linear and linear with a constant degradation rate respectively. Lastly, a 'PVLife toolbox' based on the data-driven algorithms has been developed in this research with a simplified interface to be applicable by any one even without deep knowledge in data analysis.

Finally, the two approach are combined into a hybrid model to achieve a good forecasting accuracy by deploying data-driven algorithms and also to have a physical understanding of the evaluated rates through physical models. The hybrid model has been benchmarked with physical model to evaluate the lifetime of three aforementioned experimental monocrystalline modules and it proves to provide more consistent results. The proposed hybrid model will aid to have more reliable long-term degradation forecast as well as having a physical understanding of the dominating degradation mechanisms influencing the performance degradation. We believe such a model is useful to calculate more reliable levelized cost of energy and thus the economic viability of solar energy as well as to aid in PV materials development that can withstand the different environmental conditions.

Bibliography

Annigoni, E., A. Virtuani, M. Cavvicio, G. Friesen, D. Chianese, and C. Ballif (2019). 35 years of photovoltaics: Analysis of the TISO-10-kW solar plant, lessons learnt in safety and performance – Part 2. 38

Annigoni, E., A. Virtuani, F. Sculati-Meillaud, and C. Ballif (2017, June). Modeling Potential-Induced Degradation (PID) of Field-Exposed Crystalline Silicon Solar PV Modules: Focus on a Regeneration Term. In 2017 IEEE 44th Photovoltaic Specialist Conference (PVSC), pp. 2794–2798. 14, 46

Ascencio-Vasquez, J. (2020). Modelling and worldwide assessment of performance and aging of photovoltaic modules and systems. 75, 76

Ascencio-Vásquez, J., K. Brecl, and M. Topič (2019, October). Methodology of Köppen-Geiger-Photovoltaic climate classification and implications to worldwide mapping of PV system performance. Solar Energy 191, 672–685. 38, 47

Bala Subramaniyan, A., R. Pan, J. Kuitche, and G. TamizhMani (2018, September). Quantification of Environmental Effects on PV Module Degradation: A Physics-Based Data-Driven Modeling Method. IEEE Journal of Photovoltaics 8(5), 1289–1296. 1, 17, 19, 46, 47

Bosco, N., T. J. Silverman, and S. Kurtz (2016, July). Climate specific thermomechanical fatigue of flat plate photovoltaic module solder joints. Microelectronics Reliability 62, 124–129. 17

Braisaz, B., C. Duchayne, M. Van Iseghem, and K. Radouane (2014, September). PV Aging Model Applied to Several Meteorological Conditions. In 29th PVSEC Proceedings, Amsterdam, pp. 2303–2309. 8, 14, 15, 16, 17

Brownlee, J. (2017, February). Introduction to Time Series Forecasting With Python: How to Prepare Data and Develop Models to Predict the Future. Machine Learning Mastery. 37

Buck, A. L. (1981, December). New Equations for Computing Vapor Pressure and Enhancement Factor. Journal of Applied Meteorology 20(12), 1527–1532. 30

(C3S) (2017). Era5: Fifth generation of ecmwf atmospheric reanalyses of the global climate . copernicus climate change service climate data store. Technical report, https://cds.climate.copernicus.eu/cdsapp, Paris. 29

Cañete, C., J. Carretero, and M. Sidrach-de Cardona (2014, February). Energy performance of different photovoltaic module technologies under outdoor conditions. Energy 65, 295–302. 36

Chen Xiongzi, Yu Jinsong, Tang Diyin, and Wang Yingxun (2011, August). Remaining useful life prognostic estimation for aircraft subsystems or components: A review. In IEEE 2011 10th International Conference on Electronic Measurement Instruments, Volume 2, pp. 94–98. 6, 35

Crommelynck, D. and A. Joukoff (1990, January). A simple algorithm for the estimation of the spectral radiation distribution on a horizontal surface, based on global radiation measurements. Solar Energy 45(3), 131–137. 30

DKASC, A. S. (2019). DKASC, Alice Springs | DKA Solar Centre |, http://dkasolarcentre.com.au/locations/alice-springs, 2019-11-08 . 38

Driemel, A., J. Augustine, K. Behrens, S. Colle, C. Cox, E. Cuevas-Agulló, F. M. Denn, T. Duprat, M. Fukuda, H. Grobe, M. Haeffelin, G. Hodges, N. Hyett, O. Ijima, A. Kallis, W. Knap, V. Kustov, C. N. Long, D. Longenecker, A. Lupi, M. Maturilli, M. Mimouni, L. Ntsangwane, H. Ogihara, X. Olano, M. Olefs, M. Omori, L. Passamani, E. B. Pereira, H. Schmithüsen, S. Schumacher, R. Sieger, J. Tamlyn, R. Vogt, L. Vuilleumier, X. Xia, A. Ohmura, and G. König-Langlo (2018, August). Baseline Surface Radiation Network (BSRN): structure and data description (1992–2017). Earth System Science Data 10(3), 1491–1501. 30

Dunn, L., M. Gostein, and B. Stueve (2013, February). Literature Review of the Effects of UV Exposure on PV Modules. In NREL PV Module Reliability Workshop. 16

Escobar, L. A. and W. Q. Meeker (2007, August). A Review of Accelerated Test Models. arXiv:0708.0369 [stat]. arXiv: 0708.0369. 11, 16, 24

Faiman, D. (2008). Assessing the outdoor operating temperature of photovoltaic modules. Progress in Photovoltaics: Research and Applications 16(4), 307–315. 31

Gaines, G. B., R. E. Thomas, G. T. Noel, T. S. Shilliday, V. E. Wood, and D. C. Carmichael (1978). Development of accelerated test design for service-life prediction of solar array at Mead, Nebraska. Quarterly report. 17, 18

Gok, A., D. K. Ngendahimana, C. L. Fagerholm, R. H. French, J. Sun, and L. S. Bruckman (2017, December). Predictive models of poly(ethylene-terephthalate) film degradation under multi-factor accelerated weathering exposures. PLOS ONE 12(5), e0177614. 23

Gu, X., Y. Lyu, L.-C. Yu, C.-C. Lin, and D. Stanley (2015, December). Effect of Intensity and Wavelength of Spectral UV Light on Discoloration of Laminated Glass/EVA/PPE PV Module. In 3rd Atlas-NIST Workshop on PV Materials Durability. 16

Hacke, P., S. Spataru, S. Johnston, K. Terwilliger, K. VanSant, M. Kempe, J. Wohlgemuth, S. Kurtz, A. Olsson, and M. Propst (2016, November). Elucidating PID Degradation Mechanisms and In Situ Dark I–V Monitoring for Modeling Degradation Rate in CdTe Thin-Film Modules. IEEE Journal of Photovoltaics 6(6), 1635–1640. 14

Hacke, P., S. Spataru, K. Terwilliger, G. Perrin, S. Glick, S. Kurtz, and J. Wohlgemuth (2015, November). Accelerated Testing and Modeling of Potential-Induced Degradation as a Function of Temperature and Relative Humidity. IEEE Journal of Photovoltaics 5(6), 1549–1553. 14

Halm, A., A. Schneider, V. D. Mihailetchi, L. J. Koduvelikulathu, L. M. Popescu, G. Galbiati, H. Chu, and R. Kopecek (2015, August). Potential-induced Degradation for Encapsulated n-type IBC Solar Cells with Front Floating Emitter. Energy Procedia 77, 356–363. 14

Hattendorf, J., A. Blauaermel, D. Koshnicharov, M. C. Koekten, L. Wulff, W.-M. Gnehr, R. Löw, and J. A. Esquivel (2012, October). Potential Induced Degradation in Mono-Crystalline Silicon Based Modules: An Acceleration Model. In 27th European PVSEC Proceedings, pp. 3405–3410. 14, 15

Huld, T. and A. M. G. Amillo (2015, June). Estimating PV Module Performance over Large Geographical Regions: The Role of Irradiance, Air Temperature, Wind Speed and Solar Spectrum. Energies 8(6), 5159–5181. 30, 31

Hyndman, R. J., G. Athanasopoulos, C. Bergmeir, G. Caceres, L. Chhay, M. O'Hara-Wild, F. Petropoulos, S. Razbash, E. Wang, and F. Yasmeen (2018). forecast: Forecasting Functions for Time Series and Linear Models version 8.10 from CRAN. 57

Hyndman, R. J. and Y. Khandakar (2008, July). Automatic Time Series Forecasting: The forecast Package for R. Journal of Statistical Software 27(1), 1–22. 57

IEC61724-1 (2017). Photovoltaic system performance, Part 1: Monitoring. Geneva, CH: International Electrotechnical Commission;2017. 57

Jordan, D. and S. Kurtz (2010, June). Analytical improvements in PV degradation rate determination. In 2010 35th IEEE Photovoltaic Specialists Conference, pp. 002688–002693. ISSN: 0160-8371, 0160-8371. 11

Jordan, D. C., C. Deline, M. G. Deceglie, A. Nag, G. M. Kimball, A. B. Shinn, J. J. John, A. A. Alnuaimi, A. B. A. Elnosh, W. Luo, A. Jain, M. U. Saleh, H. von Korff, Y. Hu, J.-N. Jaubert, and F. Mavromatakis (2020, January). Reducing Interanalyst Variability in Photovoltaic Degradation Rate Assessments. IEEE Journal of Photovoltaics 10(1), 206–212. 1

Jordan, D. C. and S. R. Kurtz (2013). Photovoltaic Degradation Rates—an Analytical Review. Progress in Photovoltaics: Research and Applications 21(1), 12–29. 5, 23

Jordan, D. C., T. J. Silverman, B. Sekulic, and S. R. Kurtz (2017). PV degradation curves: non-linearities and failure modes. Progress in Photovoltaics: Research and Applications 25(7), 583–591. 33

Jordan, D. C., T. J. Silverman, J. H. Wohlgemuth, S. R. Kurtz, and K. T. VanSant (2017a). Photovoltaic failure and degradation modes. Progress in Photovoltaics: Research and Applications 25, 318–326. 16

Jordan, D. C., T. J. Silverman, J. H. Wohlgemuth, S. R. Kurtz, and K. T. VanSant (2017b). Photovoltaic failure and degradation modes. Progress in Photovoltaics: Research and Applications 25(4), 318–326. 26, 42

Kempe, M. D. (2006, October). Modeling of rates of moisture ingress into photovoltaic modules. Solar Energy Materials and Solar Cells 90(16), 2720–2738. 23

Kempe, M. D. (2014, June). Evaluation of the uncertainty in accelerated stress testing. In 2014 IEEE 40th Photovoltaic Specialist Conference (PVSC), pp. 2170–2175. ISSN: 0160-8371. 17

Kempe, M. D., G. Jorgensen, K. Terwilliger, T. J. McMahon, C. E. Kennedy, and T. T. Borek (2007). Acetic Acid Production and Glass Transition Concerns with Ethylene-Vinyl Acetate Used in Photovoltaic Devices. 8

Kersten, F., F. Fertig, K. Petter, B. Klöter, E. Herzog, M. Strobel, J. Heitmann, and J. W. Müller (2017). System performance loss due to LeTID. 36, 37

Klünter, C., I. Rauschen, K. Reinartz, B. Müller, B. Farnung, and K. Kiefer (2019, October). Degradation in PV Power Plants: Theory and Practice. 36th European Photovoltaic Solar Energy Conference and Exhibition, 1331–1335. 37

Koehl, M., M. Heck, and S. Wiesmeier (2012, April). Modelling of conditions for accelerated lifetime testing of Humidity impact on PV-modules based on monitoring of climatic data. Solar Energy Materials and Solar Cells 99, 282–291. 24

Koehl, M., M. Heck, and S. Wiesmeier (2018). Categorization of weathering stresses for photovoltaic modules. Energy Science & Engineering 6(2), 93–111. 27, 49

Koehl, M., M. Heck, S. Wiesmeier, and J. Wirth (2011, July). Modeling of the nominal operating cell temperature based on outdoor weathering. Solar Energy Materials and Solar Cells 95(7), 1638–1646. 27

Koehl, M., S. Hoffmann, and S. Wiesmeier (2017). Evaluation of damp-heat testing of photovoltaic modules. Progress in Photovoltaics: Research and Applications 25(2), 175–183. 23

Koehl, M., D. Philipp, N. Lenck, and M. Zundel (2009, August). Development and application of a UV light source for PV-module testing. In Proceedings of SPIE - The International Society for Optical Engineering 7412. 16

Kratochvil, J. A., W. E. Boyson, and D. L. King (2004). Photovoltaic array performance model. 31

Köntges, M., S. Kurtz, C. E. Packard, U. Jahn, K. A. Berger, K. Kato, T. Friesen, H. Liu, M. Van Iseghem, J. Wohlgemuth, D. Miller, M. Kempe, P. Hacke, F. Reil, N. Bogdanski, W. Herrmann, C. Buerhop-Lutz, G. Razongles, and G. Friesen (2014). Review of Failures of Photovoltaic Modules. Report, IEA International Energy Agency. 8, 14, 26, 33, 35

Köntges, M., G. Oreski, U. Jahn, M. Herz, P. Hacke, and K.-A. Weiß (2017). Assessment of photovoltaic module failures in the field : International Energy Agency Photovoltaic Power Systems Programme : IEA PVPS Task 13, Subtask 3 : report IEA-PVPS T13-09:2017. Technical report, International Energy Agency, Paris. 1, 6

Laayouj, N., H. Jamouli, and M. E. Hail (2016, December). Intelligent Prognostic Framework for Degradation Assessment and Remaining Useful Life Estimation of Photovoltaic Module. Journal of Engineering and Technological Sciences 48(6), 772–795–795. 32

Lausch, D., V. Naumann, A. Graff, A. Hähnel, O. Breitenstein, C. Hagendorf, and J. Bagdahn (2014, January). Sodium Outdiffusion from Stacking Faults as Root Cause for the Recovery Process of Potential-induced Degradation (PID). Energy Procedia 55, 486–493. 14

Listou Ellefsen, A., E. Bjørlykhaug, V. Æsøy, S. Ushakov, and H. Zhang (2019, March). Remaining useful life predictions for turbofan engine degradation using semi-supervised deep architecture. Reliability Engineering & System Safety 183, 240–251. 32

Marín, M. L., A. Jiménez, J. López, and J. Vilaplana (1996, July). Thermal degradation of ethylene (vinyl acetate). Journal of thermal analysis 47(1), 247–258. 23

Masuda, A., N. Uchiyama, and Y. Hara (2015, March). Degradation by acetic acid for crystalline Si photovoltaic modules. Japanese Journal of Applied Physics 54(4S), 04DR04. 8

McKay, M. D., J. D. Morrison, and S. C. Upton (1999, March). Evaluating prediction uncertainty in simulation models. Computer Physics Communications 117(1), 44–51. 31

Meyers, B., M. Deceglie, C. Deline, and D. Jordan (2019, November). Signal Processing on PV Time-Series Data: Robust Degradation Analysis without Physical Models. arXiv:1907.09456 [eess]. arXiv: 1907.09456. 1, 2

Miller, D. C., E. Annigoni, A. Ballion, J. G. Bokria, L. S. Bruckman, D. M. Burns, Xinxin Chen, L. Elliott, Jiangtao Feng, R. H. French, S. Fowler, Xiaohong Gu, P. L. Hacke, C. C. Honeker, M. D. Kempe, H. Khonkar, M. Köhl, L.-E. Perret-Aebi, N. H. Phillips, K. P. Scott, F. Sculati-Meillaud, T. Shioda, S. Suga, S. Watanabe, and J. H. Wohlgemuth (2015, June). Degradation in PV encapsulation transmittance: An interlaboratory study towards a climate-specific test. In 2015 IEEE 42nd Photovoltaic Specialist Conference (PVSC), pp. 1–6. ISSN: null. 30

Moser, D., M. D. Buono, U. Jahn, M. Herz, M. Richter, and K. D. Brabandere (2017). Identification of technical risks in the photovoltaic value chain and quantification of the economic impact. Progress in Photovoltaics: Research and Applications 25(7), 592–604. 6, 14

Munoz, M. A., M. C. Alonso-García, N. Vela, and F. Chenlo (2011, September). Early degradation of silicon PV modules and guaranty conditions. Solar Energy 85(9), 2264–2274. 16

Naumann, V., T. Geppert, S. Großer, D. Wichmann, H.-J. Krokoszinski, M. Werner, and C. Hagendorf (2014, January). Potential-induced Degradation at Interdigitated Back Contact Solar Cells. Energy Procedia 55, 498–503. 14

Ndiaye, A., A. Charki, A. Kobi, C. M. F. Kébé, P. A. Ndiaye, and V. Sambou (2013, October). Degradations of silicon photovoltaic modules: A literature review. Solar Energy 96, 140–151. 8, 23

Ngo, T., Y. Heta, T. Doi, and A. Masuda (2016, April). Effects of UV on power degradation of photovoltaic modules in combined acceleration tests. Japanese Journal of Applied Physics 55(5), 052301. 24, 49

Omazic, A., G. Oreski, M. Halwachs, G. C. Eder, C. Hirschl, L. Neumaier, G. Pinter, and M. Erceg (2019, April). Relation between degradation of polymeric components in crystalline silicon PV module and climatic conditions: A literature review. Solar Energy Materials and Solar Cells 192, 123–133. 50

Pan, R., J. Kuitche, and G. Tamizhmani (2011, January). Degradation analysis of solar photovoltaic modules: Influence of environmental factor. In 2011 Proceedings - Annual Reliability and Maintainability Symposium, pp. 1–5. ISSN: 0149-144X, 0149-144X. 8

Park, N., C. Han, and D. Kim (2013, December). Effect of moisture condensation on long-term reliability of crystalline silicon photovoltaic modules. Microelectronics Reliability 53(12), 1922–1926. 8, 23

Philipp, D., T. Geipel, P. Gebhardt, A. Schmid, T. Naeem, and E. Fokuhl (2019, October). LeTID - A Comparison of Test Methods on Module Level. 36th European Photovoltaic Solar Energy Conference and Exhibition, 816–821. 36, 37

Phinikarides, A., N. Kindyni, G. Makrides, and G. E. Georghiou (2014, December). Review of photovoltaic degradation rate methodologies. Renewable and Sustainable Energy Reviews 40, 143–152. 2, 6

Reise, C., B. Müller, D. Moser, G. Belluardo, and P. Ingenhoven (2018, April). Task 13: Uncertainties in PV System Yield Predictions and Assessments. 60, 61

Rizzo, A., A. Cester, M. V. Madsen, F. C. Krebs, and S. A. Gevorgyan (2018). A Novel Algorithm for Lifetime Extrapolation, Prediction, and Estimation of Emerging PV Technologies. Small Methods 2(1), 1700285. 33

Schwingshackl, C., M. Petitta, J. E. Wagner, G. Belluardo, D. Moser, M. Castelli, M. Zebisch, and A. Tetzlaff (2013, January). Wind Effect on PV Module Temperature: Analysis of Different Techniques for an Accurate Estimation. Energy Procedia 40, 77–86. 31

Segado, P. M., J. Carretero, and M. Sidrach-de-Cardona (2015). Models to predict the operating temperature of different photovoltaic modules in outdoor conditions. Progress in Photovoltaics: Research and Applications 23(10), 1267–1282. 31

Sharma, V. and S. S. Chandel (2013, November). Performance and degradation analysis for long term reliability of solar photovoltaic systems: A review. Renewable and Sustainable Energy Reviews 27, 753–767. 23

Sheng, Z., Q. Hu, J. Liu, and D. Yu (2019, January). Residual life prediction for complex systems with multi-phase degradation by ARMA-filtered hidden Markov model. Quality Technology & Quantitative Management 16(1), 19–35. 32

Swanson, R., M. Cudzinovic, D. DeCeuster, V. Desai, J. Jürgens, N. Kaminar, W. Mulligan, L. Rodrigues-Barbarosa, D. Rose, D. Smith, A. Terao, and K. Wilson (2005, January). The surface polarization effect in high-efficiency silicon solar cells. pp. 410. 14

Taubitz, C., M. Kröber, M. Schütze, and M. B. Köntopp (2014, November). Potential Induced Degradation: Model Calculations and Correlation between Laboratory Tests and Outdoor Occurrence. In 29th European PVSEC Proceedings, pp. 2490–2494. 14, 15

Taylor, S. J. and B. Letham (2018, January). Forecasting at Scale. The American Statistician 72(1), 37–45. 2, 33, 56

Urraca, R., T. Huld, F. J. Martinez-de Pison, and A. Sanz-Garcia (2018, August). Sources of uncertainty in annual global horizontal irradiance data. Solar Energy 170, 873–884. 28

Virtuani, A., M. Caccivio, E. Annigoni, G. Friesen, D. Chianese, C. Ballif, and T. Sample (2019). 35 years of photovoltaics: Analysis of the TISO-10-kW solar plant, lessons learnt in safety and performance—Part 1. Progress in Photovoltaics: Research and Applications 27(4), 328–339. 38

Virtuani, A., D. Strepparava, and G. Friesen (2015, October). A simple approach to model the performance of photovoltaic solar modules in operation. Solar Energy 120, 439–449. 37

Whitfield, K., A. Salomon, S. Yang, and I. Suez (2012, June). Damp heat versus field reliability for crystalline silicon. In 2012 38th IEEE Photovoltaic Specialists Conference, pp. 001864–001870. ISSN: 0160-8371, 0160-8371. 8

Wohlgemuth, J. H. (2012). Standards for pv modules and components – recent developments and challenges. Presented at the 27th European Photovoltaic Solar Energy Conference and Exhibition, Frankfurt, Germany. 1, 23

Wu, D., J. Zhu, T. R. Betts, and R. Gottschalg (2014). Degradation of interfacial adhesion strength within photovoltaic mini-modules during damp-heat exposure. Progress in Photovoltaics: Research and Applications 22(7), 796–809. 23

Zhang, S., Y. Zhang, and J. Zhu (2018, April). Residual life prediction based on dynamic weighted Markov model and particle filtering. Journal of Intelligent Manufacturing 29(4), 753–761. 32

Zhu, J., M. Koehl, S. Hoffmann, K. A. Berger, S. Zamini, I. Bennett, E. Gerritsen, P. Malbranche, P. Pugliatti, A. D. Stefano, F. Aleo, D. Bertani, F. Paletta, F. Roca, G. Graditi, M. Pellegrino, O. Zubillaga, F. J. C. Iranzo, A. Pozza, T. Sample, and R. Gottschalg (2016). Changes of solar cell parameters during damp-heat exposure. Progress in Photovoltaics: Research and Applications 24(10), 1346–1358. 23

Zorrilla-Casanova, J., M. Piliougine, J. Carretero, P. Bernaola-Galván, P. Carpena, L. Mora-López, and M. Sidrach-de-Cardona (2013). Losses produced by soiling in the incoming radiation to photovoltaic modules. Progress in Photovoltaics: Research and Applications 21(4), 790–796. 36

Mapping of global climate stress factors

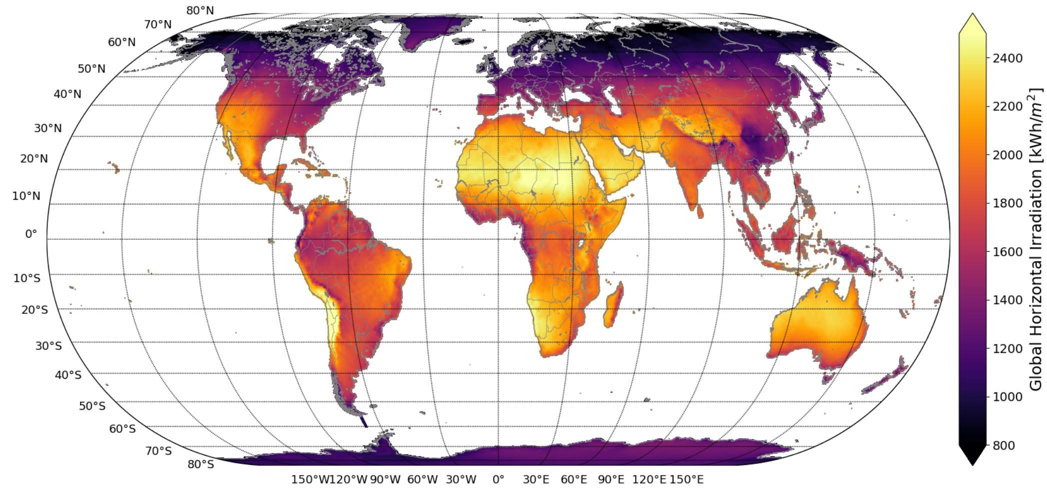

Figure 1: Global horizotal irradiation used to model UV. Since the ambient temperature is propotional to the irradiance levels, the global distribution of ambient temperatures takes the same trend. Figure reprinted from Ascencio-Vasquez (2020). The map is according to EAR5 dataset and of the year 2018

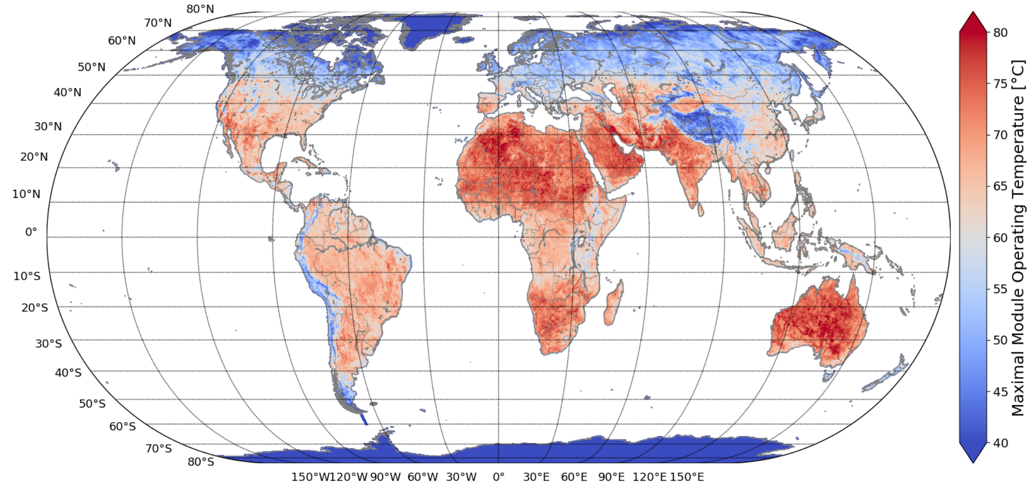

Figure 2: Maximum module temperature distribution worldwide. The module temperature is calculate from the ambient temperature using the Faiman model. Figure reprinted from Ascencio-Vasquez (2020). The map is according to EAR5 dataset and of the year 2018

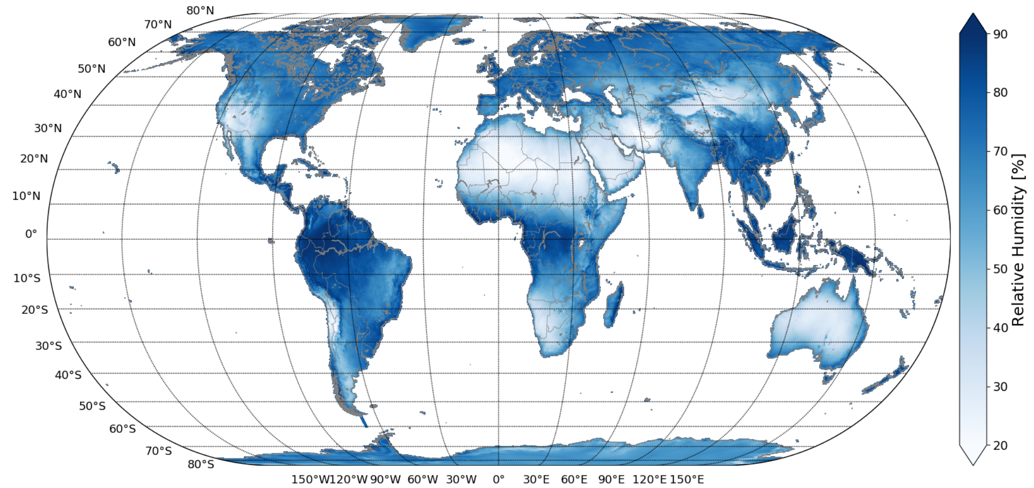

Figure 3: Distribution of relative humidity worldwide. The relative humidity is calculated from the ambient and the dew point temperatures using the Buck's formula. Figure reprinted from Ascencio-Vasquez (2020). The map is according to EAR5 dataset and of the year 2018

Supporting articles

Paper 1. S. Lindig, I. Kaaya, K.A. Weiss, D. Moser, and M. Topic, "Review of statistical and analytical degradation models for photovoltaic modules and systems as well as related improvements," IEEE J. Photovoltaic., vol. 8, no. 6, pp. 1773–1786, Nov. 2018.
This paper is reprinted from the Open Access publication available at https://ieeexplore.ieee.org/document/8472886. All rights remain with the authors and editors.
Impact factor: 3.398

Paper 2. I. Kaaya, M. Koehl, A.P. Mehilli, S. de Cardona Mariano, & K.A. Weiss, "Modeling Outdoor Service Lifetime Prediction of PV Modules: Effects of Combined Climatic Stressors on PV Module Power Degradation". IEEE Journal of Photovoltaics,vol. 9, no. 4, pp. 1105–1112, May. 2019.
This paper is reprinted from the Open Access publication available at https://ieeexplore.ieee.org/document/8720037. All rights remain with the authors and editors.
Impact factor: 3.398

Paper 3. J. A-Vásqueza, I. Kaaya, K. Brecla, K-A. Weiss and M.Topic, "Global climate data processing and mapping of degradation mechanisms and degradation rates of PV modules". energies MDPI ,vol. 12, no. 4749 Dec 2019.
This paper is reprinted from the Open Access publication available at https://www.mdpi.com/1996-1073/12/24/4749/htm. All rights remain with the authors and editors. Impact factor: 2.707

This article has been accepted for inclusion in a future issue of this journal. Content is final as presented, with the exception of pagination.

Review of Statistical and Analytical Degradation Models for Photovoltaic Modules and Systems as Well as Related Improvements

Sascha Lindig, Ismail Kaaya, Karl-Anders Weiß, David Moser, and Marko Topic

***Abstract*—In this work, we investigate practical approaches of available degradation models and their usage in photovoltaic (PV) modules and systems. On the one hand, degradation prediction of models is described for the calculation of degradation at system level where the degradation mode is unknown and hence the physics cannot be included by the use of analytical models. Several statistical models are thus described and applied for the calculation of the performance loss using as case study two PV systems, installed in Bolzano/Italy. Namely, simple linear regression (SLR), classical seasonal-decomposition, seasonal- and trend-decomposition using Loess (STL), Holt–Winters exponential smoothing and autoregressive integrated moving average (ARIMA) are discussed. The performance loss results show that SLR produces results with highest uncertainties. In comparison, STL and ARIMA perform with the highest accuracy, whereby STL is favored because of its easier implementation. On the other hand, if monitoring data at PV module level are available in controlled conditions, analytical models can be applied. Several analytical models depending on different degradations modes are thus discussed. A comparison study is carried out for models proposed for corrosion. Although the results of the models in question agree in explanation of experimental observations, a big difference in degradation prediction was observed. Finally, a model proposed for potential induced degradation was applied to simulate the degradation of PV systems maximum power in three climatic zones: alpine (Zugspitze, Germany), maritime (Gran Canaria, Spain), and arid (Negev, Israel). As expected, a more severe degradation is predicted for arid climates.**

***Index Terms*—Degradation models, performance loss, photovoltaic (PV) modules, PV systems, service life prediction.**

I. Introduction

BECAUSE of high costs and limited efficiencies, photovoltaic (PV) applications were exclusively used for space applications until the 1970's and 1980's. In the beginning of the 1970's, the dramatic price increase for fossil fuels and an energy uncertainty because of the oil crisis raised the awareness for a need of change in the energy supply [1]. Since then, the interest in renewable energies and solar energy in particular has increased, which in turn led through scientific achievements to a steady reduction in installation costs and performance improvements of terrestrial PV systems. In the late 1990's, the first large-scale PV systems were installed [2]. Nowadays, PV module manufacturers guarantee a performance reduction of no more than 20% within 25 years of operation at standard test conditions (STC) (modules tested indoor under $T_{\mathrm{STC}} = 25\ ^\circ\mathrm{C}$, $G_{\mathrm{STC}} = 1000\ \mathrm{W/m^2}$, AM 1.5) and even started to guarantee a maximum degradation of 1%/year for the first ten years. Nevertheless, the actual performance throughout the lifetime is quite uncertain and unpredictable. Laboratory or field determination of PV modules service life under real environmental conditions requires an unacceptable length of time.

PV systems are affected by continuous cycles of temperature, humidity, irradiation, mechanical stress, and soiling. These environmental mechanisms cause different degradation modes to take place within a PV module and reduce the performance of the system. Therefore, it is necessary to develop diagnostic techniques, lower the performance uncertainty, and predict the behavior of PV systems with higher accuracy.

Commonly two approaches, statistical and analytical methods, are used for evaluating degradation rates of PV modules and systems. This report describes quantitative degradation and service lifetime models currently used for PV modules and recommends further improvements. A review of available models and improvements is crucial for accurate life-time calculations of future energy PV systems. The first part of this work focuses on available metrics of variables and the most common statistical models to retrieve the performance loss based on these metrics. The second part deals with analytical models, which pinpoint specific degradation modes and their possible impact on the performance of PV systems.

We believe that a more precise prediction of PV system performance and the capability of linking performance losses to relevant degradation modes will increase public trust in solar energy. Additionally, it will help stakeholders such as investors, PV plant owners, operation and maintenance, and insurance companies as well as other parties involved to favor more beneficial and accurate business models and

Manuscript received June 1, 2018; revised July 27, 2018; accepted September 5, 2018. This work was supported by the European Union's Horizon 2020 Program under GA. No. 721452—H2020-MSCA-ITN-2016. *(Corresponding author: Sascha Lindig.)*

S. Lindig is with the Institute for Renewable Energy, EURAC Research - Viale Druso 1, 39100 Bolzano, Italy, and also with the Faculty of Engineering, University of Ljubljana, 1000 Ljubljana, Slovenia (e-mail: sascha.lindig@eurac.edu).

I. Kaaya and K. A. Weiß are with the Fraunhofer Institute for Solar Energy Systems, 79110 Freiburg, Germany (e-mail: ismail.kaaya@ise.fraunhofer.de; karl-anders.weiss@ise.fraunhofer.de).

D. Moser is with the Institute for Renewable Energy, EURAC Research - Viale Druso 1, 39100 Bolzano, Italy (e-mail: david.moser@eurac.edu).

M. Topic is with the Faculty of Engineering, University of Ljubljana, 1000 Ljubljana, Slovenia (e-mail: marko.topic@fe.uni-lj.si).

Color versions of one or more of the figures in this paper are available online at http://ieeexplore.ieee.org.

Digital Object Identifier 10.1109/JPHOTOV.2018.2870532

to more efficiently operate and maintain PV systems in the future.

II. PV Modules Degradation Modes

Degradation modes are effects that irreversibly degrade the performance of a PV module/system or may cause safety problems [3]. A great number of different degradation modes are observed in PV modules, both under outdoor operation and indoor testing. The most commonly observed degradation modes include [3]: light induced degradation (LID), solder fatigue failure, silver grid finger delamination, bypass diode failure, delamination, cell cracks, corrosion, polymeric discoloration, ultraviolet (UV) degradation of the cell, polymeric mechanical failure, and potential induced degradation (PID). Each of these degradation modes has different causes and is triggered by different stress factors. Apart from the modes listed, different technical risks, which affect the PV performance and the resulting costs, were found by Moser *et al.* [4]: glass breakage, snail track, defective backsheet, hotspot, soiling, overheating, and failure junction box. An occurring degradation mode can have an increasing impact on the PV performance over time. It develops either in isolation or in combination with other degradation modes or technical risks and might lead to the failure of a PV module. The term failure for electrotechnical devices is defined as "the termination of the ability of an item to perform a required function" [5]. While this definition serves as a clear guideline for most devices, the failure of a PV component is somewhat more complex. For example, although a PV module can still be technically usable, its power output might be too low to verify the continuation of its operation from an economical point of view. Within the scope of this work, a failure is defined as the necessity to replace a PV component, because of its ultimate, economic or safety-related failure. A clear understanding of the definition of a degradation mode is also still a challenge and stress should be put on common nomenclature to define the same degradation mode with the same terminology. For the moment, accelerated aging tests are being utilized in the study of some of these modes. However, there is no proof/evidence that the results from these tests reflect what exactly happens to the modules in outdoor conditions.

III. Degradation Modeling

Degradation models are used to relate a test item's estimated failure time with the wear and tear during its usage period. The failure time is defined as the end of the lifetime of a PV component because of its failure. Degradation models help to quantify the performance loss PV modules and systems are experiencing under operation. Degradation in PV systems is the reduction in efficiency with which a PV system is converting light of the sun into electricity over time [6]. This appears at all levels of a PV system, be it at cell, module or system level. To model PV module degradation modes, the knowledge of internal loads like temperature, chemical conditions, irradiance, and mechanical loads in/on the PV module is required. One very important part is to convert external loads to internal loads of the module.

Models for degradation are generally either data-driven or derived from physical principles via stochastic processes. Although data-driven models are more commonly applied to analyze degradation data, viewing degradation through stochastic processes helps researchers to theoretically characterize the degradation process. Therefore, a coupling of both models could enhance the knowledge of what is happening in PV systems. Data-driven models help to examine the overall performance loss of a system over time and by using analytical models conclusions of what triggered these losses might be derived.

A. Data-Driven Models

Data-driven models are often empirical employed to estimate degradation rates based on statistical analysis of given data sets. The goal of the statistical analysis is to calculate the trend of the PV performance time-series and to translate the slope of the trend to an annual loss rate, in units of %/year [7]. Although these models can provide consistent performance loss rates (PLRs), which are useful for data extrapolation and service life predictions, they do not directly provide evidence for the degradation modes taking place in the module. Other effects such as diffuse soiling, snow, shading or module mismatch have also a direct impact on the performance trend. Therefore, it is more accurate to talk about a PLR rather than a degradation rate.

B. Analytical Models

Analytical models are based on the physical/chemical theories of a specific degradation mode. These models represent the mechanism involved in complex physical/chemical processes. For well-known PV module degradation modes, several analytical models to forecast PV module degradation are available. All these models are based on the principle of understanding the underlying process, but they are still only heuristic models, which do not include the influence of material parameters.

In the following chapters, we discuss the most commonly used performance loss models.

IV. Performance Loss Models

Before applying any statistical model, the observed data are generally treated using filtering techniques depending on factors like irradiance or standard deviation ranges and subsequently averaged or added up over certain time periods. This step is performed as data preparation to minimize outliers and noise and to remove values corresponding to inhomogeneous irradiance conditions on the irradiance sensor and the PV system [8]. Afterwards, a performance metric can be applied to a pretreated data set and the PLR is calculated by using statistical methods. These steps are necessary to minimize seasonal oscillations and to eliminate outliers resulting in the reduction of the overall uncertainty in the estimation of the PLR. In the following, a short overview of the most common performance metrics as well as statistical methods is presented. In Section IV-C, a comparison of the statistical models in question is performed on a case study with data of two PV systems installed at the airport of Bolzano in Italy.

A. Performance Metrics

Statistical performance loss models need to be applied on certain PV system performance-rating parameters. The parameters are expressed through performance metrics, which are measured or calculated in a specified interval. Performance metrics are ideal to compare the performance of different systems in different climates. They can be categorized into three different groups. These are: 1) electrical parameters directly taken from *I–V* curves recorded either outdoor or indoor and corrected to STC, 2) empirical metrics such as PVUSA [9], the 6-k-values performance model (applied in the PVGIS online tool) [10] or the Sandia models [11], and 3) normalized and/or corrected metrics such as performance ratio [7]. Great care has to be taken when selecting performance metrics. The choice as well as possible corrections such as corrected power for temperature and irradiance [12] will influence the results. Therefore, the outcome of a certain performance loss model applied on a specific performance metric needs to be evaluated and put into context to understand the validity of the results.

1) Evaluation of I–V Curves: Electrical parameters of the *I–V* curve include power, voltage, and current at the maximum power point, the open circuit voltage, and the short circuit current. With these parameters, it is possible to calculate the fill factor. A PV systems performance loss is observable when comparing the values of periodically performed measurements of systems in operation [13]. If an unexpected decline in one of the parameters appears, the affected modules can be examined indoors or outdoors, for example, with electroluminescence or thermal imaging cameras. For detailed characterization, indoor measurements can lead to the most accurate results. However, removing PV modules from the field is time consuming with the possibility of damaging the modules during transport and handling. These considerations need to be taken into account to decide which strategy to follow depending on the extent and the complexity of the detected problem and which stakeholders are involved. For example, for insurance claims, outdoor measurement may be sufficient while certified indoor measurements could be required for PV module warranty claims.

2) Empirical Metrics: The empirical metrics presented are models, which aim to obtain performance data while taking into account the dependence between the PV system output and prevailing outdoor conditions [9]. The idea is to receive PV system performance parameter like the efficiency or the maximum power through the application of formulas, which consist of empirical coefficients and weather data. Two widely used models are the 6-k-values performance model and PVUSA. The 6-k-values performance model describes system performance through the relative efficiency η_{REL} correlated to STC as a function of in-plane irradiance G_{POA} and module temperature T_{mod} [14]

$$\eta_{\mathrm{REL}}(G', T') = 1 + k_1 ln(G') + k_2 ln(G')^2 + k_3 T' + k_4 T' ln(G') + k_5 T' ln(G')^2 + k_6 T'^2. \quad (1)$$

Equation (1) has to be fitted to experimental data to obtain the empirical coefficients $k_1 - k_6$. Hereby, the normalized in-plane irradiance $G' = G/G_{\mathrm{STC}}$ and the normalized temperature $T' = T_{\mathrm{mod}} - T_{\mathrm{STC}}$ are considered. An average performance model for each PV type is considered and the k-coefficients are calculated using data from different modules of the same PV technology [10], [14]. This model creates a matrix instead of a single well-defined value for the maximum power point.

Within the PVs for utility scale and applications project, another widely used model, PVUSA, was developed [15], [16]. While calculating corrected power values, it is assumed that the PV system current primarily depends on irradiance and the voltage on module temperature T_{mod}. T_{mod} in turn is strongly dependent on ambient temperature, irradiance, and wind speed. A regression of the systems maximum power output is performed against PVUSA test conditions (PTC) by

$$P_{\mathrm{MPP}} = G_{\mathrm{POA}}(A + BG_{\mathrm{POA}} + CT_{am} + Du_W)$$
$$(G_{\mathrm{PTC}} = 1000\,\mathrm{W/m^2}, T_{\mathrm{PTC}_{AM}} = 20\,^{\circ}\mathrm{C}, u_W = 1\,\mathrm{m/s}). \quad (2)$$

First, measurements at high irradiance values (G $\geq$ 800 W/m^2) in the plane of array (POA) are selected and fitted to calculate monthly values for the coefficients *A*, *B*, *C*, and *D*, applying multivariate regression. Afterwards, the coefficients are used to receive monthly ratings at PTCs (substituting meteorological data values). It should be noted that this methodology is optimized for crystalline silicon PV. An adapted version of the equation including another coefficient *E* was developed to consider thin-film technologies [7], [9].

3) Normalized and Corrected Metrics: Normalized and/or corrected metric parameters are useful when comparing different PV technologies in different climates. Here, PV system performance data are either normalized to comparable, unit-free metrics or corrected in respect to outdoor conditions. One of the most commonly used metrics is the performance ratio (PR), which is an adequate indicator for the quality of a PV installation. The PR is calculated by dividing the final (or array) yield $Y_{f(a)}$ (depending if ac- or dc-power is evaluated) with the reference yield Y_{ref} [17]. The yields are ratios of measured values of power or irradiance with values obtained under STC

$$\mathrm{PR} = \frac{Y_f}{Y_{\mathrm{ref}}} = \frac{P_{\mathrm{AC}}/P_{\mathrm{STC}}}{G_{\mathrm{POA}}/G_{\mathrm{STC}}} \quad (3)$$

$$\mathrm{PR}_{\mathrm{DC}} = \frac{Y_a}{Y_{\mathrm{ref}}} = \frac{P_{\mathrm{DC}}/P_{\mathrm{STC}}}{G_{\mathrm{POA}}/G_{\mathrm{STC}}}. \quad (4)$$

When studying the PV performance, it is advisable to use dc-related performance metrics in order to eliminate possible influences because of inverter degradation or misbehavior.

A promising correction method, presented by Belluardo *et al.* [18], evaluates the irradiance and temperature corrected power under STC conditions as follows:

$$P_{T,G\,\mathrm{corr}} = P_{\max}\frac{G_{\mathrm{STC}}}{G}\frac{1}{1 + \gamma(T_{\mathrm{mod}} - T_{\mathrm{STC}}).} \quad (5)$$

Here, γ is the temperature coefficient of the PV systems power at STC, which is stated on the datasheet. Since γ is retrieved at 1000 W/m^2 and highly temperature dependent, a preliminary data filtering, similar to the filter applied in PVUSA, should be performed to assure the accuracy of the temperature coefficient in use.

Methods, which correct absolute values like power, voltage or current, can be additionally normalized by dividing the corrected value by the nominal installed value under STC. This step simplifies a possible comparison between different PV systems. A clear advantage of these rating techniques is the possibility to evaluate the performance loss in any desired time resolution.

B. Purely Statistical Methods

Statistical analysis methods are used to retrieve trends of performance time-series. These time-series are some sort of performance metrics, which are discussed in Section IV-A. The slope of a trend function can be interpreted as the PLR. It is possible to accumulate these ratings for any given time resolution into an easily comparable annual aging value. The difficulty is to find a good estimation of the PLR since the application of a certain statistical method on a performance metric and a defined filter determines the result significantly. Statistical analysis methods can be divided into model-based methods like linear regression, classical seasonal decomposition (CSD), Holt–Winters (HW) exponential smoothing or autoregressive integrated moving average (ARIMA) and nonmodel-based methods such as seasonal and trend decomposition using Loess (STL). In the following, these commonly used methods are described.

1) Simple Linear Regression (SLR): Performance metrics of any kind are most commonly applied on linear regression because of the straight-forward approach. The fitted trend line is given by

$$\hat{y} = at + b. \tag{6}$$

Hereby, *a* represents the gradient and *b* is the intercept with the *y*-axis. The SLR-algorithm uses the method of least squares. The idea of this method is to sum up squared values of the difference between trend line and actual measurement points and to find the minimum value for this sum. Squares are used to add up only positive numbers and to put more weight on more widely scattered residuals. This method overemphasizes outliers as well as seasonal variations and can result in large uncertainties. Because of that, performance metrics, which reduce seasonal oscillation should be applied if the SLR-algorithm is used.

2) Classical Seasonal Decomposition: Another commonly used statistical model is CSD. By using CSD, the seasonality and a certain irregular component are separated from a set of measured time-series data to receive a clear trend over time. This technique helps to get a fast idea of a performance loss of the system in question. The trend is obtained by applying a centered moving smoothing on a time-series with a certain seasonal period *m*. When using monthly data, the seasonal period is usually set to 12. Here, the first value is computed by averaging over the first 12 months. Due to the 12-month centered moving average, 6 months at the beginning and 6 months at the end of the observation period are not included in the computation. To calculate the seasonality, the trend is subtracted from the measured data and each month throughout the years of surveillance is averaged. What remains at the end is an irregular component [19]. Depending on the stability of the seasonal component, an additive or a multiplicative model is used as shown in the equations below

$$\hat{y} = T_t + S_t + e_t \quad , \quad \hat{y} = T_t \times S_t \times e_t. \tag{7}$$

Here, *T* is the trend, *S* the seasonality, and *e* the remaining part of the data [7].

3) HW Seasonal model: The HW seasonal model contains a forecast equation and three smoothing equations as shown below

$$\hat{y}_{t+1|t} = l_t + b_t + s_{t-S+1} \tag{8}$$

$$l_t = A(y_t - s_{t-S}) + (1 - A)(l_{t-1} + b_{t-1}) \tag{9}$$

$$b_t = B(l_t - l_{t-1}) + (1 - B)b_{t-1} \tag{10}$$

$$s_t = C(y_t - l_{t-1} - b_{t-1}) + (1 - C)s_{t-S}. \tag{11}$$

Here, l_t is the level, b_t the slope, and s_t the seasonal component. *A*, *B*, and *C* are smoothing parameters. If monthly data are evaluated, the period of seasonality, *S*, equals to the value of 12. The HW model is either additive or multiplicative, depending on the seasonal behavior. In case of evaluating a PV systems performance, the additive method should be selected because the seasonal variations are approximately constant throughout the series. The seasonal component is then computed in absolute terms and has a mean of around zero. The level equation (9) is a weighted average between the seasonally adjusted observation $(y_t - s_{t-S})$ and the nonseasonal one-step-ahead forecast $(l_{t-1} + b_{t-1})$. The slope is a weighted average of the level at time *t* minus the level at $t - 1$, and the trend at $t - 1$. The selection of smoothing parameters determines how fast the exponential weights decline over the past observations. The HW method can be especially useful for computing the future behavior of a PV system [7], [20], [21].

4) Autoregressive Integrated Moving Average: ARIMA is a model, which can contain several methods in a multiplicative way and can be described as ARIMA (p, d, q) (P, D, Q). Here, p is the auto-regressive, d the differencing, and q the moving average order as well as P is the seasonal autoregressive, D the seasonal differencing, and Q the seasonal moving average order. Due to the flexibility of the model, seasonal variations, errors, outliers, and level shifts can be addressed in a proper way. ARIMA is applied using the following [7]:

$$\phi(T)\phi_S(T^S) \bigtriangledown^d \bigtriangledown_S^D y_t = \phi(T)\phi_S(T^S)e_t \tag{12}$$

T is the delay operator, $\phi(T) = (1 - \phi_1 T - \cdots - \phi_p T^p)$ is an autoregressive polynomial in *T* of degree *P*, $\phi(T^S)$ is an autoregressive polynomial in T^S of degree P_S, $\phi(T)$ a moving average polynomial in *T* of degree *q*, and $\phi_S(T^S)$ is a moving average polynomial of degree Q_S in T^S. Apart from that, $\bigtriangledown^d = (1 - T)^D$ is a nonseasonal differencing operator and $\bigtriangledown_S^D = (1 - T^S)^d$ is a seasonal differencing operator and grasps nonstationarity in the relevant location in consecutive periods [22].

The stationarity of the time-series determines the optimal ARIMA model; a transformation using differencing to achieve stationarity might be indispensable. Stationarity is described by a constant mean and variance, resulting in a nonexisting trend and the graph seems more like white noise. There are different

This article has been accepted for inclusion in a future issue of this journal. Content is final as presented, with the exception of pagination.

ways to difference a time-series, the simplest and most common way being first-order differencing [23]

$$\hat{y} = y_t - y_{t-1}. \tag{13}$$

Here, the differenced value is the change between two consecutive values of the original time-series. The resulting time-series has T-1 values. Seasonal or second-order differencing are further examples of how to create stationarity within the time-series in question.

The heart of the ARIMA model is the application of autoregression. To perform an autoregression, the desired variable is computed by applying a linear combination of past values of the variable. The general form of an autoregressive model of order p is

$$\hat{y} = c + \phi_1 y_{t-1} + \phi_2 y_{t-2} + \cdots + \phi_p y_{t-p} + e_t \tag{14}$$

where c is a constant and e_t is the remainder.

The moving average model used within ARIMA has a different purpose than the one for CSD. Here, the moving average uses past forecast errors in a model similar to a regression. The aim of the moving average model is to predict a forecast instead of smoothing the trend cycle of past values [21].

While using the software environment R, the function seas, a function within the R-package "seasonal" which automatically performs seasonal adjustments, automatically calculates the optimal ARIMA (p, d, q)(P, D, Q) variables to apply on the data set [24]. For the application of ARIMA within Section IV-C, the extracted parameters for both systems are (0, 1, 1) (0, 1, 1).

5) Seasonal–Trend Decomposition Using LOESS: STL is a continuation of CSD and Loess is a method to estimate nonlinear relationships. The centered moving average is replaced by a locally weighted regression to extract the trend [25]. Because of that, the estimates become more robust and are less affected by missing data and outliers. Similar to CSD, STL decomposes a seasonal time-series into three components (trend, seasonal, remainder) and is described by

$$Y_t = T_t + S_t + R_t. \tag{15}$$

STL contains an inner and an outer loop. Every time a run within the inner loop is performed, the seasonal and trend components are updated. The number of runs within the inner loop are mostly equal to 1 or 2. The outer loop includes an inner loop followed by a calculation of robustness weights. This calculation serves as an input for the following inner loop to decrease the impact of transient, abnormal behavior on the trend and seasonal parts [26].

To better grasp the idea of Loess, the method is explained when applied within the software R. Here, two parameters have to be chosen, the trend window and the seasonal window. The seasonal window is either periodic or the span of the Loess window for seasonal extraction. The smaller the values, the faster the trend and seasonal components can change. A high value for the seasonal window forces the seasonal part to be periodic, in this case just the means for the monthly values are used (seasonal component for January is mean of all January values). After calculating the seasonally adjusted data, (measured data minus seasonality) the trend is Loess-smoothened. This is done by applying local regression on a data window with a certain width. The regression curve is fitted to the data within the window. The closer the points are to the center of the window (higher weight), the greater is the impact on the regression line calculation. The weight is reduced on those points that are furthest from the regression curve. The whole step of regression and weighting is repeated several times to receive a point on the Loess-curve, which is at the center of the window. By moving the window across the data, the complete Loess curve is computed. What follows is that each point of the Loess curve is the intersect of a regression curve and the center of the respective window.

C. Comparison of Statistical Models

The statistical models presented are applied on the uncorrected performance ratio data sets of a mono-crystalline (mc-Si) and an amorphous silicon (a-Si) system using the software R. The mc-Si system contains 14 PV modules and has a rated power of 1960 Watt-peak (Wp). The second installation includes 12 amorphous silicon modules with a power of 1200 Wp. The observed data have a resolution of 15 min and were averaged over whole months. The systems in question were installed in Bolzano/Italy in August 2010 and are evaluated for seven years from March 2011 until February 2018 in order to eliminate initial degradation effects such as the Staebler–Wronski effect or short-term LID. The monitored data are prefiltered to exclude data with performance ratio values below 1% and above 200% and a POA irradiation of less than 50 W/m^2 and more than 1500 W/m^2. This was done to remove extreme outliers and measurement errors. The simplicity of the filter was chosen to intensify possible deviations among the models. The irradiance data are recorded with a pyranometer. For each model, the relative annual PLRs, the corresponding uncertainty and the intercept with the *y*-axis are given. The PLR of the more sophisticated models are calculated by applying a linear regression to the respective trend, which was extracted through the statistical model. To receive the yearly relative PLR and the corresponding uncertainty, the following formulas are used [27]:

$$\text{PLR} = \frac{12a}{b} \tag{16}$$

$$u_{\text{PLR}} = \sqrt{\left(\left(\frac{12}{b}\right)^2 \times u_a^2 + \left(\frac{-12a}{b^2}\right)^2 \times u_b^2\right)} \tag{17}$$

where a and b are the fitting coefficients of the linear regression, $u_{a,b}^2$ the variances of these fitting coefficients, and u_{PLR} the standard deviation of the PLR. This uncertainty calculation corresponds to a confidence interval of 68%.

Two definitions of the PLR can be found in the literature, in relative terms as PLR $= 12a/b$ or absolute with PLR $= 12a$ [18]. Here, the relative PLR was chosen because it makes it easier to generalize the findings to the energy yield of the array using the initial yield of the plant. The results of these calculations are less aimed to deliver the best possible combination of filtering techniques, performance metrics, and statistical models but are intended to provide a direct comparison between the presented analysis methods. While the uncertainties of the resulting PLRs

This article has been accepted for inclusion in a future issue of this journal. Content is final as presented, with the exception of pagination.

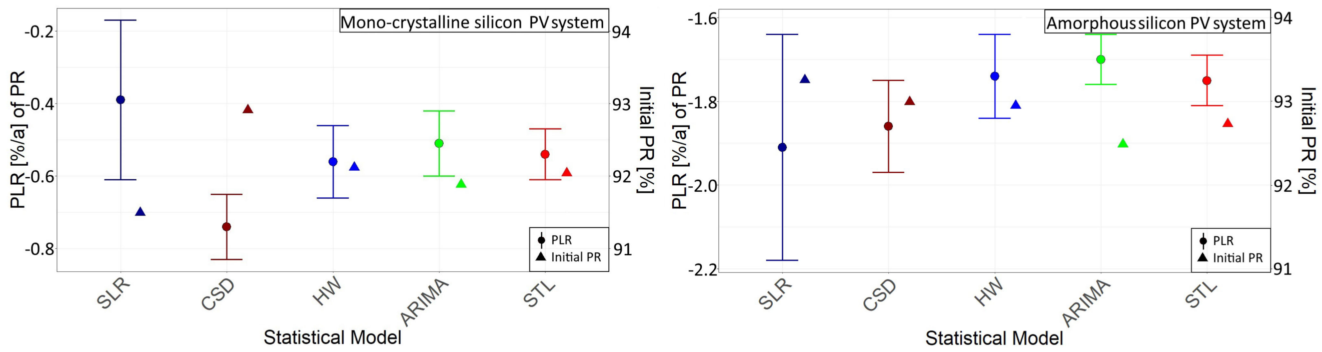

Fig. 1. Comparison of statistical models on PR-data, circles represent PLR including uncertainties (primary axis), triangles represent initial PR (secondary axis), on the left is mc-Si system, on the right is a-Si system.

TABLE I
COMPARISON OF STATISTICAL MODELS

Characteristic	SLR	CSD	HW	ARIMA	STL
Different technologies	PLR with highest uncertainty	Not well suited	Not that well suited	PLR with high accuracy	PLR with high accuracy
Filtering, outlier handling	Crucial, outlier have big impact	Crucial, outlier have big impact	Robust through weighted average	Robust through models flexibility	Robust through locally weighted regression
Time period	Longer time-series better suited	Removing of first & last observations	Shorter time series can be evaluated	Shorter time series can be evaluated	shorter time series can be evaluated
Seasonality	Sensitive to seasonality	Sensitive to seasonality	Insensitive to seasonality	Insensitive to seasonality	Insensitive to seasonality
Stationarity of time-series	Not necessary	Not necessary	Not necessary	Stationarity necessary	Not necessary

were used to rate the statistical models, the remainder, where applicable, serves as a validation of the parameter fit. The remainder should have Gaussian white noise properties, such as being uncorrelated and normally distributed.

In Fig. 1, the relative PLRs, uncertainties and initial PR values are given. The initial value is the intercept with the y-axis. The stated uncertainty is the uncertainty of the PLR against the extracted trends, computed by the individual statistical methods.

It can be seen that the performance of the mc-Si system degrades 0.5%–0.6% per year, the one of a-Si close to 1.8% per year. Because of cabling and other system losses the initial PR value is below the theoretical value under STC. As expected, linear regression shows in both cases the highest uncertainty. For all other cases, a trend was first filtered from the data set on which a linear regression was performed. This step leads to an outcome with higher certainties. While all more advanced methods show similar results with regards to the uncertainty of the mc-Si system, STL and ARIMA outperform the others when applied to the a-Si system.

In case of CSD, the loss ratio is for both systems higher in comparison and probably overestimated. In Section IV-B2, it was mentioned that, when using CSD, the first and last months of the data set are lost due to the applied centered moving average. This is visible in Fig. 2. Here, the extracted trend-lines of the PR of the mc-Si system using CSD and STL are shown. Within the first six months of observation, the trend of the PR has a roughly stable value. When applying CSD, this time period is not taken

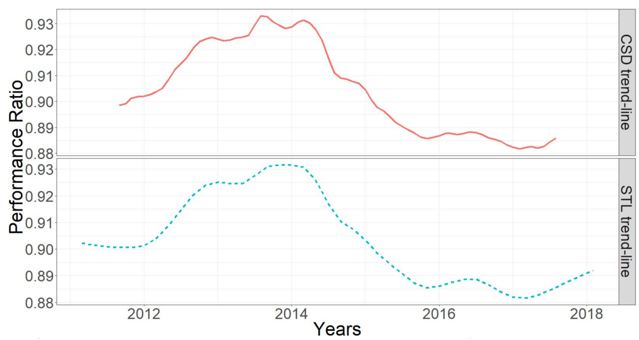

Fig. 2. Trend-lines of CSD- (red-straight) and STL-model (blue-dotted) of unfiltered monthly PR-data of a mc-Si system.

into account and because of this, the decrease is stronger over time. This in turn results additionally in an overestimation of the initial PR value.

Table I summarizes the models in respect to different characteristics of time-series. In general, SLR might serve as a first indication of a PLR determination but is not suited for accurate calculations due to its simplistic approach. It has been shown that the more sophisticated selected analysis methods perform very similar for crystalline systems, both in the estimation of the initial PR and the PLR. An exception hereby is the usage of CSD for short time-series. The exclusion of the first and last observations can falsify the final PLR. When a thin-film system

This article has been accepted for inclusion in a future issue of this journal. Content is final as presented, with the exception of pagination.

is subject of the calculations, STL and ARIMA show the best results.

When applying HW, ARIMA or STL, it is very important to perform crucial modeling steps with great care to receive the optimal results. In case of ARIMA, the time-series has to be transformed in order to reach stationarity. Since PV time-series are highly seasonal, a seasonal differentiation is essential. For the same reason, the seasonal window parameter within STL has to be set as periodic and the additive method is preferred when using the HW model.

Filtering is an integral part when computing PLR values. If performance metrics are corrected using temperature coefficients, which are retrieved at a POA irradiance of 1000 W/m^2, an appropriate POA irradiance should be selected. Within this work, the preliminary filter are treating outliers and values corresponding to measurement errors not sufficiently. This was done on purpose to amplify the impact of outliers and measurement inaccuracies on the final results. SLR and CSD treat all values with similar weights and are therefore strongly affected by outliers. HW's weighted average, STL's locally weighted regression, and the combination of similar techniques within ARIMA are well suited for outlier handling.

Another statistical method worth mentioning is the year-on-year model developed by Sunpower [28] and later improved by NREL [29]. It is implemented within the Python RdTools for the analysis of PV data. This method has a complete different approach as the here discussed models, as it is using a loss rate distribution instead of one single value. The gradient between two related data points in consecutive years (hour, day, week, month) determine a single PLR. The median of this gradient, the gradients of all remaining data points of that two years, and all following years determine the final performance loss per year. The power loss rates are computed using a 100% performance baseline value. This approach is excluded within this study. A comparison is difficult to perform because the initial value is preset and, in contrast with the performed computations, the data aggregation is done in an irradiance-weighted manner. Nevertheless, this approach is of special interest if high quality field irradiance data are not available because it can compute the PR based on a modeled clear-sky irradiance.

V. Modeling Specific Degradation Modes Using Analytical Models

In order to explain experimental observations of different degradation modes, analytical models are developed based on the physical/chemical theories of the degradation mode in question. These models are environmental stress oriented. The hypotheses of a particular degradation mode are built depending on specific environmental stresses applied, and on the assumption that the kinetics of a specific degradation mode are influenced by one dominating process. Electrical parameters such as power at maximum power point (P_{max}), short circuit current (I_{SC}), shunt (R_{sh}), and series resistance (R_s) are commonly modeled as degradation indicators. Hence, the environmental stresses and their interactions with the PV module components are assessed based on the reduction of the initial electrical parameter at time ($t = 0$) before aging and at time ($t = t$) after aging or in the field.

A. Degradation Models for Corrosion

Corrosion is one of the most occurring degradation modes in PV modules [30]. Corrosion is caused by the presence of high temperature and high humidity in the module. Humidity can enter the module through the backsheet or the layers of the encapsulant and spread into the module [31], weakening the adhesive bonds between the interfaces. One hypothesis is that humidity, which catalyzes corrosive processes, leads to a formation of acetic acid through the hydrolysis of vinyl-acetate monomers present in the EVA [32]–[34]. Corrosion attacks the metallic connections of PV cells and results in a loss of adhesive strength between the cells and the metallic frame, as well as an increased leakage current and therefore a loss in performance [32]. Empirical models based on power at maximum power point and series resistance as degradation indicators have been proposed to model corrosion according to [35]–[37]. The models are as follows.

1) The Model of Pan [35]

$$\frac{P_{\text{max}}}{P_{\text{max}(0)}} = \exp(-R_D t^{\beta}). \tag{18}$$

2) P_{max} and R_s Models According to Braisaz [36]

$$P_{\text{max}} = \frac{1-\exp(-B)}{1+\exp(R_D t - B)} \tag{19}$$

$$R_s = R_{s(0)} + \exp(R_D t - B) \tag{20}$$

where P_{max} and R_s are the output power and series resistance at time (t), $P_{\text{max}(0)}$ and $R_{s(0)}$ are the power output and series resistance at time ($t = 0$), β is the experimental parameter, B is a coefficient to be defined, and R_D is the degradation rate determined according to (21), (22), and (23).

1) Models for Degradation Rate (R_D) Calculation: Kinetic models are developed on the primary assumption that the rate of degradation is proportional to the concentration of water in PV modules and that the rate constant has a Arrhenius temperature dependence. Three models according to [19] and [38] are proposed, namely the Peck's model, the Eyring model, and the exponential model.

Peck's model:

$$R_{D.\text{Peck}} = A\exp\left(-\frac{E_a}{k_B T}\right) RH^n. \tag{21}$$

Eyring model:

$$R_{D.\text{Eyring}} = A\exp\left(\frac{-E_a}{k_B T} - \frac{b}{RH}\right). \tag{22}$$

Exponential model:

$$R_{D.\text{Exp}} = A\exp\left(\frac{-E_a}{k_B T}\right).\exp(m \times RH). \tag{23}$$

Here, E_a is the activation energy of the degradation process [eV], T the module temperature [K], k_B is the Boltzmann constant (8.62×10^{-5} eV/K), and RH is the relative humidity [%].

TABLE II
COMPARISON OF MODELS FOR DEGRADATION RATE

Degradation model	A	E_a [eV]	n,b & m	% deviation
Module 1				
Peck	0.022	0.86	2.17	0.35%
Eyring	0.07	0.71	13.5	1.4%
Exponential	0.012	0.88	0.12	0.5%
Module 2				
Peck	0.12	0.79	2.05	0.41%
Eyring	0.129	0.62	23.0	2.0%
Exponential	0.006	0.81	0.12	0.6%

A, n, b, and m are model parameters. R_D [%/h] is the inverse of the mean time to failure at a given condition. In order to obtain A, E_a, n, b, and m in (21), (22), and (23), the equations can be fitted to experimental data or represented on a logarithmic scale by a straight line, using the following equations:

$$ln(R_{D.\text{Peck}}) = ln(A) - \left(\frac{E_a}{k_B T}\right) + n \times ln(RH) \qquad (24)$$

$$ln(R_{D.\text{Eyring}}) = ln(A) - \left(\frac{E_a}{k_B T}\right) - \frac{b}{RH} \qquad (25)$$

$$ln(R_{D.\text{Exp}}) = ln(A) - \left(\frac{E_a}{k_B T}\right) + m \times RH. \qquad (26)$$

A plot of $ln(R_D)$ versus $1/T[K]$ gives an Arrhenius plot with a slope E_a/k_B and an intercept $ln(A)$.

2) Comparison of Corrosion Models: The models of Peck, Eyring, and exponential were applied to fit indoor data sets (damp heat at 85C/85% RH), of two c-Si modules, with module 1 showing a good performance stability compared with module 2. The models were compared based on the extracted parameters (see Table II) as well as the deviation from the fitted data points. All models are consistent concerning the influence of the activation energy on the degradation rate and that the predicted values are in the range of literature values for polymeric materials, which usually range between 0.6 and 2.0 eV [39]. Nevertheless, the Eyring model shows a significant difference in the extracted activation energy in comparison to that of Pecks and the exponential model. It also has the highest percentage deviation of fitted data points in both cases. Therefore, from this study, we can conclude that the Peck's model has a better fit compared with the other models.

Degradation models are utilized for the simulation of power output degradation for module 1 to predict its performance in three climatic zones: alpine (Zugspitze, Germany), maritime (Gran Canaria, Spain), and arid (Negev, Israel), assuming the degradation is because of corrosion according to Pan and Braisaz. The module temperature is given for a standard c-Si PV module type glass-backsheet construction installed at the three test sites and relative humidity was calculated from ambient conditions according to [40]. For all the simulations, annual

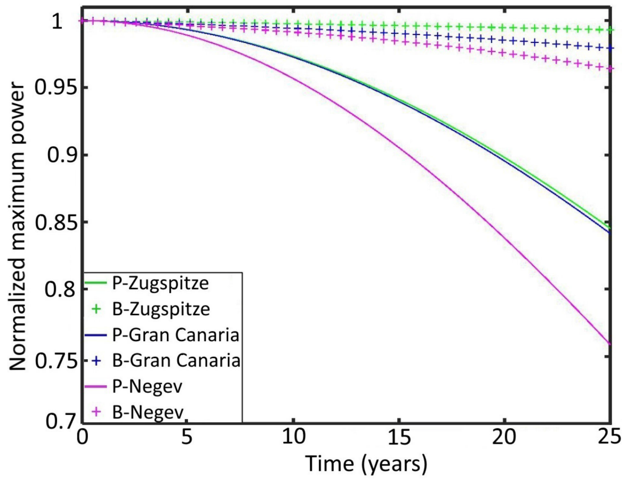

Fig. 3. Module 1. Maximum power degradation models of Pan (P) and Braisaz (B), simulated for three climates: Zugspitze (green), Gran Canaria (blue), and Negev (purple).

mean values of temperature and relative humidity were used. In both cases, the Peck's model was used for degradation rate calculation and both models were fitted to indoor data to extract the model parameters.

Both models show that temperature is the most relevant factor that influences the PV degradation process, visible by the power losses depicted in Fig. 3. This can be seen by a small loss through lower degradation in power for the module installed at Zugspitze, where the climate is characterized by low temperatures and high levels of relative humidity. However, the models completely differ in degradation predictions. According to the simulations, the model of Pan converges at a relatively fast rate compared with the one of Braisaz. This could be due to the influence of the model coefficients such as B and β. Moreover, the time parameter for the Pan model follows a power law, hence β might be an accelerating factor.

B. Degradation Models for PID

PID has been observed in all PV technologies and in almost all operating climates. It does not occur so frequently, but if it does, its effect can lead to a severe performance loss within a short period [4], [41]–[44]. In general terms, PID is caused by the difference in potential between the cells and the support structure of the module. This difference drives a leakage current that can lead to power degradation. Different types of PID occur depending on the module technology. For crystalline silicon PV, two degradation modes can be identified, PID-p (for polarization or passivation) and PID-s (for shunting). PID-p is a temporary and reversible degradation of the passivation layer, which reduces the performance due to a surface recombination increase [45]–[47]. PID-s is because of a leakage current involving an ionic flow of Na+ from the glass, encapsulant or cell surface into the cell, diffusing into the silicon stacking faults and shunting the cell [48]. The sodium incorporation in the Si surface degrades primarily the FF, the V_{oc}, and finally the I_{sc}. The relevant stress factors for PID-s include [42]; high temperature,

TABLE III
PIDHACKE MODEL

A	E_a [eV]	n
4.61	0.99	2.99

relative humidity, system voltage, light, bias-junction potential, and injected carriers. The models proposed for PID degradation according to [36], [43], [44], [49]–[51] are as follows.

1) Pidhacke Model: A parabolic model was proposed by Hacke *et al.* [44] to fit the power degradation of c-Si modules

$$\frac{P_{\max}}{P_{\max(0)}} = 1 - A\exp\left(-\frac{E_a}{k_B T}\right) RH^n \times t^2. \quad (27)$$

The constants A and n are determined by fitting the equation to experimental results. The parameters have to be determined for each module type. This parabolic model is applicable to the beginning of the degradation phases of PID-s, as it can fit the beginning of a sigmoid and does not describe the stabilization phase of the sigmoidal curve. Annigoni *et al.* [49] used the indoor data to determine coefficients of the model for distinct aging contributions (temperature, relative humidity, and time) and then applied the model including a voltage term in (28) to outdoor PID degradation for different climates

$$\frac{P_{\max}}{P_{\max(0)}} = 1 - A\exp\left(-\frac{E_a}{k_B T}\right) RH^n \times t^2 \times U. \quad (28)$$

In this study, a similar approach is adopted to extract the model coefficients in Table III and to simulate maximum power degradation because of PID in three climatic zones; alpine (Zugspitze, Germany), maritime (Gran Canaria, Spain), and arid (Negev, Israel). In all simulations, a constant voltage of 500 V was assumed. The simulation results, shown in Fig. 4, were consistent with the ones of Annigoni, saying that a more severe degradation is predicted for arid climates.

2) Exponential Model: The model was applied by Hacke *et al.* [43] to predict PID occurrence in thin-film modules in the field using accelerated tests. Considering shunting, which is the PID mode that occurs first, an exponential model based on module temperature T and relative humidity RH was found to fit well the PID rate for multiple stress levels of a CdTe module in chamber tests. The power model is of the form

$$\frac{d}{dt}\left(\frac{P_{\max}}{P_{\max(0)}}\right) = 1 - Af(U)\exp\left(-\frac{E_a}{k_B T}\right) RH^n \times t \quad (29)$$

where $f(U)$ expresses the voltage dependency.

3) Model of Hattendorf: The model of Hattendorf *et al.* [50] is based on a matrix of indoor experiments where modules are exposed to varying voltage, module temperature, and ambient humidity. The conditions are varied to determine the model

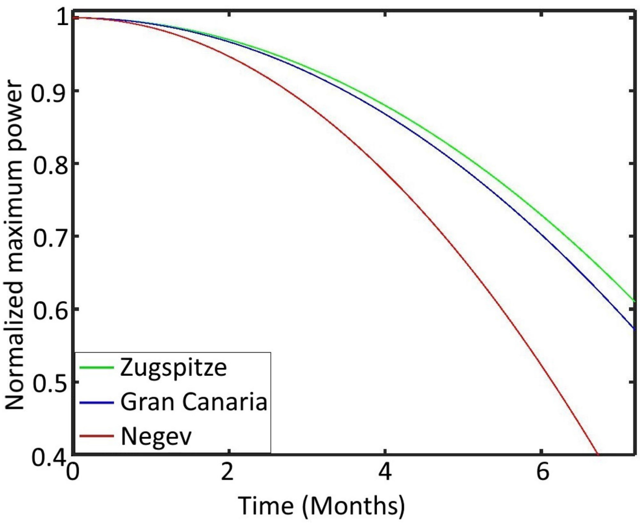

Fig. 4. Simulated normalized maximum power degradation because of PID in three climatic zones; Freiburg (green), Gran Canaria (blue) and Negev (red).

parameters for the module power. The model is written as

$$P_{\max}(U, T, RH, t) = P_{\max(0)}(1 - P(t)) \quad (30)$$

$$P(t) = P_\infty \frac{1 - \exp\left(\frac{t}{\tau_1}\right)}{1 - \exp\left(\frac{t - t_0}{\tau_2}\right)};$$

$$P(U) = \left(1 + \exp\left(\frac{U - U_0}{\Phi}\right)\right)^{-2} \quad (31)$$

$$t_0 = a \times b \times \hat{t_0}; \tau_1(T) = b^2 \times \hat{\tau}_1; \tau_2 = \hat{\tau}_2 \quad (32)$$

$$a(H) = \frac{H_0}{H}; b(T) = \exp\left(\frac{T - T_0}{\phi}\right). \quad (33)$$

The model includes six adaptation parameters: $\hat{t_0}$, U_0, $\hat{\tau}_1$, $\hat{\tau}_2$, Φ, and ϕ. H_0 and T_0 are scaling parameters. The function $P(t)$ describes the power loss caused by degradation. $P_\infty(U)$ is its limit for $t \to \infty$, and $a(H)$ and $b(T)$ are the acceleration functions of relative humidity and temperature. For $T = 0$ and $H = 0$, they are equal to 1, therefore $\hat{\tau}_1, \hat{\tau}_2$ are the time constants under these conditions. τ_2 remains constant for a given module. To determine the model's parameters, the power degradation is measured as a function of time with the system voltage U as parameters and a fixed humidity H as well as temperature T. The saturating power P_∞ is extracted by fitting $P(t)$ to the measured data.

4) Taubitz Model: Taubitz *et al.* [51] proposed a regeneration model for shunt resistance evolution over time because of PID degradation. The shunt resistance was modeled in three phases: shunting phase, regeneration phase, and transition phase as follows:

Shunting phase:

$$R_{sh}(t) = a_S \exp\left(\frac{-t}{b_S(t)}\right). \quad (34)$$

This article has been accepted for inclusion in a future issue of this journal. Content is final as presented, with the exception of pagination.

Regeneration phase:

$$R_{sh}(t) = C_R + a_R \exp\left(\frac{t}{b_R(t)}\right). \quad (35)$$

Transition phase:

$$R_{sh}(t) = a_T(T)(t + b_T(T))^2 + C_T \quad (36)$$

where a_S, b_S, C_T, b_T, $a_T(T)$, $b_S(T)$, $b_T(T)$, C_R, and a_R are constants and have to be determined for a specific module type. Some of them are dependent on the module temperature T. The constants are determined by measuring the times t_S, t_T, and t_R for reaching certain target values.

5) PID Model According to Braisaz et al. [36]: The model is based on shunt resistance R_{sh} degradation as an indicator, as it is the most important parameter for PID. The evolution of R_{sh} as a function of voltage, temperature, and relative humidity was modeled as

$$R_{sh}(t) = \frac{R_{sh(0)}}{1 + aR_D t} \quad (37)$$

$$R_D = A \times U \frac{B}{1 + \exp(-C(RH) + D)} \exp\left(-\frac{E_a}{k_B T}\right) \quad (38)$$

where R_{sh} is the shunt resistance at time (t), $R_{\text{sh}(0)}$ is the initial shunt resistance, A, B, C, and D are model coefficients, U is the applied voltage, and R_D is the degradation rate.

Recommendation: The model contains many coefficients whose usage is not clearly described, such coefficients might affect the physical interpretation of the results when used inappropriately. Therefore, we recommend that one should have a prior knowledge of the impact of the parameters on which the coefficients are being applied to the degradation process in question.

C. Models for UV Degradation

UV light exposure has been reported to cause PV module degradation in a number of ways. Exemplary, it could result in discoloration of the encapsulant material [52] or delamination at the glass encapsulant or cell encapsulant interface [53]. The parameter most impacted by UV exposure is the short circuit current (I_{sc}). Braisaz *et al.* [36] proposed a model for short circuit degradation because of UV exposure over time. They found that the degradation curve is not linear but an exponentially decreasing curve. The short circuit is modeled as a function of UV as

$$I_{sc}(t) = I_{sc(0)} - aD_{\text{UV}}(t) - b(1 - \exp(-CD_{\text{UV}})(t)) \quad (39)$$

$$D_{\text{UV}}(t) = \int_0^t E(u) \times 5.5\% \, \mathrm{d}u. \quad (40)$$

Here, D_{UV} is the UV dose in MJ/m^2 or kWh/m^2, I_{sc} is the short circuit current at time (t), $I_{\text{sc}}(0)$ is the initial short circuit current, and a, b, and C are model coefficients. The multiplication by 5.5% is because the UV radiation (280–400 nm) is approximately 5.5% of the total light spectrum $E(u)$ [54].

1) Schwarzschild Law: The Schwarzschild Law has been applied by Gu *et al.* [55] to study the effect of intensity and wavelength of spectral UV light on discoloration of laminated glass/EVA/PPE PV modules. The law is a function of intensity as

$$k = A(I)^p. \quad (41)$$

Here, k is a constant, I the intensity, and p is the Schwarzschild coefficient.

Recommendation: When applying this expression in performance (power) prediction models where other loads are also applied, the parameter p must be calibrated according to the knowledge of severity ranking [56].

D. Degradation Models for Delamination, Fatigue Solder Failure, and Cell Cracks

1) Coffin–Manson's Equation: The model is used to predict degradation modes caused by temperature cycling such as encapsulant delamination, fatigue solder failure, and cell cracks. According to Escobar and Meeker [38], the model describes the number of cycles to failure as

$$N = \frac{\sigma}{(\Delta T)^{\beta_1}} \quad (42)$$

where ΔT is the temperature range and σ and β_1 are properties of the material and test setup. The cycles-to-failure distribution for temperature cycling can also depend on the cycling rate (e.g., because of heat buildup). An empirical extension of the Coffin–Manson relationship that describes such dependencies is [38]

$$N = \frac{\sigma}{(\Delta T)^{\beta_1}} \frac{1}{(\text{freq})^{\beta_2}} \exp\left(\frac{E_a \times 11605}{T_{\max}(K)}\right) \quad (43)$$

where freq is the cycling frequency and E_a is a quasi-activation energy.

2) Crack Propagation Model: The model was suggested by Braisaz *et al.* [36] and it was applied to simulate the degradation of the short-circuit current I_{sc} due to the expansion of cell cracks caused by temperature. The model takes the form

$$C_a(t) = C_a(t-1) + \frac{1}{x\left(\frac{125}{T_a}\right)^m}. \quad (44)$$

$C_a(t)$ is the crack activation at time (t), $C_a(t-1)$ the crack activation at time $(t-1)$, T_a is the daily temperature amplitude, m a model parameter, and x is the number of thermal cycles. The crack activation/propagation model is dependent on the daily temperature amplitude T_a.

3) Damage Accumulation Model: The model was used by Bosco *et al.* [57] in order to calculate the solder fatigue damage in seven cities investigated in their study and compared with FEM simulated results. They found out that the model fits well to the simulated calculations. The model is written as

$$D = C(\Delta T)^n (r(T))^m \exp\left(-\frac{Q}{k_B T_{\max}}\right). \quad (45)$$

In this equation, ΔT is the mean daily maximum cell temperature change, $T_{\max}$ the mean maximum daily temperature, C a scaling constant, Q the activation energy, k_B Boltzmann's constant, $r(T)$ the number of times the temperature history increases or decreases across the reversal temperature, T the period of a year, and n and m are model constants similar to those in the Coffin–Manson equation.

4) Backsheet Degradation Model: The model is used to estimate a potential form of the degradation kinetics of the backsheet. This kinetic model was applied by Kempe [58] to model the uncertainty in a 25-year equivalent test for module backside exposure to irradiance and temperatures in different climatic zones. The degradation rate model is written as

$$R_D \approx I^X (b + m \times \text{TOW}) \times (T_f)^{\frac{T - T_0}{10}}. \tag{46}$$

Here, I is the light intensity, X, b, and m are fit parameters, TOW is the time of wetness, T the temperature, T_0 a reference temperature, and T_f is a multiplier for the increase in degradation for a rise in temperature in 10 K steps.

Recommendation: As also mentioned by Kempe, the parameter that describes the effect of time of wetness has very high uncertainties, we recommend careful comparison of the relative change in degradation rate with changes in TOW. In case one wants to extract thermal parameters such as activation energy, the multiplier term (T_f) can be replaced by the Arrhenius term.

E. Model Based on Multiple Stresses

Since degradation of PV modules in outdoor operation is influenced by multiple environmental stresses, models based on multiple stresses are viable for outdoor service lifetime prediction.

1) Model of Gaines: Gaines *et al.* [37] proposed a model for power output degradation based on multiple accelerated environmental stresses. The model suggested is

$$\frac{P_{\max}}{P_{\max(0)}} = [1 - R_D t]^{\frac{1}{\beta}} \tag{47}$$

$$R_D = A f_T f_{RH} f_M f_G f_\omega \tag{48}$$

where R_D is the degradation rate and the factors f_T, f_{RH}, f_M, f_G, and f_ω are associated with a decrease in power output due to effects of temperature T, relative humidity RH, mechanical stresses M (due to temperature differences), gaseous concentration G, and the frequency of the temperature excursion. The mathematical form of each factor is formulated to represent the underlying physical phenomena. An Arrhenius form is used for

$$f_T = \exp\left(-\frac{B}{T}\right). \tag{49}$$

B denotes a constant parameter and T denotes temperature. The effect of relative humidity f_{RH} is represented by

$$f_{\text{RH}} = 1 + (\text{RH})_0 \exp\left(C_0\left(\frac{1}{T_C} - \frac{1}{T_0}\right)\right)^{C - \frac{D}{T}}. \tag{50}$$

The second term in the bracket corrects the relative humidity as a function of temperature, given a specified relative humidity at T_0. C and D are constant parameters. The mechanical/temperature excursion factor f_M is represented by

$$f_M = \left[\frac{\exp\left(G_1\left(\frac{1}{T} - \frac{1}{T_b}\right)\right) + \exp\left(-G_2\left(\frac{1}{T} - \frac{1}{T_b}\right)\right)}{D_0}\right] \times \exp(J\Delta T). \tag{51}$$

The first term in the bracket reflects the stresses arising from differences in expansion coefficients of bonded materials. The constants G_1, G_2, D_0, and T_b are chosen to represent the estimated magnitudes of these fatigue effects. The factor $\exp(J\Delta T)$ estimates the effect of the magnitude of the temperature excursion ΔT, where J is a constant

$$f_G = \left[1 + \frac{G}{G_o}\right]^{E - \frac{F}{T}}. \tag{52}$$

Here, E and F denote constant parameters and T is the temperature. The frequency of the temperature excursion f_ω is represented by

$$f_\omega = \left[1 + \frac{\omega}{\omega_o}\right]^{P - \frac{Q}{T}}. \tag{53}$$

ω is the frequency and P as well as Q are constant parameters. In a constant temperature test, T is a constant and ω is taken to be zero. In the cyclic temperature tests, reciprocal temperature is considered to be a sinusoidal function of time

$$\frac{1}{T}(t) = \tau + \Delta\tau \sin(\omega t) \tag{54}$$

$$\tau = \frac{1}{2}\left[\frac{1}{T_{\min}} - \frac{1}{T_{\max}}\right]. \tag{55}$$

$T_{\min}$ and $T_{\max}$ are the minimum and maximum temperatures associated with the temperature cycles.

Recommendation: The model of Gaines presents the previous approach on multiple stress modeling, however, the user should take caution that this model was developed and applied on PV modules that had a different construction from today's modules. Therefore, its application might need some modification to fit the current PV module construction types.

2) Model of Subramaniyan: Another model to calculate the degradation rate because of combined environmental stresses has been proposed recently by Subramaniyan *et al.* [59]. The model takes into account the effect of both static and cyclic temperature, UV radiation and relative humidity as

$$\text{Rate}(T, \Delta T, \text{UV}, \text{RH}) = \beta_0 \exp\left(-\frac{\beta_1}{k_B T_{\max}}\right) \times (\Delta T_{\text{daily}})^{\beta_2} \times (UV_{\text{daily}})^{\beta_3} \times (RH_{\text{daily}})^{\beta_4} \tag{56}$$

where $\text{Rate}(T, \Delta T, UV, RH)$ is the reaction rate, $T_{\max}$ the daily maximum temperature of the module [K], ΔT_{daily} the daily cyclic temperature of the module [K], UV_{daily} the daily daytime average irradiance [W/m^2], RH_{daily} the daily average relative humidity [%], and k is the Boltzmann constant. The model parameters β_0, which is the frequency factor [s^{-1}], β_1, the activation energy [eV], β_2, the effect of cyclic temperature, β_3, the effect of UV radiation and β_4, the effect of RH, can be estimated from measured data through data fitting techniques. In the scope of this paper, the model is presented but has not been applied or tested in any way due to a lack of combined stress data. A more detailed description and application of the model can be found in [59].

VI. Discussion and Conclusion

In this paper, several PV system performance loss methodologies are reviewed. Hereby, statistical and analytical models are taken into account.

First, a discussion about statistical models to determine the PLR of PV systems from available outdoor data is presented. The performance loss trend is retrieved by applying filters, performance metrics, and statistical models on data sets. By performing detailed in-depth performance studies, it might be possible to gain a greater understanding about the root causes of the decrease in the power output of PV systems over time. Especially when considering current and voltage behavior, specific degradation modes could be identified and at a later stage verified by visual inspection techniques.

As a first measure, appropriate filtering techniques have to be applied on the data set in question. The choice of the filter will strongly depend on the performance metric and/or statistical model and, in case of an inappropriate filter window, will falsify the final outcome. On the other hand, pretreatment of the data set is necessary to eliminate outliers, noise, and minimize seasonal oscillation. Before deciding which performance metric or statistical model to use, the PV system technology, the length of the observed period, climatic conditions, and mounting system (rack, tracker) should be taken into consideration. Prevailing seasonality, temperature/irradiance dependency of the *I–V* curve parameters and noncorrelated outliers (data errors, shading effects, etc.) will increase the uncertainty of the results and influence the final PLR. The final aim is to receive a clear performance trend. In Section IV-C, the discussed statistical models have been applied on monitored field data of one monocrystalline silicon and one amorphous silicon system to retrieve long-term performance trends. Thereby, the application of SLR resulted in performance ratings with the greatest uncertainties in comparison. The usage of CSD produced performance rates with low uncertainties but due to the elimination of the first and last months of monitored data through the centered moving average, this technique is not recommended for data sets, which just consider short time periods. It was seen that CSD overestimated the performance loss of both systems. The remaining techniques, namely HW exponential smoothing, ARIMA, and STL, are performed on a similar high level of accuracy and the results are almost identical. HW experiences a slightly higher uncertainty when applied to the amorphous silicon PV system. It seems that ARIMA and STL are better suited for noncrystalline PV systems due to their favorable treatment of the temperature behavior of the system in question. These three techniques exclude the seasonal part in time-series of PV performance metrics, which is an important modeling step in order to receive a clear performance trend. Nevertheless, it has to be stressed that the application of statistical models, especially ARIMA, has to be performed with great care and that it is not a rudimentary exercise to retrieve accurate model parameters for more advanced models. In case of ARIMA, the time-series has to be stationary. The model parameters need to be chosen based on the time-series behavior. That means that PV-related parameters, like the varying temperature dependency of different PV technologies, or the prevailing weather conditions have to be taken into account.

Unfortunately, it is not possible to determine if a (or which) degradation mode occurs on the basis of calculated PLRs. Apart from degradation modes, other factors such as shading or soiling might be a reason for a reduced performance. Because of that, it is important to not only study the data of a PV system, but also to undertake regularly visual and electrical inspections and connect the findings with the calculated PLR. An idea of how to isolate the occurrence of degradation modes within a module under surveillance might be the application of the presented models on the short-circuit current, the open-circuit voltage and the fill factor. Hence, it might be possible, together with the inclusion of results from the studies of accelerated tests, to find patterns in the trends of these values.

In the second part of this work, several analytical models for specific degradation modes, which trigger the aforementioned performance losses to a large extent, are further studied. The models proposed for corrosion and PID were implemented to simulate the maximum power degradation in three climatic zones. A strong influence of the climate is evident in all the simulation results where, as expected, a more severe degradation is predicted for arid climates. The key observations in this study are as follows.

1) Although these models give a preliminary approximation of the time-evolution of power performance, they do not provide any information on the physical processes taking place within the module.
2) The models are developed based on numerous assumptions and simplifications, moreover the hypotheses of a particular degradation mode are modeled depending on environmental stress factors and do not take into consideration the influence of material parameters.
3) None of the models is universal, that is, they can well describe the degradation of a specific type of a PV technology and fail on the other. Therefore, it is necessary to be certain that a chosen degradation model is valid for a specific application.
4) The analytical models are developed and validated based on indoor data from accelerated tests. Although some authors went on to simulate outdoor conditions based on indoor observations, a big challenge remains of how to interpret the results for multiple environmental stresses using indoor data.

According to these observations, we recommend further developments for models that take into account both material and multiple environmental stress factors. The development of such models need to be related to indoor as well as outdoor observations.

Acknowledgment

This project has received funding from the European Union's Horizon 2020 research and innovation programme in the framework of the project "SolarTrain" under the Marie Sklodowska-Curie GA No 721452.

REFERENCES

[1] C. S. Solanki, *Solar Photovoltaics - Fundamentals, Technologies and Applications vol. 2*. New Delhi, India: PHI Learning Private Limited, 2012.

[2] I. M. Peters, H. Liu, T. Reindl, and T. Buonassisi, "Global prediction of photovoltaic field performance differences using open-source satellite data," *Joule*, vol. 2, no. 2, pp. 307–322, Feb. 2018.

[3] M. Kontges *et al.*, *Assessment of Photovoltaic Module Failures in the Field*. Report IEA PVPS T13-09:2017, Subtask 3, 2017.

[4] D. Moser *et al.*, "Identification of technical risks in the photovoltaic value chain and quantification of the economic impact," *Prog. Photovolt.: Res. Appl.*, vol. 25, no. 7, pp. 592–604, 2017.

[5] *International Electrotechnical Vocabulary. Chapter 191: Dependability and Quality of Service*, IEC60050-191, International Electrotechnical Comission, Geneva, CH, Standard, 1990.

[6] D. C. Jordan and S. R. Kurtz, "Photovoltaic degradation rates - An analytical Review: Photovoltaic degradation rates," *Prog. Photovolt.: Res. Appl.*, vol. 21, no. 1, pp. 12–29, Jan. 2013.

[7] A. Phinikarides, N. Kindyni, G. Makrides, and G. E. Georghiou, "Review of photovoltaic degradation rate methodologies," *Renew. Sustain. Energy Reviews*, vol. 40, pp. 143–152, Dec. 2014.

[8] D. Moser, M. Pichler, and M. Nikolaeva, "Filtering procedures for reliable outdoor temperature coefficients in different photovoltaic technologies | journal of solar energy engineering | ASME DC," *J. Solar Energy Eng.*, vol. 136, no. 2, pp. 021006-1–021006-10, 2013.

[9] C. M. Whitaker *et al.*, "Application and validation of a new PV performance characterization method," in *Proc. Conf. Record 26th IEEE Photovolt. Spec. Conf.*, Sep. 1997, pp. 1253–1256.

[10] G. H. Yordanov, "Relative efficiency revealed: Equations for k1-k6 of the PVGIS model," in *Proc. IEEE 40th Photovolt. Specialist Conf.*, Jun. 2014, pp. 1393–1398.

[11] D. L. King, J. A. Kratochvil, and W. E. Boyson, "Photovoltaic array performance model," Tech. Rep. SAND2004-3535, 919131, Sandia Nat. Lab., Albuquerque, NM, USA, Aug. 2004.

[12] E. Skoplaki and J. A. Palyvos, "On the temperature dependence of photovoltaic module electrical performance: A review of efficiency/power correlations," *Solar Energy*, vol. 83, no. 5, pp. 614–624, May 2009.

[13] D. C. Jordan, J. H. Wohlgemuth, and S. R. Kurtz, "Technology and climate trends in PV module degradation," in *Proc. 27th EU PVSEC Proc.*, 2012, pp. 3118–3124.

[14] T. Huld *et al.*, "A power-rating model for crystalline silicon PV modules," *Solar Energy Mater. Solar Cells*, vol. 95, no. 12, pp. 3359–3369, Dec. 2011.

[15] C. Jennings, "PV module performance at PG&E," in *Proc. Conf. Rec. 20th IEEE Photovolt. Spec. Conf.*, Sep. 1988, pp. 1225–1229.

[16] C. Whitaker, T. Townsend, and H. Wenger, "Effects of irradiance and other factors on PV temperature coefficients," in *Proc. Conf. Rec. 22nd IEEE Photovolt. Spec. Conf.*, Oct. 1991, pp. 608–613.

[17] *Photovoltaic System Performance Monitoring—Guidelines for Measurement, Data Exchange and Analysis*, IEC61724:1998, International Electrotechnical Comission, Geneva, CH, Standard, 1998.

[18] G. Belluardo *et al.*, "Novel method for the improvement in the evaluation of outdoor performance loss rate in different PV technologies and comparison with two other methods," *Solar Energy*, vol. 117, pp. 139–152, Jul. 2015.

[19] D. C. Jordan and S. R. Kurtz, "Analytical improvements in PV degradation rate determination," in *Proc. 35th IEEE Photovolt. Spec. Conf.*, Jun. 2010, pp. 688–693.

[20] C. C. Holt, "Forecasting seasonals and trends by exponentially weighted moving averages," *Int. J. Forecasting*, vol. 20, no. 1, pp. 5–10, Jan. 2004.

[21] R. J. Hyndman and G. Athanasopoulos, *Forecasting: Principles and Practice*. Melbourne, Australia: OTexts, 2013.

[22] A. Phinikarides, G. Makrides, N. Kindyni, A. Kyprianou, and G. E. Georghiou, "ARIMA modeling of the performance of different photovoltaic technologies," in *Proc. 39th IEEE Photovolt. Spec. Conf.*, Jun. 2013, pp. 0797–0801.

[23] S. G. Makridakis and S. C. Wheelwright, *Forecasting*, 3rd ed. New York, NY, USA: Wiley, Jan. 1998.

[24] C. Sax, *Seasonal: R Interface to X-13-ARIMA-SEATS*, R package version 1.6.1. 2017. [Online]. Available: https://CRAN.R-project.org/package=seasonal

[25] A. Phinikarides, G. Makrides, and G. E. Georghiou, "Comparison of analysis method for the calculation of degradation rates of different photovoltaic technologies," in *Proc. 27th EU PVSEC Proc.*, 2013, pp. 3211–3215.

[26] R. B. Cleveland, W. S. Cleveland, J. E. McRae, and I. Terpenning, "STL: A seasonal-trend decomposition procedure based on loess," *J. Official Statist.*, vol. 6, no. 1, pp. 3–33, 1990.

[27] *Evaluation of Measurement Data—Guide to the Expression of Uncertainty in Measurement,"*International Bureau of Weights and Measures, BIPM-JCGM-100:2008, Sevres, FR, Guide, 2008.

[28] E. Hasselbrink *et al.*, "Validation of the PVLife model using 3 million module-years of live site data," in *Proc. IEEE 39th Photovolt. Spec. Conf.*, Jun. 2013, pp. 0007–0012.

[29] D. C. Jordan, C. Deline, S. R. Kurtz, G. M. Kimball, and M. Anderson, "Robust PV degradation methodology and application," *IEEE J. Photovolt.*, vol. 8, no. 2, pp. 525–531, Mar. 2018.

[30] A. Ndiaye *et al.*, "Degradations of silicon photovoltaic modules: A literature review," *Solar Energy*, vol. 96, pp. 140–151, Oct. 2013.

[31] N. Park, C. Han, and D. Kim, "Effect of moisture condensation on long-term reliability of crystalline silicon photovoltaic modules," *Microelectron. Rel.*, vol. 53, no. 12, pp. 1922–1926, Dec. 2013.

[32] M. D. Kempe *et al.*, "Acetic acid production and glass transition concerns with ethylene-vinyl acetate used in photovoltaic devices," *Solar Energy Mater. Solar Cells*, vol. 91, no. 4, pp. 315–329, Feb. 2007.

[33] K. Whitfield, A. Salomon, S. Yang, and I. Suez, "Damp heat versus field reliability for crystalline silicon," in *Proc. 38th IEEE Photovolt. Spec. Conf.*, Jun. 2012, pp. 1864–1870.

[34] A. Masuda, N. Uchiyama, and Y. Hara, "Degradation by acetic acid for crystalline Si photovoltaic modules," *Jpn. J. Appl. Phys.*, vol. 54, no. 4S, pp. 04DR04-1–04DR04-6, Mar. 2015.

[35] R. Pan, J. Kuitche, and G. Tamizhmani, "Degradation analysis of solar photovoltaic modules: Influence of environmental factor," in *Proc. Annu. Rel. Maintainability Symp.*, Jan. 2011, pp. 1–5.

[36] B. Braisaz, C. Duchayne, M. Van Iseghem, and K. Radouane, "PV aging model applied to several meteorological conditions," in *Proc. 29th PVSEC Proc.*, Amsterdam, The Netherlands, Sep. 2014, pp. 2303–2309.

[37] G. B. Gaines *et al.*, "Development of an accelerated test design for predicting the service life of the solar array at mead, nebraska," Quarterly Techn. Rep., NASA, USA, Feb. 1979.

[38] L. A. Escobar and W. Q. Meeker, "A review of accelerated test models," *Statist. Sci.*, vol. 21, no. 4, pp. 552–577, Nov. 2006.

[39] R. Laronde, A. Charki, D. Bigaud, and P. Excoffier, "Reliability evaluation of a photovoltaic module using accelerated degradation model," in *Proc. SPIE*, 2011, vol. 8112.

[40] M. Koehl, M. Heck, and S. Wiesmeier, "Modelling of conditions for accelerated lifetime testing of Humidity impact on PV-modules based on monitoring of climatic data," *Solar Energy Mater. Solar Cells*, vol. 99, pp. 282–291, Apr. 2012.

[41] J. Berghold *et al.*, "Potential-induced degradation (PID) and its correlation with experience in the field," *Photovolt. Int.*, vol. 19, pp. 85–92, 2013.

[42] M. Kontges *et al.*, "Review of failures of photovoltaic modules," Report IEA PVPS T13-01:2014, Subtask 3.2, 2014.

[43] P. Hacke *et al.*, "Elucidating PID degradation mechanisms and in-situ dark I-V monitoring for modeling degradation rate in CdTe thin-film modules," *IEEE J. Photovolt.*, vol. 6, no. 6, pp. 1635–1640, Nov. 2016.

[44] P. Hacke *et al.*, "Accelerated testing and modeling of potential-induced degradation as a function of temperature and relative humidity," *IEEE J. Photovolt.*, vol. 5, no. 6, pp. 1549–1553, Nov. 2015.

[45] V. Naumann *et al.*, "Potential-induced degradation at interdigitated back contact solar cells," *Energy Procedia*, vol. 55, pp. 498–503, Jan. 2014.

[46] A. Halm *et al.*, "Potential-induced degradation for encapsulated n-type IBC solar cells with front floating emitter," *Energy Procedia*, vol. 77, pp. 356–363, Aug. 2015.

[47] R. Swanson *et al.*, "The surface polarization effect in high-efficient silicon solar cells," in *Proc. 15th Int. PVSEC Proc.*, Jan. 2005.

[48] D. Lausch *et al.*, "Sodium outdiffusion from stacking faults as root cause for the recovery process of potential-induced degradation (PID)," *Energy Procedia*, vol. 55, pp. 486–493, Jan. 2014.

[49] E. Annigoni *et al.*, "Modeling potential-induced degradation (PID) in crystalline silicon solar cells: From accelerated-aging laboratory testing to outdoor prediction," in *Proc. 32nd EU PVSEC Proc.*, Munich, Germany, Jun. 2016, pp. 1558–1563.

[50] J. Hattendorf *et al.*, "Potential induced degradation in mono-crystalline silicon based modules: An acceleration model," in *Proc. 27th Eur. PVSEC Proc.*, Oct. 2012, pp. 3405–3410.
[51] C. Taubitz, M. Krber, M. Schtze, and M. B. Koentopp, "Potential induced degradation: Model calculations and correlation between laboratory tests and outdoor occurrence," in *Proc. 29th Eur. PVSEC Proc.*, Nov. 2014, pp. 2490–2494.
[52] L. Dunn, M. Gostein, and B. Stueve, "Literature review of the effects of UV exposure on PV modules," in *NREL PV Module Reliab. Workshop*, Feb. 2013.
[53] M. A. Munoz, M. C. Alonso-Garcia, and Vela, "Early degradation of silicon PV modules and guaranty conditions," *Solar Energy*, vol. 85, no. 9, pp. 2264–2274, 2011.
[54] M. Koehl, D. Philipp, N. Lenck, and M. Zundel, "Development and application of a UV light source for PV-module testing," in *Proc. SPIE - Int Soc. for Opt. Eng. 7412*, Aug. 2009, pp. 7412021–7412027.
[55] X. Gu, Y. Lyu, L.-C. Yu, C.-C. Lin, and D. Stanley, "Effect of intensity and wavelength of spectral UV light on discoloration of laminated Glass/EVA/PPE PV module," in *3rd Atlas-NIST Workshop PV Mater. Durability*, Dec. 2015.
[56] D. C. Jordan, T. J. Silverman, J. H. Wohlgemuth, S. R. Kurtz, and K. T. VanSant, "Photovoltaic failure and degradation modes," *Progress Photovoltaics: Res. Appl.*, vol. 25, pp. 318–326, 2017.
[57] N. Bosco, T. J. Silverman, and S. Kurtz, "Climate specific thermomechanical fatigue of flat plate photovoltaic module solder joints," *Microelectron. Rel.*, vol. 62, pp. 124–129, Jul. 2016.
[58] M. D. Kempe, "Evaluation of the uncertainty in accelerated stress testing," in *Proc. IEEE 40th Photovolt. Spec. Conf.*, Jun. 2014, pp. 2170–2175.
[59] A. B. Subramaniyan, R. Pan, J. Kuitche, and G. TamizhMani, "Quantification of environmental effects on PV module degradation: A physics-based data-driven modeling method," *IEEE J. Photovolt.*, vol. 8, no. 5, pp. 1289–1296, Sep. 2018.

Sascha Lindig received the B.Eng. degree in photovoltaic and semiconductor technologies from the University of Applied Science Jena, Jena, Germany, in 2011, and the M.Eng. degree in environmental and energy engineering from the Leipzig University of Applied Sciences, Leipzig, Germany, in 2014. He is currently working toward the Ph.D. degree in electrical engineering with the University of Ljubljana, Ljubljana, Slovenia, in collaboration with EURAC Research, Bolzano, Italy.

He is working in the frame of the Marie Sklodowska Curie SOLAR-TRAIN project on statistical performance loss models of PV systems, degradation patterns and solar economics.

Ismail Kaaya was born in Uganda. He received the B.S. degree in applied physics from the International University of Africa, Khartoum, Sudan, in 2013, the Postgraduate Diploma degree in condensed matter physics from the Abdus-Salam International Center for Theoretical Physics, Trieste, Italy, in 2015, and the M.S. degree in renewable energy science and technology from Ecole Polytechnique, Palaiseau, France, in 2016. He is currently working toward the Ph.D. degree in photovoltaics with Fraunhofer Institute for Solar Energy Systems, Freiburg, Germany.

His research interests includes advanced characterization of hydrogenated amorphous silicon, modeling spatial inhomogenities/(microscopic defects) in solar cells, and development of service life models for PV modules.

David Moser received the B.Sc. and M.Sc. degrees from the University of Trento, Italy, in 2003 and 2006, respectively, the Ph.D. degree in physics from the Salford University, Salford, U.K., in 2010.

He coordinates the activities of the research group Photovoltaic Systems, Institute for Renewable Energy, EURAC, Bolzano, Italy. His work focuses on characterizing indoor and outdoor behavior, performance, and reliability of photovoltaic (PV) modules and systems, building integration of PV systems, and monitoring of outdoor PV plants. He is also active in PV potential studies on a regional scale and member of the Board of Directors of The Association of European Renewable Energy Research Centres.

Karl-Anders Weiß received the Diploma degree in physics and economics and the Ph.D. degree in physics from the University of Ulm, Germany, in 2005 and 2014, respectively.

He is Head of the Service Life Analysis Group, Fraunhofer Institute for Solar Energy Systems, Freiburg, Germany. His areas of interest include degradation of materials in solar applications, accelerated testing of components and materials of solar systems, numerical simulations, methods to analyze degradation of polymers, nondestructive analytical methods climatic loads and service life prediction.

Marko Topic received the Ph.D. degree from the University of Ljublana, Slovenia, in 1996.

He is the Head of Laboratory of Photovoltaics and Optoelectronics, University of Ljubljana, Ljubljana, Slovenia, acts as the Chairman of the European Technology and Innovation Platform Photovoltaics (ETIP-PV) since 2016 and previously as the Chairman of European Photovoltaic Technology Platform (since 2014). He is currently a full Professor with the Faculty of Electrical Engineering at the University of Ljubljana, and he has a very broad research experience in photovoltaics, thin-film semiconductor materials, electron devices, optoelectronics, electronic circuits, and reliability engineering.

Dr. Topic is a member of the Slovenian Academy of Engineering and has received several prestigious awards, including the "Zoisova nagrada" in 2008 (the highest award of the Republic of Slovenia for Scientific and Research Achievements).

Modeling Outdoor Service Lifetime Prediction of PV Modules: Effects of Combined Climatic Stressors on PV Module Power Degradation

Ismail Kaaya, Michael Koehl, Amantin Panos Mehilli, Sidrach de Cardona Mariano, and Karl Anders Weiss

***Abstract*—Photovoltaic modules are exposed to a variety of climatic loads during outdoor operation. Over time, these loads trigger a number of degradation modes within the modules leading to performance loss. This paper quantifies the impact of combined climatic loads on the module's maximum power output using a mathematical approach. Three degradation precursor reactions, namely, hydrolysis, photodegradation, and thermomechanical degradation, are assumed to be necessary for service lifetime prediction. For each reaction, an empirical kinetics model is proposed and validated with indoor test measurements. A generalized model to quantify the effects of combined climatic loads is proposed. The generalized model is calibrated and validated using outdoor test measurements. The model is then applied to predict the annual degradation rates and a 20% performance loss of three identical monocrystalline modules installed in three benchmarking climates: maritime (Gran Canaria, Spain), arid (Negev, Israel), and alpine (Zugspitze, Germany) using real monitored meteorological data. A degradation of 0.74%/year corresponding to 21.4 years operation time was predicted as the highest for an arid environment, compared with 0.50%/year and 0.3%/year degradation for maritime and alpine environments, respectively. The proposed models will find applications in outdoor predictions as well as in the combined stress accelerated tests to develop test designs.**

***Index Terms*—Climatic zones and service lifetime prediction, degradation model, degradation modes, photovoltaic (PV) module.**

I. Introduction

THE search for a combined stress model for photovoltaic (PV) module lifetime prediction dates back to the 1970s, for example, Gaines *et al*. [1] proposed a quantitative model for accelerated testing using multiple environmental stresses, which was used to develop the test design. Recently, Subramaniyan *et al*. [2] have proposed a model to link the module degradation path and environmental variables. According to our previous publication [3], the current state-of-the-art degradation models available for PV modules and systems were reviewed. Among the key observations was that most of the degradation models are developed for specific degradation modes using controlled test conditions and are validated based on indoor measurements from accelerated tests. Since a PV module in outdoor operation experiences numerous climatic loads, which, in turn, might lead to different degradation modes, combined stress models are a prerequisite to estimate PV module degradation.

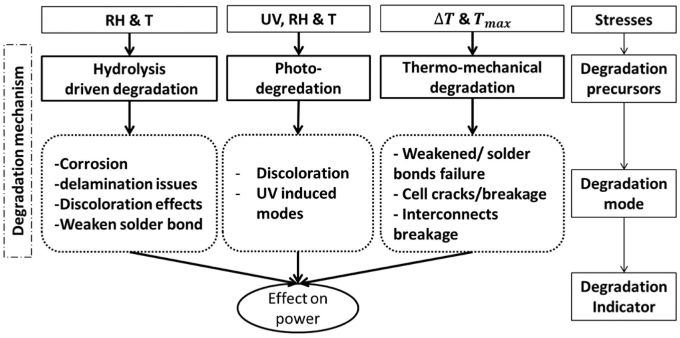

Fig. 1. Schematic diagram of the modeling hypotheses.

The main motivation of this paper is to bridge the gap toward service lifetime prediction of PV modules in outdoor operation. A combined stress model is proposed based on the physics of failure. The approach deployed in this paper is based on analyzing and modeling degradation modes under various climatic stresses. The input stresses are assumed to be responsible for triggering a specific reaction that might induce specific degradation modes (see Fig. 1). The effect of the applied stresses has been evaluated with experimental data using accelerated ageing tests. We assume that it is a crucial step to first evaluate the effects of different stresses in controlled conditions using accelerated tests. This is needed to correlate the power degradation to specific degradation modes using different characterization methods. It also helps to understand the physics of failure of the different degradation modes.

Three main aspects need to be considered for a modeling approach applicable for PV service lifetime prediction.

1) *Impact of PV material variations:* New materials are proposed frequently to improve PV performance.

Manuscript received January 31, 2019; revised March 21, 2019 and April 26, 2019; accepted May 3, 2019. This work was supported in the framework of the European Union's Horizon 2020 Marie Skłodowska-Curie Actions Program (SOLAR-TRAIN project) under Grant 721452. *(Corresponding author: Ismail Kaaya.)*

I. Kaaya is with the Fraunhofer Institute of Solar Energy, 79110 Freiburg, Germany, and also with the University of Malaga, 29016 Malaga, Spain (e-mail: ismail.kaaya@ise.fraunhofer.de).

M. Koehl, A. P. Mehilli, and K. A. Weiss are with the Fraunhofer Institute of Solar Energy, 79110 Freiburg, Germany (e-mail: Michael.koehl@ise.fraunhofer.de; amantin-Panos.mehilli@ise.fraunhofer.de; karl-anders.weiss@ise.fraunhofer.de).

S. de Cardona Mariano is with the University of Malaga, 29016 Malaga, Spain (e-mail: msidrach@ctima.uma.es).

Color versions of one or more of the figures in this paper are available online at http://ieeexplore.ieee.org.

Digital Object Identifier 10.1109/JPHOTOV.2019.2916197

2) *Different operating climatic conditions:* PV modules operate in different climates, for example, in arid, maritime, tropical climates.
3) Different PV technologies, for example, crystalline silicon (c-Si), thin films, and different module designs like bifacial, glass–glass, or glass–backsheet.

All these factors might lead to different degradation modes, rates, and performance degradation. To our knowledge, it is a rather complex challenge to have a single model taking into account all the above aspects. In this paper, a simplified approach is proposed, as a first approximation to take into account some of the above aspects in a single model.

II. Power Degradation Function and Degradation Rate Models

The fact that the module is exposed to several stress factors at the same time, and that outdoor conditions have a stochastic nature, makes it difficult to model outdoor conditions. A model that includes all the above dependences requires a huge number of unknown coefficients to be evaluated. Some of the required coefficients might require experimental procedures to be evaluated, making it time consuming and expensive.

One way to overcome these obstacles is to use an approach that minimizes the number of coefficients to be evaluated. Assumptions should be made based on the dominating loads, processes, impacts, or mechanisms for degradation evaluation. Constant or average quantities might be used to compute the average rates, in order to overcome the stochastic behavior of input parameters. Using accelerated tests to quantify the impact of applied loads on power degradation and to evaluate the sensitivity of model parameters for varying controlled test conditions helps to start with modeling before investigating outdoor conditions. This also helps to relate the performance losses to specific degradation modes. However, one of the major pitfalls of accelerated testing is that it may focus on one degradation mode while masking others. The masked degradation modes could be the first to show up or dominate in the field under different operating conditions [4]. Therefore, the underlying physics and chemistry related to the degradation must be known to avoid these obstacles. The assumptions and hypotheses used in this paper are based on the prior knowledge and studies [5]–[9], [11]–[15], which deal with the underlying physical and or chemical degradation kinetics. Fig. 1 summarizes the hypothesized degradation mechanisms that are known to be induced by the applied loads.

The models should be calibrated using nonextreme test conditions in order to obtain a good correlation of the indoor accelerated conditions to outdoor conditions. As already mentioned, very extreme conditions might generate new degradation modes that might never happen outdoors [4]; using these conditions for calibration of the model might result in high uncertainties. Moreover, some of the degradation patterns observed in accelerated tests are unlikely to occur in natural aging leading to misinterpretations. For example, during an extended damp heat (DH) test, three phases of power degradation were described by Koehl *et al*. [15] as induction, degradation, and saturation phases. One way to use such a degradation pattern for outdoor ageing would be to use the induction and the onset of the degradation phase as it might be a good representation of natural degradation.

A. Module Output Power Degradation Function

Since the module power at the maximum power point (P_{MPP}) is a quantity commonly used by manufacturers to set warranties, it has been selected for use as a degradation indicator in this paper. Hence, in this context, degradation is defined as the gradual deterioration in the module P_{MPP} over time. The effects of applied climatic stresses are then quantified by how much they lead to a reduction in the initial power over time. The module output power as a function of time is proposed as

$$\frac{P_{\mathrm{MPP}}(t)}{P_{\mathrm{MPP}}(0)} = 1 - \exp\left(-\left(\frac{B}{k_i t}\right)^{\mu}\right) \tag{1}$$

where $P_{\mathrm{MPP}}(t)$ and $P_{\mathrm{MPP}}(0)$ are the module output power at time t and the initial output power, respectively. B is the power susceptibility, which is assumed to be a material property, μ is the shape parameter, and k_i is the degradation rate constant of degradation process i.

B. Degradation Rate Models for Controlled Indoor Conditions

Empirical kinetics models to evaluate the degradation rate constant k_i are proposed depending on the applied stresses as presented in the following general reaction equation:

$$\text{Stress } A + \text{Stress } B + \ldots \text{Stress } N \rightarrow \text{Degradation precursor.} \tag{2}$$

In this paper, three main degradation precursor reactions are assumed to be hydrolysis, photodegradation, and thermomechanical degradation. Depending on the applied stresses, a reaction constant is evaluated to quantify the impact of the applied stresses on power degradation over a specified time period.

1) Hydrolysis-Driven Degradation Due to Temperature and Relative Humidity:

$$k_H = A_H . rh_{\mathrm{eff}}^{n} . \exp\left(-\frac{E_H}{k_B . T_m}\right) \tag{3}$$

where k_H is the rate constant, k_B is the Boltzmann constant (8.62×10^{-5}), T_m is the module temperature (Kelvin), A_H is the pre-exponential constant, $rh_{\mathrm{eff}}(\%)$ is the effective module relative humidity (RH) proposed by Koehl *et al.* [16], and n is a model parameter that indicates the impact of RH on power degradation. In this context, E_H is defined as the activation energy for power degradation. Equation (3) is the commonly used Peck's model, which evaluates the degradation impact due to RH and temperature [17]. The Peck's model was selected based on the study of our previous article [3], since the model showed the best performance in DH result calibration.

2) Photodegradation Due to UV Dose, Temperature, and Relative Humidity:

$$k_P = A_P . (\mathrm{UV_{dose}})^{X} . \left(1 + rh_{\mathrm{eff}}^{n}\right) . \exp\left(-\frac{E_P}{k_B . T_m}\right) \tag{4}$$

where k_P is the rate constant, $\mathrm{UV_{dose}}$ is the integral UV dose (kW/m^2), E_P is the activation energy for power degradation due

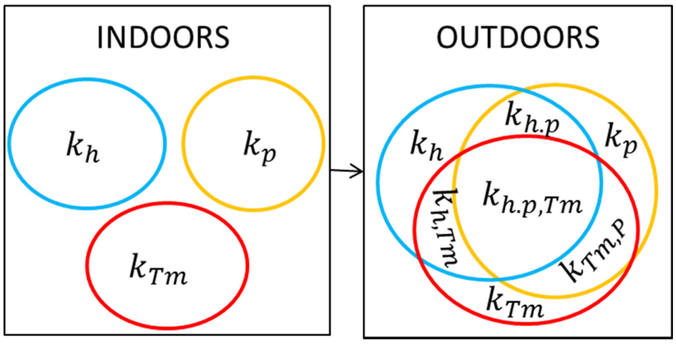

Fig. 2. Schematic diagram showing rates in controlled indoor conditions and the synergistic nature of outdoor conditions.

to photoreaction, and X is a model parameter that indicates the impact of UV dose on power degradation.

3) Thermomechanical Degradation Due to Temperature Cycles: The most commonly used model for thermal cycling (TC) is the Coffin–Manson relationship. According to Escobar and Meeker [17], the effect of temperature cycling can depend largely on the maximum temperature T_U. The cycle-to-failure distribution for temperature cycling can also depend on the cycling rate (e.g., due to heat buildup). Therefore, a modified form of the Coffin–Manson relationship including this effect is

$$k_{Tm} = A_{Tm}.(\Delta T)^{\theta}.C_N.\exp\left(-\frac{E_{Tm}}{k_B.T_U}\right) \quad (5)$$

where $\Delta T = (T_U - T_L)$ is the temperature difference (Kelvin), C_N is the cycling rate, T_U and T_L are the module upper and lower limit temperatures, and E_{Tm} is the activation energy of power degradation.

C. Degradation Rate Model for Outdoor Conditions

The transition from indoor degradation rate evaluation to outdoor is a challenging task due to not yet knowing enough how different stresses, degradation processes, and the induced degradation interact.

The underlying assumption deployed in this paper is that some degradation processes might lead to specific degradation modes independent of the others, and that some might have a synergistic nature (see Fig. 2), which results in a variety of degradation modes. Hence, this assumption allows us to evaluate the total degradation rate as the sum of both independent and dependent processes. The mathematical form of the total rate is expressed as

$$k_T = A_N.\,(1 + k_h)\,(1 + k_p)\,(1 + k_{Tm}) - 1 \quad (6)$$

$$k_T = A_N.\prod_{i=1}^{n}(1 + k_i) - 1 \quad (7)$$

where k_T $(\%/\text{year})$ is the total degradation rate $(\%/\text{year})$, k_i is the ith rate constant, and n is the total number of degradation processes. A_N is the normalization constant of the physical quantities; in this case, it takes the units $(\text{year}^{-2}/\%)$.

Using (1) and (7) and defining failure time (t_f) as a 20% loss in maximum power output (common manufacturer's warranty), the failure time can be calculated using the following relation:

$$t_f = \frac{B}{k_T \times [|\log(0.2)|]^{\frac{1}{\mu}}}. \quad (8)$$

TABLE I
EXPERIMENTAL (EXP) CONDITIONS FOR DH COMBINED UV/DH AND TC TESTS

Exp	Models calibration test Conditions	Models Validation test conditions
DH	75°C/85%RH (6500 hours)	85°C/85%RH (6500 hours)
UV/DH	180W/m^2/65°C/55% RH (4000 hours)	180W/m^2/85°C/55% RH (4000 hours)
TC	-40°C/40°C (3500 cycles)	-40°C/85°C (1200 cycles)

III. Model Calibration

Two basic approaches were applied for the calibration of the different degradation rate models: 1) optimization of model performances; and 2) through prior knowledge from previous studies. Optimization of model performance, which compares measured and simulated data, was applied with the help of a built-in nonlinear least-squares solver in the *GNU Octave* software. Prior knowledge, with the aid of sensitivity analysis, was used as a baseline to select the initial fitting guesses and also as a confirmation that the extracted values are in meaningful range.

A. Experimental Indoor

Distributed DH, TC, and combined DH-UV stress tests were carried out at different test conditions under the framework of the SOPHIA project at different test laboratories. Table I shows the different test conditions used in this paper for model calibration and validation. The studied modules are from the same manufacturer. They are P-type homojunction c-Si with thermoplastic encapsulant material and without an aluminium layer as additional moisture barrier.

B. Experimental Outdoor

Three identical monocrystalline silicon (mc-Si) modules are under monitoring in three climatic zones: maritime (in Gran Canaria, Spain), arid (in Negev, Israel), and alpine (in UFS Zugspitze, Germany). In Gran Canaria, the tilt angle is 23°, and the azimuth angle 169° for the PV module. In Negev, the tilt angle is 31°, and the azimuth angle 180° for PV modules. The module in Gran Canaria has been exposed for over seven years, and the ones in Negev and Zugspitze have been exposed over five years outdoors.

Apart from the performance measurements, the modules temperatures are also recorded every 10 min. The sensors for measuring module temperatures are located under one of the central cells. They are Pt100 sensors, which are attached from the back using adhesive aluminum tapes. Other meteorological data such as RH, global irradiation, UV irradiance, and wind speed are

This article has been accepted for inclusion in a future issue of this journal. Content is final as presented, with the exception of pagination.

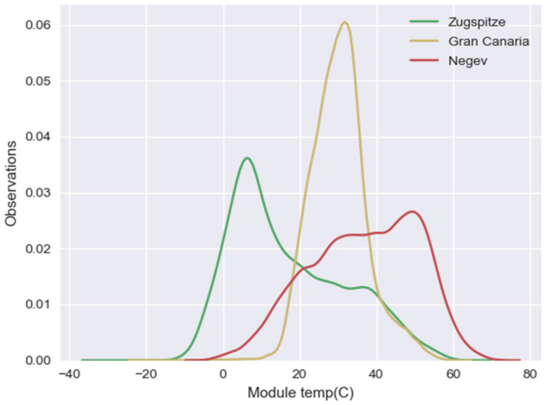

Fig. 3. Distribution of module temperature in the three climatic zones.

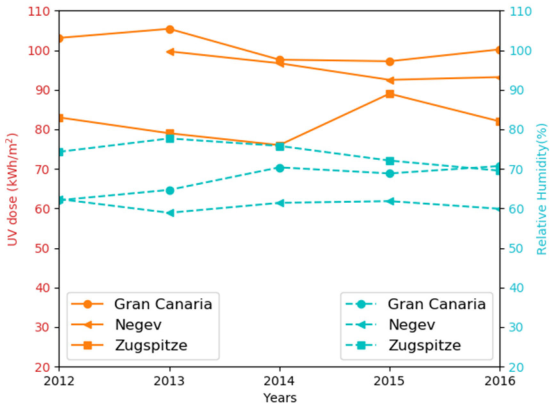

Fig. 4. Total UV dose and average annual RH for the three zones measured for five years.

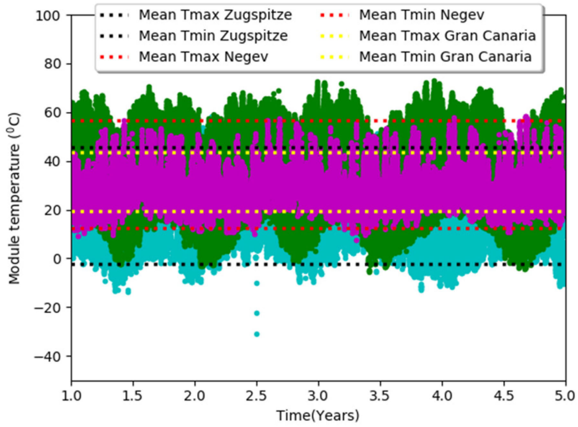

Fig. 5. Ten minutes values of module temperature for five years. The dotted lines show the mean maximum and minimum temperatures.

TABLE II
SUMMARY OF FIVE YEARS AVERAGE CLIMATIC INPUTS USED IN SIMULATION

Location	RH (%)	T_m (°C)	UV dose (kWh/m^2)	T_U (°C)	T_L (°C)
Negev	61.0	36.8	87.7	56.7	12.5
Canaria	68.0	30.6	101.0	43.6	19.6
Zugspitze	74.0	18.7	81.0	44.7	-2.30

also under monitoring in all the three zones with a 1-min resolution. The annual averages of UV dose and RH are as shown in Fig. 4.

Five years of measured datasets were used to evaluate the averages (see Table II), to ensure that the values used in degradation prediction correspond to what a module will experience during its lifetime. The mean value of the module minimum and maximum temperature has been computed considering upper and lower temperature bins as in Fig. 5.

IV. RESULTS AND DISCUSSION

A. Model Properties

It is rather complex to develop a generalized model that covers all these requirements for taking into account innovations in materials and designs. Moreover, validation of such a model requires a huge amount of data and experimental campaigns. Although the model parameters are technology or module specific, the formulations presented in this paper are flexible and can be adapted for application in other modules designs and technologies.

On the one hand, extracting model parameters for each evaluated PV module type makes degradation prediction more complex and rather expensive and time consuming. In this case, a model parameter B in (1), the so-called power susceptibility, is introduced. It could allow simulating a percentage increase in performance due to an improvement in materials of different PV modules when other model parameters are kept constant.

On the other hand, we assume that the power degradation shapes could be linked to module technologies or module design. For example, a faster degradation at early stages of exposure and followed by stabilization is commonly observed in thin-film modules [18]. The other speculation is made on the module design, for example, glass–glass modules have less moisture pathways and moisture ingress compared with glass–backsheet modules. This means that moisture-induced degradation modes are slower at the earlier stages of the module lifetime. However, as the breathable pathways and drying are also limited, the moisture will accumulate over the years, leading to a dramatic increase in the degradation rate. For this case, one could expect a degradation shape like that in Fig. 6 when $\mu = 0.96$.

The proposed power degradation function includes a shape parameter μ, making it possible to optimize all the possible degradation shapes. Fig. 6 shows degradation shapes optimization by changing the value of μ.

Moreover, it is very crucial to optimize the power degradation shapes, since they are linked to energy yield evaluation as the yield corresponds to the integral of power with respect to operation time, hence the area under the curves in Fig. 6.

B. Sensitivity Analysis of Input Loads

A sensitivity analysis of climatic input loads of temperature, RH, and UV dose on the failure time was carried out. Temperature (T), RH, and UV dose bins between (15–55 °C), (40–100%), and (80–100 kW/h/m^2), respectively, were used to generate 500

This article has been accepted for inclusion in a future issue of this journal. Content is final as presented, with the exception of pagination.

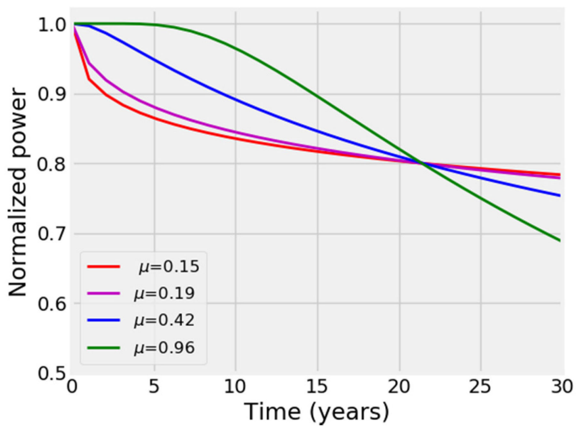

Fig. 6. Optimization of power degradation shapes by altering the shape parameter μ.

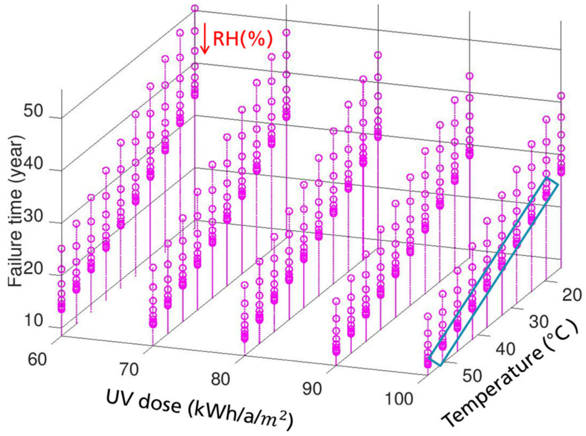

Fig. 7. Sensitivity analysis of T, UV, and RH. The arrow indicates increasing RH represented by the dots.

Fig. 8. Schematic diagram of models' calibration and validation procedure using for both indoor and outdoor datasets.

TABLE III
EXTRACTED MODEL PARAMETERS FOR INDOOR MODULES AND THE PERCENTAGE DEVIATION (DEV) FROM THE FITTED DATA

Model	A_i	n	X, θ	$E_a(eV)$	dev
Hydrolysis (3)	6.11e4	1.90	-	0.91	0.5%
Photo-degradation (4)	1.20e-3	1.80	0.63	0.43	0.2%
Thermo-mechanical (5)	9.10e-5	-	2.24	0.40	1.6%

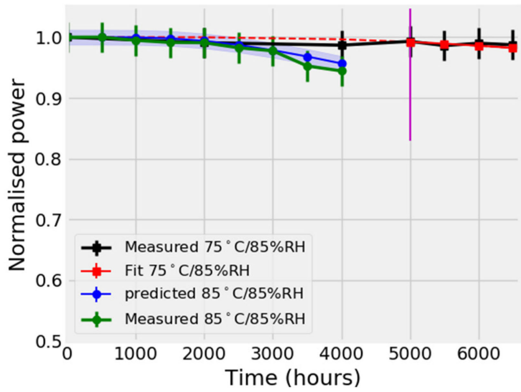

Fig. 9. Hydrolysis model (3) calibration and validation. The blue patch is the 95% confidence interval of prediction; the violet line represents the optimized data points.

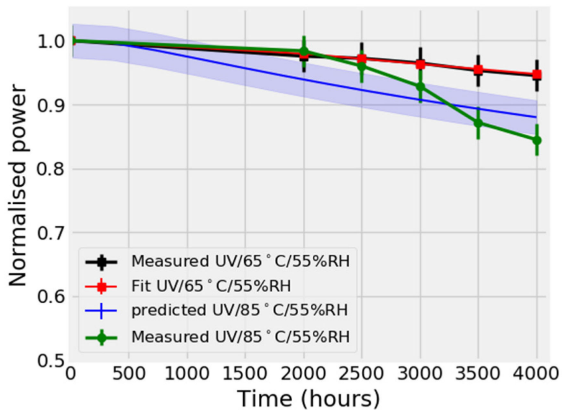

Fig. 10. Photodegradation model (4) calibration and validation. The blue patch is the 95% confidence interval of prediction.

combinations of T, RH, and UV. The variation of failure time to each combination set is shown in Fig. 7.

According to this analysis, the model is more sensitive to temperature as compared with RH and UV dose; this can be explained by the Arrhenius temperature dependence in the rate models. Moreover, during the sensitivity analysis, a threshold of RH (highlighted in blue) was observed. This was linked to the Peck's model for hydrolysis. Simulations using the peck's model only to evaluate the failure time confirmed this tendency at humidity levels above 80%. The model is still applicable, since these conditions are not usually the case outdoors, and in this paper, the varying input load was temperature for indoor conditions.

C. Model Validation

As for any predictive model, the crucial part is to validate the model. There are several ways of model validation. In this paper, the approach used is verification with real experimental measurements. Fig. 8 shows the steps used for validation of the models.

1) Model Validation With Indoor Datasets: The proposed models (3)–(5) were calibrated using indoor experimental data for specific test conditions. The extracted rate models parameters are presented in Table III. The parameter B in (1) was normalized to one, and the extracted shape parameter μ was 0.7 for Fig. 9 and 0.4 for Figs. 10 and 11.

It should be noted that the extracted parameters are valid only for a particular module type. The parameters have to be evaluated for each different module separately. The models were then

This article has been accepted for inclusion in a future issue of this journal. Content is final as presented, with the exception of pagination.

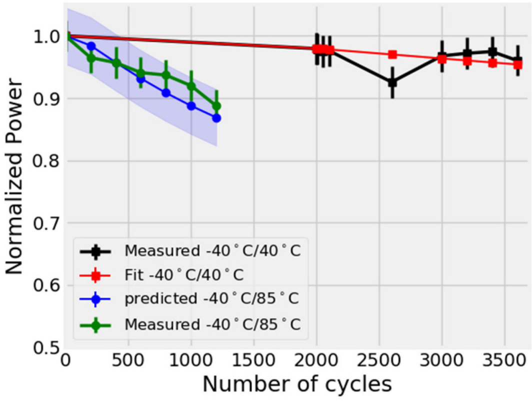

Fig. 11. Thermomechanical model (5) calibration and validation. The blue patch is the 95% confidence interval of prediction.

applied to predict the degradation when the test conditions are varied. The model predictions are compared with experimental outcomes for validation.

Fig. 9 shows calibration and validation results for the hydrolysis model (3). In black is the measured power for DH 75 °C/85RH; red is the respective model fit with a violet line at 5000 h representing the optimized data points. The blue line is the predicted power at DH 85 °C/85RH, the light blue patch is the 95% prediction confidence interval; green represents the measured power at DH 85°C/85RH, used for model validation. The vertical lines on measured data points indicate a 2.5% measurement uncertainty. The color usage and explanation above are consistent with Figs. 10 and 11 for photodegradation (4) and thermomechanical (5) models using respective datasets. For all the models, the predictions are satisfactory and are within a 95% confidence interval. The observable variations could be linked with the measurement uncertainties.

To correlate the uncertainties in model calibration with the predictions, the percentage mean square error of prediction (MSEP) [19] was evaluated as

$$\mathrm{MSEP} = 100 \times \left[V\left[P_p\right] + \left(\mu_{P_p} - \mu_{P_m}\right)^2\right] \tag{9}$$

where P_p and P_m are the predicted and measured power, respectively, V is the variance of the predicted power, and μ_{P_p} and μ_{P_m} are the mean of predicted and measured powers, respectively.

A 0.5% deviation led to 0.025% MSEP for the hydrolysis model, 1.65% deviation resulted into 0.216% MSEP for the thermomechanical model, and 0.19% deviation led to 0.168% MSEP for the photodegradation model. Although there is a correlation of the uncertainties due to model calibration as it is evaluated in the thermomechanical model, the uncertainties in experimental datasets used for validation can also influence the evaluated mean square error; therefore, it is also useful to evaluate the confidence interval of the prediction.

2) Model Validation With Outdoor Datasets: The power degradation model (1) with $k_i = k_T$ [total degradation rate (6)] was calibrated using the monitored dataset of Gran Canaria. The dataset from Gran Canaria was selected over Negev and Zugspitze because the module in Gran Canaria has been exposed for quite a long time compared with the ones in Negev

TABLE IV
EXTRACTED MODEL PARAMETERS FOR OUTDOOR MODULES

Model	A_i	n, X, θ	$E_a(eV)$
Hydrolysis (3)	4.91e7	1.90	0.74
Photo-degradation (4)	71.83	0.63	0.45
Thermo-mechanical (5)	2.04	2.24	0.43

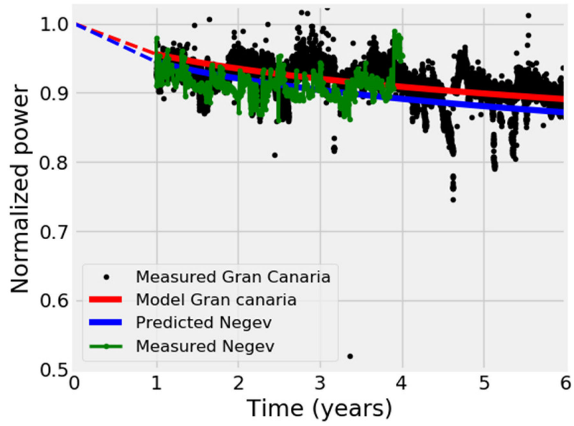

Fig. 12. Combined model (7) calibration and validation with 5-min resolution.

and Zugspitze, and moreover, it shows a clear degradation trend. A filter at module temperature (30–35 °C) and irradiance (800–1200 W/m^2) was used because it is the most frequent temperature that a module experiences over its lifetime in this region (see Fig. 3). The irradiance bin ensures that only clear sky conditions were considered in order to have irradiance conditions near to standard test conditions (STC) and to model a common situation for all the climates. The power was corrected to STC of irradiance. To make sure that the power degradation observed for outdoor modules is not due to soiling effects, periodic cleaning of the modules is done.

The extracted rate model parameters are presented in Table IV. The percentage deviation of the fitted data points was 2.34% and the derived parameters were $B = 190$ and $\mu = 0.19$ for the power function (1).

Fig. 12 shows calibration and validation results. The black dots are the measured power for Gran Canaria; the red line is the respective model fit. The blue line is the predicted power for Negev, and the measured power for Negev is in green. The dotted lines indicate normalization to the initial laboratory power values before outdoor exposure. The alpine predictions were left out to avoid too much information on the graph due to data fluctuations. The outdoor predictions show a good agreement with the measured power degradation.

D. Degradation Rates and Lifetime Prediction

Depending on the climate a module is installed in, different degradation modes might dominate over the others. Using the proposed degradation models (3)–(5) and (7) and the outdoor derived model parameters, it is possible to predict the dominating degradation precursor and the total degradation rate, as well as the failure time (8) for any location with known climatic loads.

TABLE V
PREDICTED DEGRADATION RATES USING (3)–(5) AND (7) OF THE mc-Si MODULES AND FAILURE TIME (8) IN THE THREE CLIMATIC ZONES

Location	k_h (%/year)	k_P (%/year)	k_{Tm} (%/year)	k_T (%/year)	Failure time (years)	Lower 95% CI (years)	Upper 95% CI (years)
Negev	0.169	0.216	0.225	0.74	21.4	16.7	27.1
Canaria	0.122	0.212	0.104	0.50	31.6	25.0	40.0
Zugspitze	0.043	0.103	0.129	0.30	52.8	42.7	65.0

In this paper, annual degradation rates of the mc-Si modules were predicted using input climatic loads of Zugspitze, Gran Canaria, and Negev, as shown in Table V.

High thermomechanical degradation is predicted for Zugspitze in comparison with Gran Canaria because of high module temperature variations in this climate zone. On the contrary, small degradation due to hydrolysis is predicted in Zugspitze despite the high levels of RH. This could be explained by the low average module temperatures experienced in this region, hence slowing hydrolysis processes and the absolute water vapor concentration. In all cases, high rates are predicted in Negev. This can be explained again by the higher temperatures in this zone that determines the reaction rates for other degradation processes caused by other degradation factors such as hydrolysis by humidity and photodegradation by UV dose. The predicted failure time defined as a 20% loss in power, as expected, shows more severe degradation of the maximum power output in arid climates where temperatures are higher. This further confirms the previous studies [20] that temperature could be the primary accelerator of degradation.

E. Evaluation of Uncertainties Due to Data Quality

The module power measurements were done every 5 min; such high-resolution measurements and the frequently fluctuating environmental conditions outdoors lead to unavoidable noise even after applying filters and corrections. By using a moving average of 1 h to minimize the noise in the datasets, the process of model calibration and validation was repeated. The effect of the noise to the derived model parameters as well as on failure time estimation was evaluated. Because of the high sensitivity of the models parameters, E_a, n, X, and θ, they were assumed constant, and the variations in calibration and lifetime estimations due to the noise effect are evaluated using the parameter B of the power degradation function (1).

Fig. 13 shows the calibration and validation results for hourly resolution. The deviation of the fitted data points reduced to 2.04%, and the derived model parameter reduced to $B = 182.3$

Table VI shows the MSEP and relative difference in failure time estimation with 5-min data and hourly averaged data. Although the fitting deviation improved from 2.23% to 2.04% using hourly resolution, the improvement did not considerably led to reduction in MSEP, but the effect is visible in failure time estimation with a relative difference of 4.05%. This is consistent with the observations from indoor results that the uncertainties in experimental datasets used for validation can also influence the evaluated MSEP.

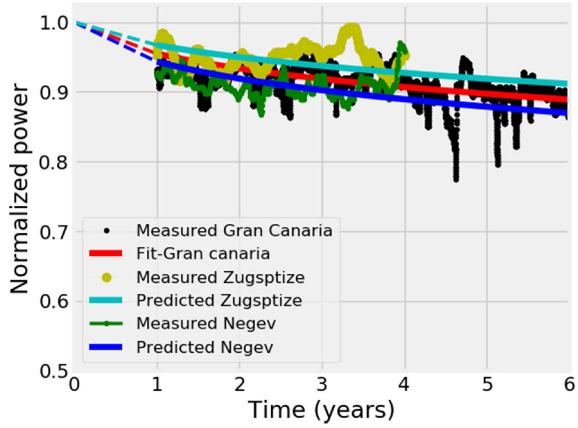

Fig. 13. Combined model (7) calibration and validation with hourly resolution.

TABLE VI
PERCENTAGE MEAN ERROR IN PREDICTION (MSEP) AND RELATIVE DIFFERENCE (REL-DIFF) OF THE ESTIMATED FAILURE TIME (t_f) FOR DIFFERENT DATA RESOLUTIONS (DATA RES)

Model	Data res	B	MSEP (%)	t_f (years)	Rel-diff
Negev	5 min	190.0	0.0230	21.4	4.05%
	Hourly	182.3	0.0240	20.5	
Zugspitze	5 min	190.0	0.0152	52.8	4.05%
	Hourly	182.3	0.0150	50.7	

V. CONCLUSION

A degradation model for quantifying the impact of combined climatic stresses on module maximum power output degradation has been introduced. Degradation rate models have been proposed and validated with indoor measurements for specific degradation precursors. A combined degradation rate model has been proposed and validated with real field datasets. The model has been applied for the evaluation of the degradation rates and the prediction of losses in the power output of monocrystalline modules installed in three climatic zones: maritime, arid, and alpine. A stronger degradation has been predicted in an arid climate, which could be explained by a higher mean module temperature, as well as high temperature variations in this zone.

In addition, a correlation of dominating degradation precursors to the operating climate has been analyzed for the three climates. Thermomechanically induced modes dominate in Zugspitze and Negev due to high temperature variations in these zones. In Gran Canaria, photodegradation dominates due to high UV values and relatively high average module temperatures experienced in this region.

The proposed power degradation model presented in this paper has been calibrated and validated using specific modules design and technology. However, the formulations are flexible and could be applied to other modules designs and technologies.

Apart from the uncertainties due to models' derived parameters and input datasets, some degradation modes might be outcomes of other degradation modes and might appear at certain stages of a module's lifetime. This makes the predictions more complex using only analytical models like the one described in this paper, hence impacting the model accuracy especially for longer time predictions. One way to solve this problem could be to apply a combination of analytical models with data-driven models or apply computer algorithms embedded with analytical models to determine the best solution for predicting outdoor service lifetime.

References

[1] G. B. Gaines, R. E. Thomas, G. T. Noel, T. S. Shilliday, and V. E. Wood, "Development of an accelerated test design for predicting the service life of the solar array at Mead, Nebraska," Jet Propulsion Lab, Pasadena, CA, USA, Tech. Rep. DOE/JPL-954328-79/11, Jun. 1979.

[2] A. B. Subramaniyan, R. Pan, J. Kuitche, and G. TamizhMani, "Quantification of environmental effects on PV module degradation: A physics-based data-driven modeling method," *IEEE J. Photovolt.*, vol. 8, no. 5, pp. 1289–1296, Sep. 2018.

[3] S. Lindig, I. Kaaya, K. Weiß, D. Moser, and M. Topic, "Review of statistical and analytical degradation models for photovoltaic modules and systems as well as related improvements," *IEEE J. Photovolt.*, vol. 8, no. 6, pp. 1773–1786, Nov. 2018.

[4] W. Q. Meeker and L. A. Escobar, "Pitfalls of accelerated testing," *IEEE Trans. Rel.*, vol. 47, no. 2, pp. 114–118, Jun. 1998.

[5] J. Zhu, D. Montiel-Chicharro, T. R. Betts, and R. Gottschalg, "Correlation of degree of EVA crosslinking with formation and discharge of acetic acid in PV modules," in *Proc. 33rd Eur. Photovolt. Sol. Energy Conf. Exhib.*, 2017, pp. 1795–1798.

[6] M. Kempe, "Modeling of rates of moisture ingress into photovoltaic modules," *Sol. Energy Mater. Sol. Cells*, vol. 90, pp. 2720–2738, Oct. 2006.

[7] V. Sharma and S. S. Chandel, "Performance and degradation analysis for long term reliability of solar photovoltaic systems: A review," *Renew. Sustain. Energy Rev.*, vol. 27, pp. 753–767, Nov. 2013.

[8] A. Ndiaye *et al.*, "Degradations of silicon photovoltaic modules: A literature review," *Sol. Energy*, vol. 96, pp. 140–151, Oct. 2013.

[9] A. Gok *et al.*, "Predictive models of poly(ethylene-terephthalate) film degradation under multi-factor accelerated weathering exposures," *PLoS ONE*, vol. 12, no. 5, May 2017, Art. no. e0177614.

[10] J. Zhu *et al.*, "Changes of solar cell parameters during damp-heat exposure," *Prog. Photovolt. Res. Appl.*, vol. 24, no. 10, pp. 1346–1358, Oct. 2016.

[11] D. C. Jordan, T. J. Silverman, J. H. Wohlgemuth, S. R. Kurtz, and K. T. VanSant, "Photovoltaic failure and degradation modes," *Prog. Photovolt. Res. Appl.*, vol. 25, no. 4, pp. 318–326, 2017.

[12] M. L. Marín, A. Jiménez, J. López, and J. Vilaplana, "Thermal degradation of ethylene (vinyl acetate)," *J. Thermal Anal.*, vol. 47, no. 1, pp. 247–258, Jul. 1996.

[13] N. Park, W. Oh, and D. H. Kim, "Effect of Temperature and humidity on the degradation rate of multicrystalline silicon photovoltaic module," *Int. J. Photoenergy*, vol. 2013, Dec. 2013, Art. no. 925280.

[14] D. Wu, J. Zhu, T. R. Betts, and R. Gottschalg, "Degradation of interfacial adhesion strength within photovoltaic mini-modules during damp-heat exposure," *Prog. Photovolt. Res. Appl.*, vol. 22, no. 7, pp. 796–809, Jul. 2014.

[15] M. Koehl, S. Hoffmann, and S. Wiesmeier, "Evaluation of damp-heat testing of photovoltaic modules," *Prog. Photovolt. Res. Appl.*, vol. 25, no. 2, pp. 175–183, Feb. 2017.

[16] M. Koehl, M. Heck, and S. Wiesmeier, "Modelling of conditions for accelerated lifetime testing of humidity impact on PV-modules based on monitoring of climatic data," *Sol. Energy Mater. Sol. Cells*, vol. 99, pp. 282–291, Apr. 2012.

[17] L. A. Escobar and W. Q. Meeker, "A review of accelerated test models," *Statist. Sci.*, vol. 21, no. 4, pp. 552–577, Nov. 2006.

[18] D. C. Jordan, T. J. Silverman, B. Sekulic, and S. R. Kurtz, "PV degradation curves: Non-linearities and failure modes," *Prog. Photovolt. Res. Appl.*, vol. 25, no. 7, pp. 583–591, Jul. 2017.

[19] M. D. McKay, "Evaluating prediction uncertainty," Nucl. Regulatory Commission, Rockville, MD, USA, Rep. NUREG/CR-6311, 1995.

[20] E. Annigoni *et al.*, "Modeling potential-induced degradation (PID) in crystalline silicon solar cells: From accelerated-aging laboratory testing to outdoor prediction," in *Proc. 32nd Eur. Photovolt. Sol. Energy Conf. Exhib.*, 2016, pp. 1558–1563.

Authors' photographs and biographies not available at the time of publication.

energies

MDPI

Article

Global Climate Data Processing and Mapping of Degradation Mechanisms and Degradation Rates of PV Modules

Julián Ascencio-Vásquez [1,*], Ismail Kaaya [2,3], Kristijan Brecl [1], Karl-Anders Weiss [2] and Marko Topič [1]

1 Faculty of Electrical Engineering, University of Ljubljana, Tržaška cesta 25, 1000 Ljubljana, Slovenia; kristijan.brecl@fe.uni-lj.si (K.B.); marko.topic@fe.uni-lj.si (M.T.)

2 Fraunhofer Institute of Solar Energy, Heidenhofstr. 2, 79110 Freiburg im Breisgau, Germany; ismail.kaaya@ise.fraunhofer.de (I.K.); karl-anders.weiss@ise.fraunhofer.de; (K.-A.W.)

3 School of Industrial Engineering, University of Malaga, 29016 Malaga, Andalucia, Spain

* Correspondence: julian.ascencio@fe.uni-lj.si

Received: 17 October 2019; Accepted: 7 December 2019; Published: 12 December 2019

check for updates

Abstract: Photovoltaic (PV) systems are the cheapest source of electricity in sunny locations and nearly all European countries. However, the fast deployment of PV systems around the world is bringing uncertainty to the PV community in terms of the reliability and long-term performance of PV modules under different climatic stresses, such as irradiation, temperature changes, and humidity. Methodologies and models to estimate the annual degradation rates of PV modules have been studied in the past, yet, an evaluation of the issue at global scale has not been addressed so far. Hereby, we process the ERA5 climate re-analysis dataset to extract and model the climatic stresses necessary for the calculation of degradation rates. These stresses are then applied to evaluate three degradation mechanisms (hydrolysis-degradation, thermomechanical-degradation, and photo- degradation) and the total degradation rate of PV modules due to the combination of temperature, humidity, and ultraviolet irradiation. Further on, spatial distribution of the degradation rates worldwide is computed and discussed proving direct correlation with the Köppen-Geiger-Photovoltaic climate zones, showing that the typical value considered for the degradation rate on PV design and manufacturer warranties (i.e., 0.5%/a) can vary ± 0.3%/a in the temperate zones of Europe and rise up to 1.5%/a globally. The mapping of degradation mechanisms and total degradation rates is provided for a monocrystalline silicon PV module. Additionally, we analyze the temporal evolution of degradation rates, where a global degradation rate is introduced and its dependence on global ambient temperature demonstrated. Finally, the categorization of degradation rates is made for Europe and worldwide to facilitate the understanding of the climatic stresses.

Keywords: photovoltaic; degradation; PV systems; climate zones; climate data

1. Introduction

The current worldwide energy transition from conventional to renewable energy sources already proves and even more forecasts the expansion of photovoltaic systems to new and diverse locations. On a global scale, we are rapidly approaching the so-called "Terawatt-scale Photovoltaics" era, which indicates the surpass of 1 TW of installed capacity of photovoltaic (PV) systems and highlights an important milestone for the PV industry [1]. This milestone is also boosted by the decrease in prices of the PV technologies, which are already the cheapest source of electricity in many countries of Europe [2].

However, this diversification is presenting some constraints in terms of financial and technical risks, due to the unclear response of PV modules and materials under different climate conditions. The financial risks are related to the estimation of the long-term energy yield, mainly due to degradation rate calculations and solar resource variability, as represented by calculations of Levelized-Cost-Of-Electricity (LCOE) for PV systems. The technical risks are related to the failure modes prone to occur for different Bill-of-Materials (BOM) and Balance-of-System (BOS) under different climatic stresses which will vary from location to location. For example, while in deserts the risk of sand-storms is high, in highlands wind gusts and snow loads can damage the PV installations. Important findings and calculation methods about the climatic triggers of degradation modes under different climate zones have been presented in [3–11]. Irradiation, temperature, and humidity have been identified as the main degradation precursors, leading to different degradation mechanisms depending on the stress level in each climate zone. In qualitative terms, some generalizations can be made by climate: in tropical climates, the combination of high humidity and high temperature is stated as being the harshest for PV reliability, where the PV modules are prone to delamination, corrosion or Potential-Induced-Degradation (PID). Desert and steppe climates stimulate degradation modes, such as encapsulant discoloration, backsheet chalking or delamination. Temperate, cold and polar climates typically present low degradation due to the low climatic stress, but modules are prone to fast power drops due to hail, storms or snow loads inducing cell cracks, glass cracks and interconnect breakage. In quantitative terms, Jordan et al. have been the pioneers in the degradation rate assessment under different climate conditions [4], but the complexity of the issue does not yet allow the conclusion of a generalized estimation model per climate zone. The synergy of climate stressors makes the estimation and prediction of the degradation rates (i.e., expressed as a reduction of the power per year, %/a) not trivial, given that not only different module types react differently regarding the climate but also that material interactions will behave differently [6].

Studies at a global scale present the mapping of PV performance indicators (e.g., performance ratio and energy yield) using different Geographic Information Systems (GIS) datasets and approaches [12–14]. Regarding the long-term operation of PV systems, usually this issue is simplified by considering a typical value (i.e., 0.5%/a for crystalline PV modules), also stated on manufacturer performance warranties. However, it is known that the impact of climate on material properties and energy production will vary over time and location. Interesting approaches to calculate the degradation rates have been proposed in references [10,15]. Both models consider as main climate degradation factors the average temperatures, temperature changes, humidity, and ultraviolet (UV) irradiation, which is in line with indoor testing and standards for PV reliability. However, those models have not been applied at global scale and a PV degradation mapping has not been published so far.

In this paper, the ERA5 climate reanalysis dataset [16] is processed to extract and further to model the essential climate variables for the study of PV degradation (temperature, humidity, and UV irradiation). The estimated climate data is compared and validated with real ground-measurements taken from different sources [17–19]. Then, the module temperature and degradation rates are estimated globally. Using the Köppen-Geiger-Photovoltaic (KGPV) climate classification [12], the spatial distribution of degradation rates in view of climate zones is evaluated. Then, the temporal evolution of degradation rates compared with the global increase in ambient temperature is presented. The global mapping of degradation mechanisms and total degradation rates are provided, together with a categorization of degradation rates in Europe and worldwide.

2. Climate Data Processing

The studies over large geographical regions can be made by processing GIS data estimated from Numerical Weather Predictions (NWP) including satellite or reanalysis models [20]. Even though satellite-based estimations can be more accurate than the reanalysis-based ones, the advantage of the second is the possibility to extract all the essential variables together in the same dataset, without gaps and identical timestamps.

One of the latest datasets released is the "ERA5" created by the European Centre for Medium-Range Weather Forecasts (ECMWF). In comparison with previous datasets (e.g., ERA-Interim), ERA5 provides a spatial resolution of 31 km and temporal resolution of hourly data from 1979 [16]. Also in the literature, the improvement on the accuracy of the global horizontal irradiance (*GHI*) is reported [20].

Although not all variables required are directly available from the ERA5, we calculate the missing local climate variables, wind speed (*WS*), relative humidity (*RH*), and UV irradiance (*UV*), using existing models.

2.1. Local Climate Variables

While high wind speed (*WS*) can increase mechanical loads on the PV installation [21] and be a trigger of further degradation processes, we use it only to estimate the PV module temperature (T_{mod}) due to the related cooling effect on materials. The *WS* is calculated and height-corrected according to Equations (1) and (2) [22,23], where $\overline{u}_{wind}$ and $\overline{v}_{wind}$ are the vector components of the wind, h_{ERA} is the height from ground which the wind is modelled in the ERA5 dataset, and h_{mod} is the assumed height of the PV modules equal to 2 m. The 2 m height assumed is in accordance with the height of modelled ambient temperature (T_{amb}) and dew point temperature (T_{dew}) given by the ECMWF.

$$WS_{ERA} = \sqrt{\overline{u}_{wind}^2 + \overline{v}_{wind}^2} \tag{1}$$

$$WS = \left(\frac{h_{mod}}{h_{ERA}}\right)^{0.2} \cdot WS_{ERA} \tag{2}$$

The relative humidity (*RH*) is also not extracted directly from ERA5, so it is estimated using Equations (3) and (4). The saturation water vapor pressure (*WVP*) over water and ice is calculated using Buck's Formula [24,25] from the dew point temperature (T_{Dew}) and ambient temperature (T_{amb}).

$$WVP(T)[kPa] = \begin{cases} 0.61115 \cdot exp^{\left(23.036 - \frac{T}{333.70}\right)\cdot\left(\frac{T}{279.82+T}\right)} & \text{for } T < 0 \\ 0.61121 \cdot exp^{\left(18.678 - \frac{T}{234.84}\right)\cdot\left(\frac{T}{257.14+T}\right)} & \text{for } T \geq 0 \end{cases} \tag{3}$$

$$RH[\%] = \frac{WVP(T_{dew})}{WVP(T_{amb})} \cdot 100[\%] \tag{4}$$

UV irradiance given in the ERA5 dataset covers a wavelength range up to 440 nm. However, this variable is usually referred for wavelengths below 400 nm. This distinction can cause large differences of the estimated UV irradiation. For example, measurements in Ljubljana, Slovenia lead to an overestimation of 45% of the energy in the UV part (see Figure 1).

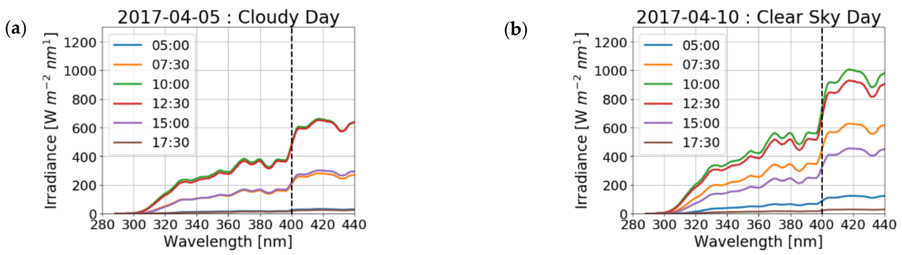

Figure 1. (**a**) Spectral irradiance from 280 nm to 440 nm under a day of cloudy sky conditions. (**b**) Spectral irradiance from 280 nm to 440 nm under a day of clear sky conditions.

For this reason, we neglect the UV irradiance data given by ERA5, and model it up to 400 nm using a method proposed in ref. [26] and expressed in Equations (5)–(8), which is based on the clearness index (k_t) and the global horizontal irradiance (*GHI*). The k_t is calculated by dividing the *GHI* and the top-of-atmosphere irradiance extracted from ERA5. Unfortunately, the lack of valid measurements disallows that we validate the model worldwide.

$$k_t^* = max(0.1, min(k_t, 0.7)) \tag{5}$$

$$UV_B = \left(1.897 \ - 0.860 \ k_t^*\right) \cdot 1e^{-3} \cdot GHI \tag{6}$$

$$UV_A = \left(7.210 \ - 2.365 \ k_t^*\right) \cdot 1e^{-2} \cdot GHI \tag{7}$$

$$UV = UV_A + UV_B \tag{8}$$

The GIS data extracted and computed is compared with 15 ground meteorological stations involved in the World Radiation Monitoring Center - Baseline Surface Radiation Network (WRMC-BSRN) [17], one station in Alice Springs, Australia provided by the Desert Knowledge Australia (DKA) Solar Centre [18] and one station in the Atacama Desert provided by Universidad de Chile [19]. The station locations are shown in Figure 2 and more details are presented in Table A1 in the Appendix A. At these stations, GHI, T_{amb}, and RH are measured. The comparison is carried out on a daily average resolution for the years 2016, 2017, and 2018, except for the Chilean station where the time frame ranges from 2010 to 2014. We use the inverse distance weighting (IDW) as interpolation method [27] to calculate the estimated values at specific location reducing the geographical mismatch between measured and computed values.

The time-series for each location are compared by the cumulative distribution function (CDF) and the coefficient-of-determination (R^2). In Figure 3, locations with high and low accuracy are presented, while the rest of the locations are presented in Table A2 in the Appendix A. For example, on one hand, data in Cabauw (The Netherlands) show almost perfect fitting for the three variables (T_{amb}, GHI, and RH), evidencing that ERA5 can be used as synthetic data in some locations. On the other hand, in Howrah (India), the accuracy of GHI and RH is low but could be improved with a post-processing algorithm, e.g., ref. [28].

An excellent agreement of T_{amb} was noticed possibly because of the high number of observational data in ERA5. GHI and RH also show good performance even though they are purely modelled.

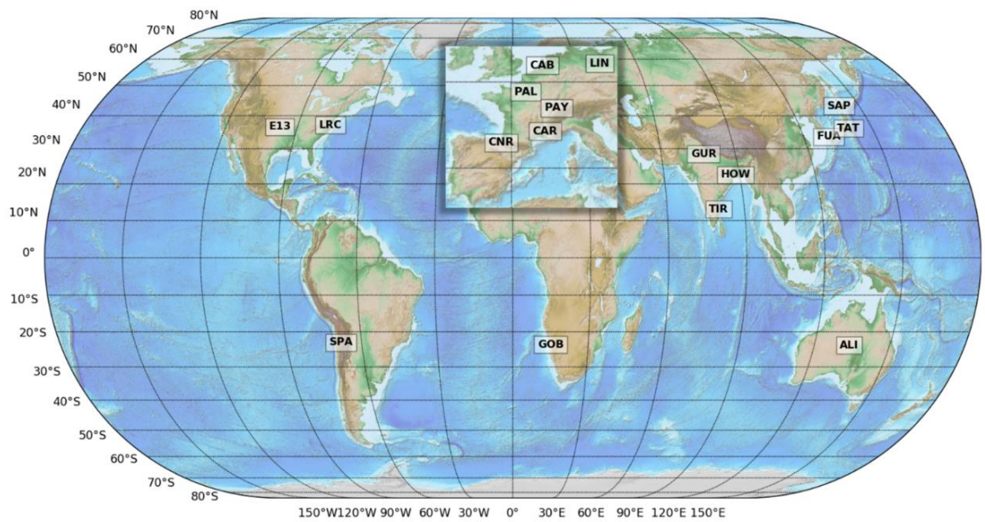

Figure 2. Location of meteorological stations used to compare the GHI, T_{amb}, and RH with the modelled data from ERA5 reanalysis dataset.

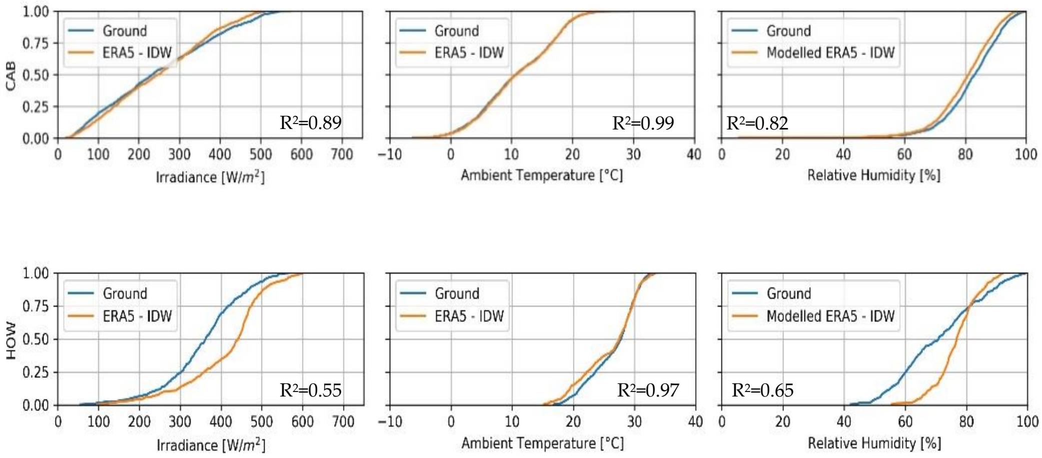

Figure 3. Cumulative distribution functions (CDFs) and statistical indicators for comparison of ground-measurements and modelled data from the ERA5 reanalysis dataset and the inverse distance weighting (IDW) interpolation. We present a high accuracy and low accuracy case, Cabauw (CAB, Lopik, Utrecht, The Netherlands) and Howrah (HOW, West Bengal, India). The comparison of the other 15 locations is presented in Table A2 in the Appendix A.

2.2. Operating Conditions of PV Modules

One of the most important climatic loads to analyze the degradation is the PV module temperature (T_{mod}). Typically this variable is estimated by using the Ross model [29], which is a function of the ambient temperature, irradiance and the Ross coefficient (k_{Ross}) as presented in Equation (9). However, a higher accuracy of T_{mod} estimations under different climate conditions for crystalline silicon PV modules can be achieved by using the Faiman model (see Equation (10)) [22,30]. In Figure 4, a visual comparison of the estimated T_{mod} is illustrated. The main differences are presented in areas with high wind speed where the cooling effect will be taken into account when using the Faiman model.

Further calculations in this paper are based on the Faiman model to estimate the PV module temperature as a function of the T_{amb}, GHI, and WS, considering u_0 equal to 26.9 W/m^2/°C and u_1 equal to 6.2 Ws/m^3/°C [23], which are typical values reported for c-Si PV modules in the open-rack mounting configuration.

$$T_{mod} = T_{amb} + k_{Ross} \cdot GHI \tag{9}$$

$$T_{mod} = T_{amb} + \frac{GHI}{u_0 + u_1 \cdot WS} \tag{10}$$

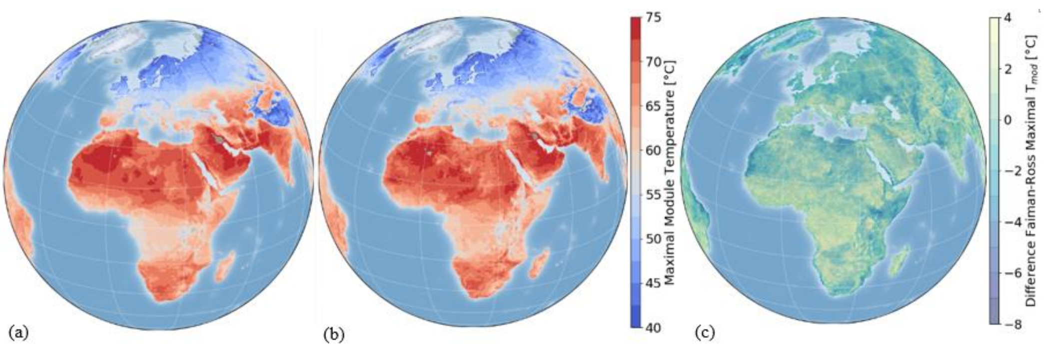

Figure 4. (**a**) Maximal module temperature using the Ross model. (**b**) Maximal module temperature using the Faiman model. (**c**) Absolute difference between the estimated T_{mod} using Faiman and Ross models. Annual average data from 2016 to 2018.

3. Spatial Distribution of PV Degradation Rates

Degradation mechanisms will be triggered not only from one individual degradation factor but due to a combination of them. In ref. [10], three degradation processes are defined and empirically expressed due to the combination of climate degradation factors: Hydrolysis-degradation (k_H) related to the effect of temperature and humidity, photo-degradation (k_P) depends on temperature, humidity and UV irradiance, and thermo-mechanical-degradation (k_{Tm}) due to high temperature and temperature differences. The models are presented in Equations (11) to (14):

$$k_H = A_H \cdot rh_{eff}^n \cdot \exp\left(-\frac{E_H}{k_B \cdot T_m}\right), \tag{11}$$

$$k_P = A_P \cdot (UV_{dose})^X \cdot \left(1 + rh_{eff}^n\right) \cdot \exp\left(-\frac{E_P}{k_B \cdot T_m}\right), \tag{12}$$

$$k_{Tm} = A_{Tm} \cdot (\Delta T)^\theta \cdot C_N \cdot \exp\left(-\frac{E_{Tm}}{k_B \cdot T_U}\right), \tag{13}$$

$$k_T = A_N \prod_{i=1}^{n} (1 + k_i) - 1, \tag{14}$$

where the parameters are:

k_H: Hydrolysis degradation rate (%)
k_P: Photo-degradation rate (%)
k_{Tm}: Thermomechanical degradation rate (%)
k_T: Total degradation rate (%)
k_B: Boltzmann constant (8.62×10^{-5})
E_H: Activation Energy for Hydrolysis degradation (eV)
E_P: Activation Energy for Photo-degradation (eV)
E_{Tm}: Activation Energy for Thermomechanical degradation (eV)
A_H: Pre-exponential constant for Hydrolysis degradation
A_P: Pre-exponential constant for Photo-degradation
A_{Tm}: Pre-exponential constant for Thermomechanical degradation
rh_{eff}: effective relative humidity
UV_{dose}: integral UV dose (kW/m^2)
T_m: average module temperature
T_U: upper module temperature
T_L: lower module temperature
$\Delta T = T_U - T_L$: temperature difference
n: model parameter that indicates the impact of RH on power degradation.
X: model parameter that indicates the impact of UV dose on power degradation.
θ: model parameter that indicates the impact of ΔT on power degradation.
C_N: Cycling rate
A_N: normalization constant of the physical quantities (a^{-2}/%)

The degradation mechanisms are quantified by using the fitting coefficients published in ref. [10] for a high-performance monocrystalline silicon PV module installed in the open-rack mounting configuration.

Further on, the calculated degradation rates can be directly related to climate zones. To simplify the spatial distribution analysis of degradation rates, we use the Köppen-Geiger-Photovoltaic (KGPV) scheme proposed in ref. [12] to compare the climate zones in terms of annual degradation rates, as shown in Figures 5 and 6. Each KGPV climate zone is defined by two letters, the first one implies the relation of temperature and precipitation (*TP*-zones) and the second is related to the irradiation level, as *H*-zones. The definition of each letter is as follows:

Temperature-Precipitation (*TP*) Zones
A: Tropical climate
B: Desert climate
C: Steppe climate
E: Temperate climate
D: Cold climate
F: Polar climate

Irradiation (*H*) Zones
K: Very high irradiation
H: High irradiation
M: Medium irradiation
L: Low irradiation

Hydrolysis-degradation presents the smallest contribution in almost all the KGPV zones, but is considerably higher for the tropical climates (AH and AK), which zones are related to high precipitation levels (humid areas) and temperature levels. This process can provoke moisture ingress leading to delamination of polymers or corrosion of solder bonds [31].

Photo-degradation has the second-highest contribution to the total degradation rate. This indicator combines the humidity, temperature, and UV irradiance impacting the PV module. The impact is similar to hydrolysis-degradation but higher in terms of absolute values due to the process triggered by UV irradiation. For desert areas, even though the UV irradiation is high, the low humidity in the air decreases the estimated damage of the PV cells due to this mechanism. The photo-degradation is considerable high in tropical zones (AH and AK) due to the high climatic stresses of all variables (temperature, humidity, and UV irradiation).

Thermo-mechanical degradation exhibits the highest contribution to the total degradation rate in all zones, except in the AH zone, where the temperature variations are minimal. This parameter is affected by seasonal temperature cycling (the difference between the maximum and minimum temperature of the year) and also the annual average maximum ambient temperature.

The total degradation rates calculated by the combination of the previous three degradation mechanisms Equation (13) are also evaluated per each KGPV climate zone. In accordance with the literature [6], the highest degradation rate is identified in tropical areas (hot and humid). Interestingly, the AK (tropical with very high irradiation) presents lower degradation than the AH (tropical with high irradiation), due to lower photo-degradation contribution (related to lower humidity).

The steppe climate has higher humidity than the deserts and therefore, the total degradation rate is increased by higher hydrolysis-degradation and photo-degradation. As expected CK (steppe with very high irradiation) might be more stressful for PV modules than CH (steppe with high irradiation), due to higher UV irradiation.

Temperate climates (DM and DH) result in average degradation rates of 0.42%/a and 0.58%/a, respectively. Those climate zones are predominant in Europe, and their values are in accordance with the typical 0.5%/a degradation rate assumed along within the PV community. However, the spread of the values can range around ± 0.3%/a in the temperature zones across Europe.

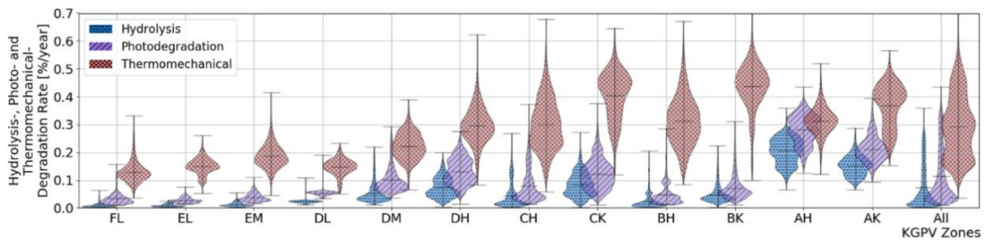

Figure 5. Spatial distribution of the degradation mechanisms in view of the Köppen-Geiger-Photovoltaic (KGPV) climate zones.

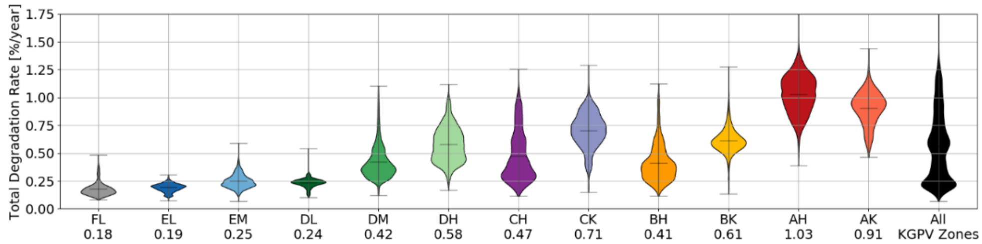

Figure 6. Spatial distribution of the total degradation rates in view of the KGPV climate zones. The average of total degradation rate per climate zone is indicated below each label in %/a.

Cold and polar areas present average degradation rates around or below 0.2%/a. In real operating conditions, we expect higher values due to external degradation factors, such as snow accumulation over the PV systems or mechanical loads due to wind gusts which are not included in the calculations as yet.

Desert areas exhibit similar average degradation rates than temperate areas. In absolute climate values, desert areas are hotter and dryer than temperate areas. However, in the relative contribution of degradation mechanisms, the high thermomechanical stress together with low hydrolysis and photo-degradation makes the average similar to the moderate climate stressors of the temperate climate. In real operating conditions, external degradation factors, such as soiling might increase the degradation rate if taken into account, but the degradation presented here assumes only gradual and non-reversible degradation processes.

4. Mapping of Degradation Mechanisms and Total Degradation Rate

The worldwide mapping of the degradation mechanisms (hydrolysis-degradation, photo-degradation and thermomechanical-degradation) are presented in Figure A1 in the Appendix B. As mentioned before, the simulations are based on the degradation model developed in ref. [10], and coefficients fitted for a specific PV module (high-performance mono-crystalline silicon PV module). The climate datasets used were extracted, modelled and averaged from the ERA5 reanalysis dataset for the years 2016, 2017, and 2018.

Figure A2 in the Appendix B shows the calculated worldwide degradation rate combining the three degradation mechanisms based on the main climate degradation factors.

To facilitate the visualization and possible use of our degradation maps, we categorize the locations into bins of 0.2%/a ranging from 0% to 0.8%/a for Europe and ranging from 0% to 1.4%/a around the World. The categorized maps are shown in Figures 7 and A3, respectively. The total degradation rates could reach 0.8%/a in the hottest areas of the south of Spain and Portugal for Europe, and globally the highest degradation rates (above 1.4%/a) are identified in locations next to the equator line.

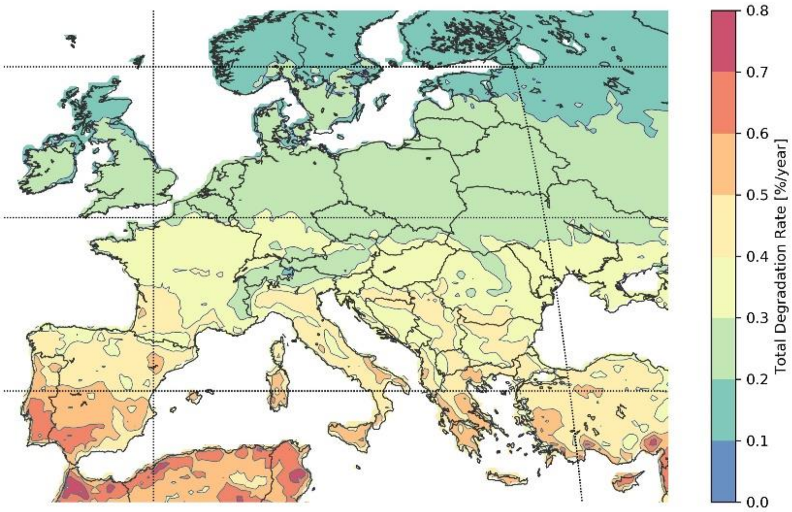

Figure 7. European categorization of total degradation rate based on temperature, humidity, and UV irradiance for a specific monocrystalline silicon PV module.

5. Uncertainty over Time-Temporal Evolution

The temporal evolution of the climate also might be a factor to consider while estimating the degradation rates of PV modules. In ref. [12] the decrease of the Performance Ratio due to climate change effect is already reported. Hereby, the annual degradation rates are simulated for the PV module described previously, using historical data from ERA5. For convenience in terms of computational resources, degradation rates based on hourly data are calculated only for the years 1980, 1990, 2000, 2010, 2016, 2017, and 2018. The ambient temperature is extracted for every year from 1979 to 2018.

In Figure 8, the evolution of the ambient temperature and degradation rates is shown. The global calculations represent the average values for land-surface between the Latitudes −60° and 60°. We notice that an increase in the ambient temperature also increases the degradation of the PV modules over time.

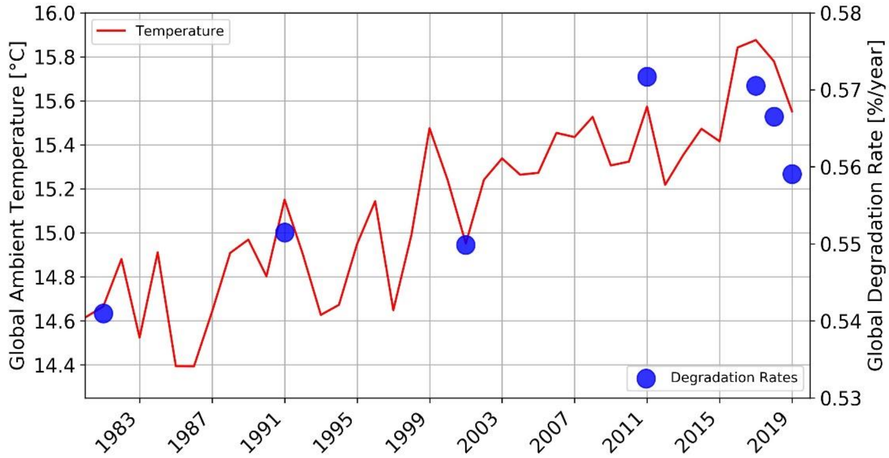

Figure 8. Temporal evolution of the global ambient temperature and the total degradation rates. The calculations are limited to the land-surface between the latitudes −60° and 60°.

6. Discussions

The used degradation model currently takes into account pure climate degradation factors and it does not include temporal or external degradation factors or failure modes such as light-induced degradation (LID), light and elevated temperature degradation (LeTID), potential-induced-degradation (PID) or mechanical damage due to wind or snow loads. Neither the underperformance due to soiling or snow covering is considered. Also, the final results of total degradation rates represent the value at steady conditions (for example, after LID). The calculations presented in this paper are related to a specific monocrystalline silicon PV module, and the values could be different for devices with different BOM but we expect the trend to remain the same for all crystalline silicon technologies.

The correlation with the KGPV climate zones shows a good agreement with the literature. Tropical climates are again presented as the harshest for PV modules due to the high humidity and high temperature. Desert and steppe climates present high degradation rates due to high daily temperature changes, even excluding soiling. Under no consideration of wind and snow loads, the temperate, cold and polar climates present low degradation rates.

Even though the results are coherent, some climate and degradation modelling topics need further investigation: (1) lack of UV irradiation measurements spread around the world does not allow a representative validation of models, (2) moisture ingress and related triggering of degradation processes, such as corrosion or delamination, need to be understood for different interactions of materials, and (3) the understanding of degradation mechanisms under high UV irradiance and extremely low humidity exposure.

Despite the current limitations, the average degradation rates calculated agree with the typical values used in manufacturer warranties and developers, showing that in the worst case (e.g., tropical climates) an average degradation of 1%/a can offer more than 20 years of performance above 80%, and the global average degradation rate of 0.5%/a could promise a lifetime operation of 40 years. Additionally, the mapping and results presented can give a new perspective of the climatic stresses worldwide when considering the installation of PV modules at different locations. Also, the high resolution of the GIS data, including ambient temperature, UV irradiation and humidity, together with the module operating temperature, helps to identify relevant variables for PV systems where measured data is not available. The degradation mechanisms and the total degradation rates calculated for the land-surface are available as Supplementary Materials attached to this article.

7. Conclusions

In this paper, we used the ERA5 climate reanalysis dataset for the modelling of PV degradation mechanisms and total degradation rates worldwide. We demonstrated that by extracting the ambient and dew point temperature, the relative humidity can be estimated at any location. Also, by extracting the global and top-of-atmosphere irradiances, the ultraviolet irradiance was estimated. Then, the extracted and modelled variables (temperature, irradiance, and humidity) were combined to compute the degradation of PV modules in terms of photo-degradation, hydrolysis-degradation, and thermo-mechanical-degradation. The quantification of each degradation mechanism allowed us to estimate the total degradation rate globally for a specific monocrystalline silicon PV module.

To validate the estimation of climate variables, we extracted the time series of 17 ground measurement stations from the World Radiation Monitoring Center - Baseline Surface Radiation Network (WRMC-BSRN), Desert Knowledge Australia (DKA) Solar Centre, and Universidad de Chile which include ambient temperature, global horizontal irradiance and relative humidity. The cumulative distribution function and coefficient-of-determination (R^2) were calculated to prove the good agreement between the ground measurements and the modelled data from ERA5 interpolated using the Inverse-Distance-Weighting method. For the validation, we considered daily average values from 2016 to 2018.

In terms of global spatial distribution, we found a clear correlation between the Köppen-Geiger-Photovoltaic (KGPV) climate classification and the estimated degradation rates. In the temperate zones of Europe, the average degradation rate is in accordance with the typical degradation rate of 0.5%/a considered widely by the PV community, however, this value can vary around ± 0.3%/a for a specific year.

From our calculations, thermomechanical degradation is the harshest for the studied PV module in nearly all climate zones, presenting the highest impact in very high irradiation zones, such as CK, BK, and AK. Photo-degradation and hydrolysis-degradation show similar global spatial distribution, but the former is higher since it also comprises UV irradiation as a degradation factor.

The temporal evolution of the degradation rates is directly correlated with the global ambient temperature and it is evidence that climate change could impact the long-term performance of PV systems.

We developed new maps for degradation mechanisms and the total degradation rate for the studied PV module which can be directly integrated as a new layer over the KGPV climate classification map and provide a rapid understanding of performance and degradation globally. However, due to the high uncertainty in the real degradation rate of PV systems (solar resource, methodology of calculation, quality of operational data, bill-of-materials of PV modules, etc.), the maps are presented as a guide to identify possible risk areas in terms of climate stress but not to give quantified degradation rates for specific locations for any PV module or PV system.

Supplementary Materials: The datasets generated in this article are available online as Mendeley data at https://data.mendeley.com/datasets/3nt652dwwx/1.

Author Contributions: J.A.-V., I.K. worked on the data processing, simulations and analyses. K.B., K.-A.W., and M.T. discussed the results and helped to improve the schemes. All the authors discussed the results and contributed, read and commented on the manuscript.

Funding: This project received funding from the European Union's H2020 programme SOLAR-TRAIN under grant agreement No 721452 and research programme P2-0197 funded by the Slovenia Research Agency.

Acknowledgments: The authors would like to thank the organizations ECMWF, DKA Solar Centre, Universidad de Chile and WRMC-BSRN for providing climate datasets.

Conflicts of Interest: The authors declare no conflict of interest.

Appendix A Meteorological Stations and Data Validation

Table A1. Details of meteorological stations used for the validation of *GHI*, T_{amb}, and *RH*.

Label	Location	Latitude	Longitude	Elevation [m]	Available Time Frame
ALI	Alice Springs, Australia	−23.76	133.88	560	2008-09 to 2019-11
CAB	Cabauw, Netherlands	52.0	4.9	0	2005-02 to 2019-05
CAR	Carpentras, France	44.1	5.1	100	1996-09 to 2018-12
CNR	Pamplona, Spain	42.8	−1.6	471	2009-07 to 2019-02
E13	Oklahoma, USA	36.6	−97.5	318	1994-01 to 2017-05
FUA	Fukuoka, Japan	33.6	130.4	3	2010-04 to 2019-04
GOB	Gobabeb, Namibia	−23.6	15.0	407	2012-05 to 2019-05
GUR	Gurgaon, India	28.4	77.2	259	2014-07 to 2019-01
HOW	Howrah, India	22.6	88.3	51	2014-10 to 2019-01
LIN	Lindenberg, Germany	52.2	14.1	125	1994-10 to 2017-01
LRC	Virginia, USA	37.1	−76.4	3	2014-12 to 2019-05
PAL	Palaiseau, France	48.7	2.2	156	2003-06 to 2019-02
PAY	Payerne, Switzerland	46.8	6.9	491	1992-10 to 2019-03
SAP	Sapporo, Japan	43.1	141.3	17	2010-04 to 2019-04
SPA	San Pedro de Atacama, Chile	−22.98	−68.16	2390	2009-05 to 2014-06
TAT	Tateno, Japan	36.1	140.1	25	1996-02 to 2019-03
TIR	Tiruvallur, India	13.1	80.0	36	2014-08 to 2019-01

Table A2. Cumulative Distribution Function (CDF) for *GHI*, T_{amb} and *RH* to compare ground stations from BSRN, DKA Solar Centre and Universidad de Chile with modelled and interpolated data from ERA5 climate reanalysis.

Cumulative Distribution Functions	Var.	R^2
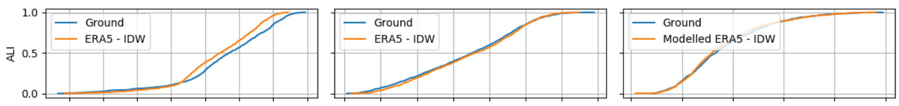	*GHI* T_{amb} *RH*	0.76 0.98 0.91
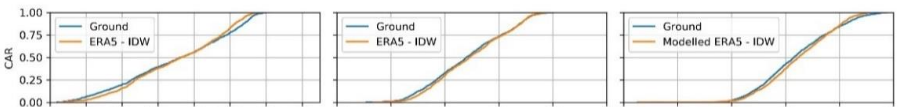	*GHI* T_{amb} *RH*	0.89 0.98 0.82
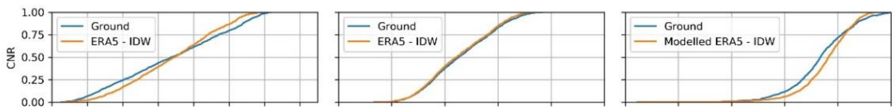	*GHI* T_{amb} *RH*	0.78 0.98 0.64
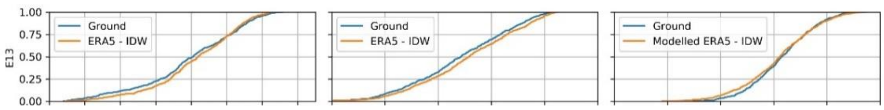	*GHI* T_{amb} *RH*	0.81 0.99 0.85
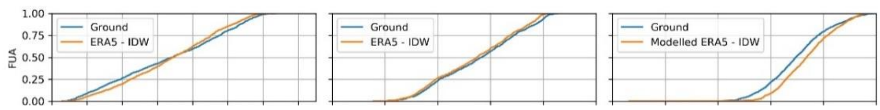	*GHI* T_{amb} *RH*	0.82 0.99 0.80
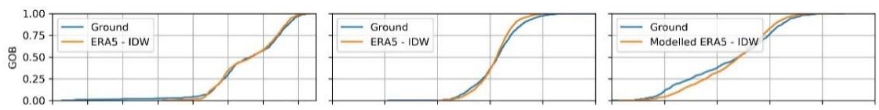	*GHI* T_{amb} *RH*	0.65 0.72 0.71

Table A2. *Cont.*

Cumulative Distribution Functions	Var.	R^2
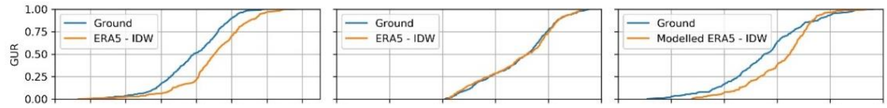	*GHI* T_{amb} *RH*	0.63 0.98 0.82
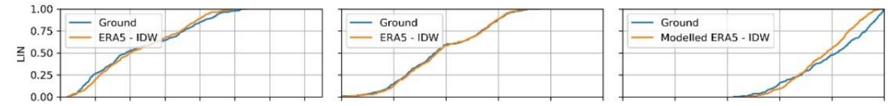	*GHI* T_{amb} *RH*	0.90 0.99 0.93
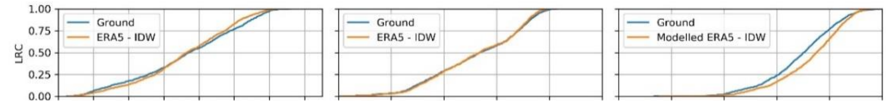	*GHI* T_{amb} *RH*	0.89 0.99 0.78
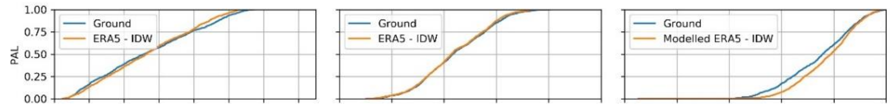	*GHI* T_{amb} *RH*	0.87 0.99 0.83
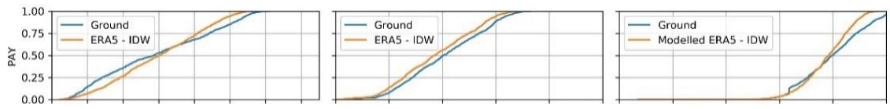	*GHI* T_{amb} *RH*	0.79 0.98 0.47
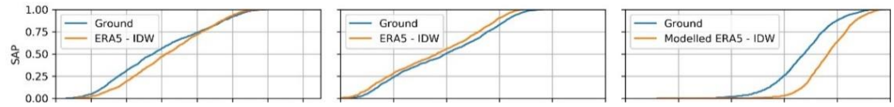	*GHI* T_{amb} *RH*	0.72 0.99 0.62
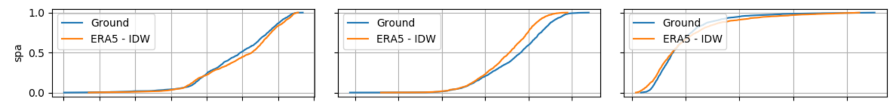	*GHI* T_{amb} *RH*	0.79 0.84 0.75
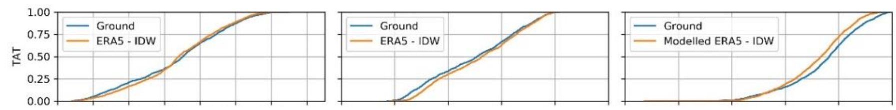	*GHI* T_{amb} *RH*	0.86 0.99 0.86
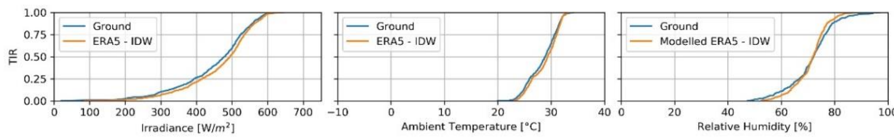	*GHI* T_{amb} *RH*	0.49 0.96 0.75

Appendix B Mapping of Degradation Mechanisms and Total Degradation Rate

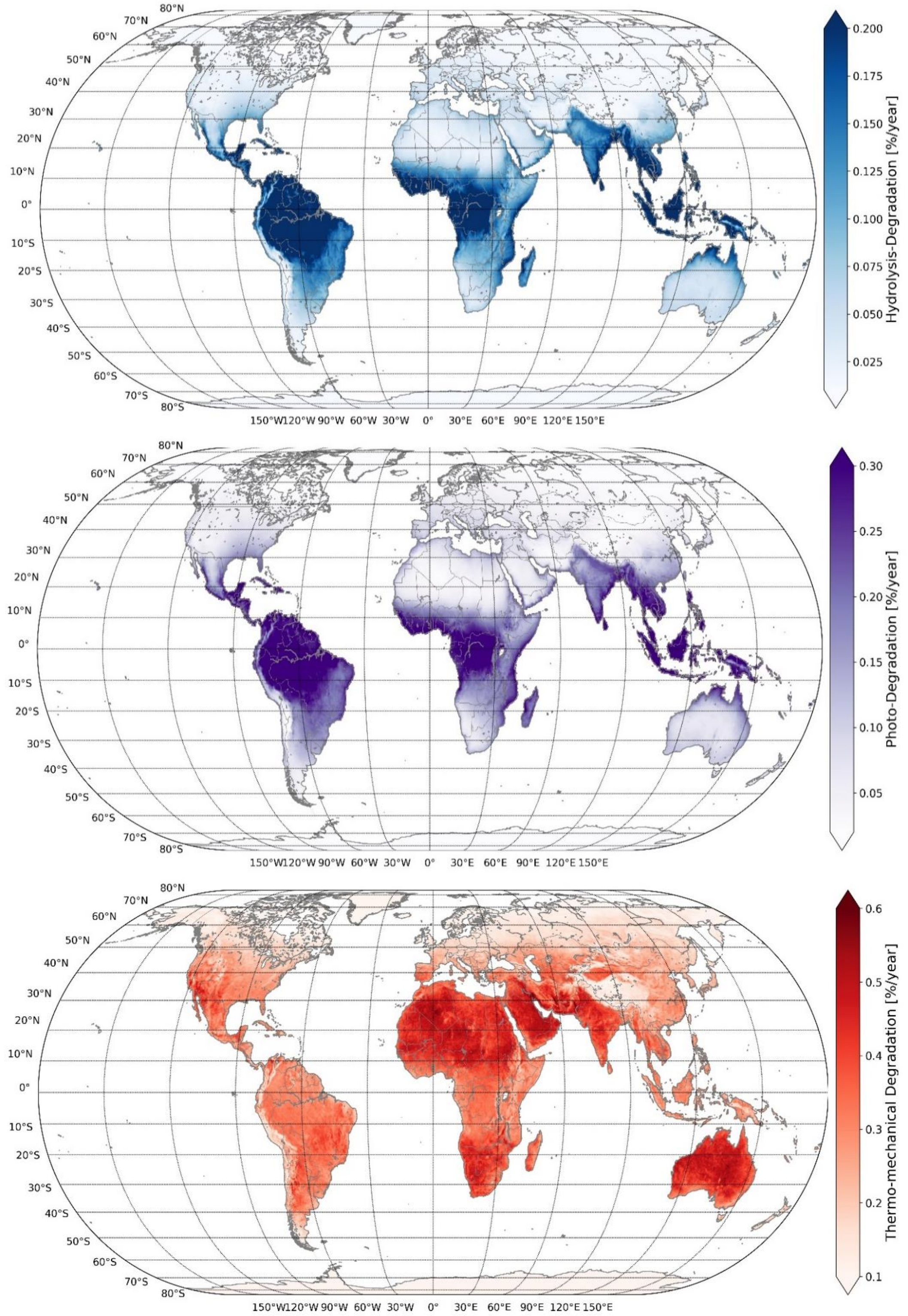

Figure A1. Global mapping of degradation mechanisms. **top** Hydrolysis-degradation, **middle** photo-degradation and **bottom** thermomechanical degradation.

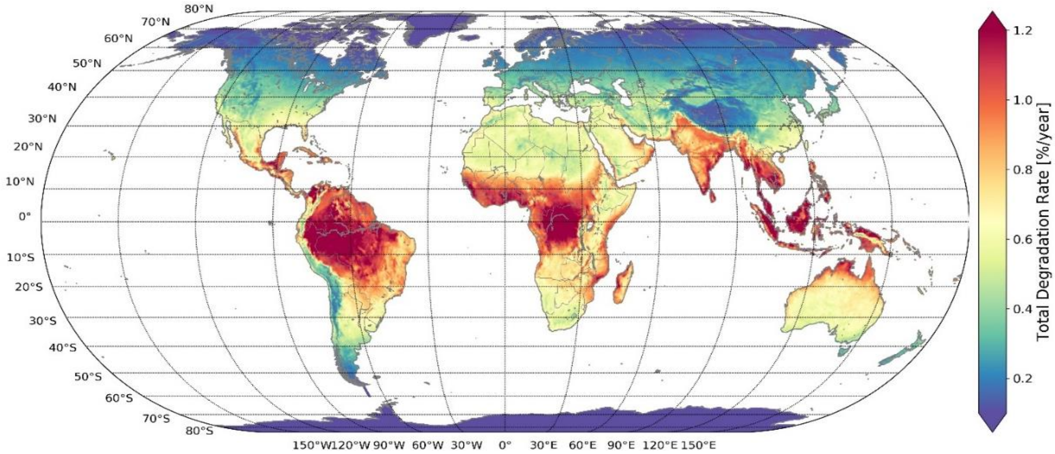

Figure A2. Total degradation rates for a specific mono-crystalline silicon PV module using the Kaaya model. Climate data from ERA5 for the average between 2016 and 2018.

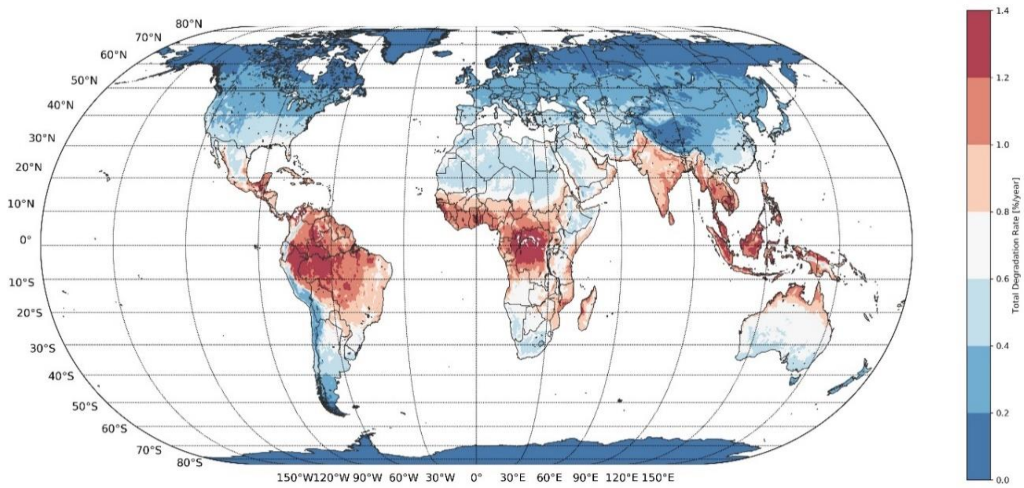

Figure A3. Categorization of total degradation rates for a specific mono-crystalline silicon PV module using the Kaaya model. Climate data from ERA5 for the average between 2016 and 2018.

References

1. Haegel, N.M.; Atwater, H.; Barnes, T.; Breyer, C.; Burrell, A.; Chiang, Y.-M.; De Wolf, S.; Dimmler, B.; Feldman, D.; Glunz, S.; et al. Terawatt-scale photovoltaics: Transform global energy. *Science* **2019**, *364*, 836–838. [CrossRef] [PubMed]
2. Vartiainen, E.; Masson, G.; Breyer, C.; Moser, D.; Román Medina, E. Impact of weighted average cost of capital, capital expenditure, and other parameters on future utility-scale PV levelised cost of electricity. *Prog. Photovolt. Res. Appl.* **2019**. [CrossRef]
3. Jordan, D.C.; Wohlgemuth, J.H.; Kurtz, S.R. Technology and Climate Trends in PV Module Degradation. In Proceedings of the 27th European Photovoltaic Solar Energy Conference and Exhibition, Frankfurt, Germany, 24–28 September 2012.
4. Jordan, D.C.; Kurtz, S.R.; VanSant, K.; Newmiller, J. Compendium of photovoltaic degradation rates: Photovoltaic degradation rates. *Prog. Photovolt. Res. Appl.* **2016**, *24*, 978–989. [CrossRef]
5. Jordan, D.C.; Silverman, T.J.; Wohlgemuth, J.H.; Kurtz, S.R.; VanSant, K.T. Photovoltaic failure and degradation modes: PV failure and degradation modes. *Prog. Photovolt. Res. Appl.* **2017**, *25*, 318–326. [CrossRef]
6. Omazic, A.; Oreski, G.; Halwachs, M.; Eder, G.C.; Hirschl, C.; Neumaier, L.; Pinter, G.; Erceg, M. Relation between degradation of polymeric components in crystalline silicon PV module and climatic conditions: A literature review. *Sol. Energy Mater. Sol. Cells* **2019**, *192*, 123–133. [CrossRef]

7. Halwachs, M.; Neumaier, L.; Vollert, N.; Maul, L.; Dimitriadis, S.; Voronko, Y.; Eder, G.C.; Omazic, A.; Mühleisen, W.; Hirschl, C.; et al. Statistical evaluation of PV system performance and failure data among different climate zones. *Renew. Energy* **2019**, *139*, 1040–1060. [CrossRef]
8. Eder, G.C.; Voronko, Y.; Dimitriadis, S.; Knöbl, K.; Újvári, G.; Berger, K.A.; Halwachs, M.; Neumaier, L.; Hirschl, C. Climate specific accelerated ageing tests and evaluation of ageing induced electrical, physical, and chemical changes. *Prog. Photovolt. Res. Appl.* **2018**, 1–16. [CrossRef]
9. Dubey, R.; Chattopadhyay, S.; Kuthanazhi, V.; Kottantharayil, A.; Singh Solanki, C.; Arora, B.M.; Narasimhan, K.L.; Vasi, J.; Bora, B.; Singh, Y.K.; et al. Comprehensive study of performance degradation of field-mounted photovoltaic modules in India. *Energy Sci. Eng.* **2017**, *5*, 51–64. [CrossRef]
10. Kaaya, I.; Koehl, M.; Mehilli, A.P.; de Cardona Mariano, S.; Weiss, K.A. Modeling Outdoor Service Lifetime Prediction of PV Modules: Effects of Combined Climatic Stressors on PV Module Power Degradation. *IEEE J. Photovolt.* **2019**, *9*, 1105–1112. [CrossRef]
11. Lindig, S.; Kaaya, I.; Weis, K.-A.; Moser, D.; Topic, M. Review of Statistical and Analytical Degradation Models for Photovoltaic Modules and Systems as Well as Related Improvements. *IEEE J. Photovolt.* **2018**, *8*, 1773–1786. [CrossRef]
12. Ascencio-Vásquez, J.; Brecl, K.; Topič, M. Methodology of Köppen-Geiger-Photovoltaic climate classification and implications to worldwide mapping of PV system performance. *Sol. Energy* **2019**, *191*, 672–685. [CrossRef]
13. Peters, I.M.; Liu, H.; Reindl, T.; Buonassisi, T. Global Prediction of Photovoltaic Field Performance Differences Using Open-Source Satellite Data. *Joule* **2018**, *2*, 307–322. [CrossRef]
14. Victoria, M.; Andresen, G.B. Using validated reanalysis data to investigate the impact of the PV system configurations at high penetration levels in European countries. *Prog. Photovolt. Res. Appl.* **2019**, *27*, 576–592. [CrossRef]
15. Bala Subramaniyan, A.; Pan, R.; Kuitche, J.; TamizhMani, G. Quantification of Environmental Effects on PV Module Degradation: A Physics-Based Data-Driven Modeling Method. *IEEE J. Photovolt.* **2018**, *8*, 1289–1296. [CrossRef]
16. Copernicus Climate Change Service (C3S) ERA5: Fifth Generation of ECMWF Atmospheric Reanalyses of the Global Climate. Copernicus Climate Change Service Climate Data Store (CDS) 2017. Available online: https://cds.climate.copernicus.eu/cdsapp#!/home (accessed on 13 October 2019).
17. Driemel, A.; Augustine, J.; Behrens, K.; Colle, S.; Cox, C.; Cuevas-Agulló, E.; Denn, F.M.; Duprat, T.; Fukuda, M.; Grobe, H.; et al. Baseline Surface Radiation Network (BSRN): Structure and data description (1992–2017). *Earth Syst. Sci. Data* **2018**, *10*, 1491–1501. [CrossRef]
18. Desert Knowledge Australia Centre Download Data. Location: Alice Springs. Available online: http://dkasolarcentre.com.au/historical-data/download (accessed on 25 November 2019).
19. Molina, A.; Falvey, M.; Rondanelli, R. A solar radiation database for Chile. *Sci. Rep.* **2017**, *7*, 14823. [CrossRef]
20. Urraca, R.; Huld, T.; Martinez-de-Pison, F.J.; Sanz-Garcia, A. Sources of uncertainty in annual global horizontal irradiance data. *Sol. Energy* **2018**, *170*, 873–884. [CrossRef]
21. Camus, C.; Offermann, P.; Weissmann, M.; Buerhop, C.; Hauch, J.; Brabec, C.J. Site-specific assessment of mechanical loads on photovoltaic modules from meteorological reanalysis data. *Sol. Energy* **2019**, *188*, 1134–1145. [CrossRef]
22. Schwingshackl, C.; Petitta, M.; Wagner, J.E.; Belluardo, G.; Moser, D.; Castelli, M.; Zebisch, M.; Tetzlaff, A. Wind Effect on PV Module Temperature: Analysis of Different Techniques for an Accurate Estimation. *Energy Procedia* **2013**, *40*, 77–86. [CrossRef]
23. Huld, T.; Amillo, A. Estimating PV Module Performance over Large Geographical Regions: The Role of Irradiance, Air Temperature, Wind Speed and Solar Spectrum. *Energies* **2015**, *8*, 5159–5181. [CrossRef]
24. Buck, A.L. New Equations for Computing Vapor Pressure and Enhancement Factor. *J. Appl. Meteorol.* **1981**, *20*, 1527–1532. [CrossRef]
25. Buck Research Instruments, LLC. *CR-1A User's Manual*; Buck Research Instruments, LLC: Aurora, CO, USA, 2012.
26. Wald, L. *A Simple Algorithm for the Computation of the Spectral Distribution of the Solar Irradiance at Surface*; Research Report; Mines ParisTech: Paris, France, 2018.
27. Kuo, P.-H.; Chen, H.-C.; Huang, C.-J. Solar Radiation Estimation Algorithm and Field Verification in Taiwan. *Energies* **2018**, *11*, 1374. [CrossRef]

28. Yang, D. Post-processing of NWP forecasts using ground or satellite-derived data through kernel conditional density estimation. *J. Renew. Sustain. Energy* **2019**, *11*, 026101. [CrossRef]
29. Skoplaki, E.; Palyvos, J.A. Operating temperature of photovoltaic modules: A survey of pertinent correlations. *Renew. Energy* **2009**, *34*, 23–29. [CrossRef]
30. Faiman, D. Assessing the outdoor operating temperature of photovoltaic modules. *Prog. Photovolt. Res. Appl.* **2008**, *16*, 307–315. [CrossRef]
31. Koehl, M.; Heck, M.; Wiesmeier, S. Categorization of weathering stresses for photovoltaic modules. *Energy Sci. Eng.* **2018**, *6*, 93–111. [CrossRef]